REACTION OF MERCURY WITH A Ag-Sn DENTAL AMALGAM ALLOY

J. R. ABBOTT, B.Sc. Dent., M.D.S.

A thesis submitted for the degree of

Doctor of Philosophy

Department of Chemical Engineering,
Material Engineering Group,
The University of Adelaide.

JUNE 1981

DECLARATION

This thesis contains no material which has been accepted for the award of any other degree or diploma in any university and to the best of my knowledge and belief, contains no material previously published or written by another person, except where due reference is made in the text.

JOHN R. ABBOTT

ACKNOWLEDGEMENTS

I wish to thank my supervisor Professor D.R. Miller for his encouragement and valuable advice during the investigation and for his guidance in the preparation of this thesis.

The author is particularly grateful to Mr. D.J. Netherway for his collaboration in computer programming and electron diffraction analyses.

Special thanks to Mr. R.A. Legge, Mr. I.H. Brown and Mr. L. Bray for their assistance and helpful discussions. I am most grateful to Miss J.E. Nash who typed the drafts of this thesis and to Miss V.A. Greenwood for photographic assistance.

The author would also like to register appreciation to the Workshop's staff for the assistance given and particular thanks to Mr. B.H. Ide for the maintenance of equipment associated with this project.

Finally, acknowledgement is given to the National Health and Medical Research Council for supporting this project with a Dental Post-Graduate Scholarship.

SUMMARY

The objective of the present investigation was to examine the reaction mechanism between the γ phase of the silver-tin system and mercury. In order to achieve this objective it was necessary to prepare a single γ phase alloy whose homogeneity was established by improved optical metallographic techniques and by transmission electronmicroscopy. X-ray and electron diffraction in conjunction with structure factor and intensity calculations, confirmed that the γ phase alloy had an ordered orthorhombic crystal lattice and conformed to the Pmmn - D_{2h}^{13} No. 59 space group with lattice parameters a = 5.967 Å, b = 4.781 and c = 5.183.

Scanning electron microscope studies of mercury attack on plastically deformed single crystals of γ phase of known orientation, revealed that preferential attack occurred along well defined crystallographic planes. These crystal planes were identified as the (011), (01$\bar{1}$) and (010) planes. Additional structural information obtained from transmission electron microscope studies, interpreted using computerised crystallographic programs, showed that plastic deformation occurred both by crystallographic slip on the (010) plane and by deformation twinning on the ($\bar{2}$11), (0$\bar{1}$1) and (011) planes.

The significance of these results as related to an understanding of the reaction mechanism between mercury and the γ phase is discussed.

TABLE OF CONTENTS

TABLE OF CONTENTS (continued)

TABLE OF CONTENTS (continued)

CHAPTER 1

INTRODUCTION

1.1 HISTORICAL BACKGROUND

From the earliest times, strenuous efforts have been made to alleviate the extremely painful complaint of toothache, particularly that caused by dental decay or dental caries which accompanies the development of visible holes or cavities in teeth.

The early attempts at treatment (e.g. cauterization) were rudimentary but widely used and they persisted in various forms until well into the 19th century. Although a procedure like cauterization may have resulted in some temporary relief of pain due to the destruction of live tissue, a recurrence within a few days or weeks of treatment would be expected. Early attempts to fill teeth would likewise have had little success in preventing the progress of decay, although some temporary structural support for teeth weakened by decay may have been achieved. One such procedure, documented at the time of Christ, was to restore decayed teeth with fillings of lead or linen. In the 9th century Persian dentists plugged cavities with alum and over the following millenium a wide variety of non-metallic compounds, some mixed with herbs and drugs such as opium (which may have been at least partially

successful in easing pain) were tried. The performance of these materials has not been recorded but as the biology of dental caries was not understood, in general, no attempt would have been made to remove decay from the tooth prior to insertion of the material so that any relief from the progress of decay must have been short lived. This would also have been true of teeth filled with metallic materials such as gold which appears to have been first used for this purpose in the 15th century.

The use of gold foil pluggings was both a tedious and expensive procedure and it caused considerable discomfort to the patient. The alternative at the beginning of the 19th century was one or other of the eutectic type lead base alloys such as "Newtons Alloy" (52% Bi, 32% Pb, 16% Sn, melting point 95°C), "D'arcets Alloy" (50% Bi, 25% Pb, 25% Sn, melting point 93°C) and Woods Metal (50% Bi, 25% Pb, 12.5% Sn and 12.5% Cd, melting point 73°C) which were either melted and cast into the tooth cavity or plugged into the cavity in the solid state and then "buttered" into place with a hot instrument. However, the discomfort which their use imposed on the patient was so great that the desirability of finding an alternative metallic restorative material which could be inserted in the tooth in the liquid state and then hardened without the need for the application of heat, was all too apparent to both patient and dentist.

In response to this need, Pepys and Fox in 1805 produced what they described as a "fusible metal" which contained mercury as one of its principal ingredients. Although the alloy was not successful clinically, it was notable in being the first amalgam preparation to be used in restorative dentistry. Other mercury preparations appeared soon after. In 1818, for example, Regnart developed an alloy which could be "softened" by the application of mercury. "Silver paste" (a mixture of pure silver and mercury) was introduced in 1826 by the French dentist, Taveau, and over the following seven or eight years silver-mercury amalgams, usually prepared from coarse filings of French silver coins, came to be used by dental practitioners in Europe and the U.S.A. The initial response of patients to these amalgams may have been one of relief at being spared the trauma of having molten Woods Metal poured into their aching teeth. Unfortunately, however, the apparent ease with which amalgam could be inserted into a cavity not only betrayed many dental practitioners into careless clinical procedures but it encouraged the activities of unqualified and often incompetent entrepreneurs who were quick to capitalize on the lucrative business opportunities afforded by this new "painless" procedure for filling teeth. The clinical performance of these early amalgams was quite disastrous and reaction against them mounted to such an extent that the American Society of Dental Surgeons resolved, in 1845, that all its members pledge to abandon the insertion of

amalgam fillings and any member contravening this resolution was to be expelled!

In spite of the strong stand taken by the ASDS, some dental practitioners continued to recognize the potential benefits offered by amalgams. One of these preparations, copper amalgam, which consisted of 69.3% Hg, 28.2% Cu and 2.2% Sn, was supplied in the form of pellets which were heated to about 95°C in an iron spoon until mercury droplets appeared. It was then ground in a mortar and pestle and mulled in the hand until a consistency suitable for packing was attained. This material had poor long term stability as its corrosion resistance in the oral cavity was low but it found considerable support in preserving children's deciduous teeth. Its use continued well into the present century and indeed as recently as 1964 (Lind et al. 1964) reported the results of clinical studies of the bacteriostatic action of copper amalgams brought about by the slow release of copper.

Of far greater significance, however, was the fact that in 1895, G.V. Black published the first of a series of papers (Black 1895 a, b, c, 1896 a, b, 1897) describing the results of carefully controlled experiment on amalgams prepared from silver-tin alloys with compositions in the range 42-75% Ag and 30-58% Sn. Black observed that amalgams sometimes expanded and sometimes contracted during setting and he established that these dimensional changes, the

clinical significance of which he was quick to appreciate, were dependent on the alloy composition, the particle size of the filings of the alloy which were mixed with mercury, the ratio of mercury to alloy in the mix, the type of mixing vessel (e.g. mortar and pestle), used to prepare the amalgam and the procedure used to pack the amalgam into the tooth cavity. He noted that the reaction was markedly affected by annealing the filings at 100°C before mixing with mercury and that this resulted in a reduction in the amount of mercury required to produce a "working mix" of the right consistency. The compressive strengths and the dimensional changes which occurred on setting were determined for a range of amalgams prepared from Ag-Sn alloys and Ag-Sn alloys containing additions of elements such as Au, Pb, Zn, Bi, Pd, Al and Cu. From this massive investigation and his astute observations on the clinical performance of the amalgam restorations which he had inserted over a period of some 40 years of dental practice (notwithstanding the ASDS edict!), Black was able to make firm recommendations not only on the clinical procedures to be adopted in correctly cutting the cavity, mixing and inserting the amalgam into the cavity etc., but also on metallurgical factors such as the composition of the silver-tin alloy (Black suggested 70% Ag, 30% Sn), the preparation and heat-treatment of the alloy filings, the optimum mercury:alloy ratio etc.

Black's contribution to the knowledge of the behaviour of silver-tin dental amalgam, made long before

the silver-tin phase diagram had been determined and without the assistance of metallographic techniques, was enormous. But perhaps his greatest achievement was in successfully persuading a dental profession, initially prejudiced (perhaps justifiably so!) against mercury preparations, that provided the silver-tin amalgam restorations were correctly formulated and inserted using the guidelines which he had drawn up, they did, indeed, represent a major advance in the practice of restorative dentistry.

Black's work was supported by other studies in America and in England and Germany. By 1925, when the U.S. Federal Specification No. 356 (Dental Amalgam Alloys) was issued, the use of silver-tin amalgams of composition approximately 70% Ag 30% Sn was widespread.

1.2 CONSTITUTION OF ALLOYS OF SILVER AND TIN

The early attempts, e.g. by Heycock and Neville (1897), Petrenko (1907), to establish the phase diagram for the Ag-Sn system were shown by Murphy (1926) to be inadequate. Murphy's phase diagram, Fig. 1.1, now accepted as essentially correct, establishes the presence of two peritectic reactions in the system. The first, at a temperature of 724°C and 14.5% Sn, results in the formation of the β-phase with a composition ranging from approximately Ag_5Sn to Ag_6Sn while the second, which occurs at 480°C and 26.9% Sn produces the γ-phase which

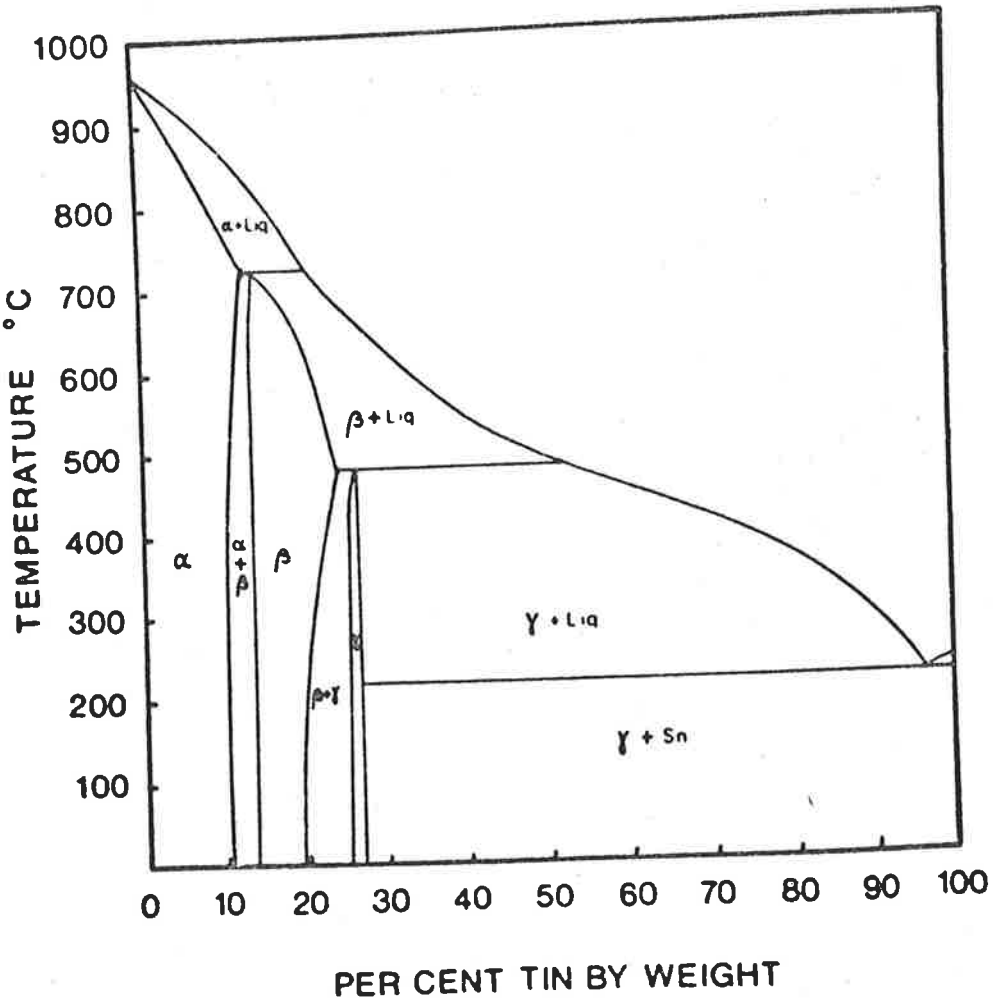

FIGURE 1.1 The constitution diagram of the silver-tin system as described by Murphy (1926).

was believed to have a composition corresponding to the formula Ag_3Sn which exists as a single phase at room temperature over the range 26.0 to 26.9% Sn. Beyond about 27% Sn a eutectic structure of γ and almost pure Sn exists.

1.3 CRYSTAL STRUCTURE OF THE γ PHASE

There appears to have been considerable controversy surrounding the determination of the crystal structure and lattice parameters of the γ phase. The earliest X-ray diffraction studies were carried out in 1926 by Preston, a colleague of Murphy's at the National Physical Laboratories, who observed (Murphy 1926) that the X-ray powder diffraction pattern was consistent with the material having a hexagonal close packed structure with a = 2.98 Å and c/a = 1.61. In reply to the criticism of his work by Hume-Rothery that such a structure contains 2 atoms per unit cell which is inconsistent with the composition of the compound Ag_3Sn, Preston pointed out that powder diffraction data was inadequate to enable the crystal structure to be determined unequivocally and that such a determination must await the availability of single crystals of the compound. Later, however, Nial, Almin and Westgren (1931), again using X-ray powder diffraction techniques suggested that Ag_3Sn had a deformed hexagonal structure which could be described by an orthorhombic lattice with constants a = 2.989 Å, b = 4.771 and c = 5.149. (NOTE: These parameters have

been re-allocated to conform with the nomenclature adopted by Fairhurst and Cohen (1972)). This work was supported, again on the basis of powder diffraction data, by Waterstrat and Hicho (1964).

However, Fairhurst (1966) and later Fairhurst and Cohen (1972) carried out a complete X-ray structural analysis using a single crystal of Ag_3Sn in a precession camera as well as very accurate X-ray powder diffraction observations. This approach led them to conclude that the space group conformed to one of 2 possible space groups listed in the International Tables for X-ray Crystallography Vol. 1. Since one of these possibilities could be eliminated for Ag_3Sn on the basis of packing requirements and observations of the intensities of the diffraction peaks, they were led to the conclusion that the space group of the compound Ag_3Sn was the orthorhombic Pmmn - D_{2h}^{13} No. 59 the lattice parameters for which are a = 5.968 Å, b = 4.7802, c = 5.1843, i.e. an "a" value twice that of Nial et al.. The unit cell for this crystal contains 8 atoms, 6 silver and 2 tin.

Notwithstanding this work of Fairhurst and Cohen, the use of the lattice parameters of Nial et al. has persisted. Malhotra and Lawless (1975) for example, used Nial dimensions for the identification of Ag_3Sn in studies of ternary alloys of silver, tin and gold: Wood and Jacombs (1976) and Wood and King (1978) determined the interplanar spacings of splat quenched Ag_3Sn and found them to be in

agreement with Nial's results but inconsistent for the larger "a" value determined by Fairhurst. Resolution of this continuing conflict in the structure of the γ-phase of the Ag-Sn system will be presented in Chapter 3 of the present thesis.

1.4 REACTION OF THE γ PHASE WITH MERCURY

Following the identification of the compound Ag_3Sn by Petrenko in 1907 and the recognition of its importance as a dental amalgam alloy, a number of attempts were made (Joyner 1911, McBain and Joyner 1912, Knight and Joyner 1913, Gray 1919, 1921, 1922, 1923 etc.) to determine the nature of the amalgamation reaction products by chemical methods. Previous work of Ogg (1895) and Reinders (1904) on silver mercury alloys had established the presence of a compound Ag_3Hg_4 ("Arbor Dianae") and as this appeared to be the only familiar compound discovered in the reaction products of Ag_3Sn with mercury, the reaction was believed to be as follows:

$$Ag_3Sn + 4Hg \rightarrow Ag_3Hg_4 + Sn$$

In 1931, however, Murphy and Preston carried out an X-ray diffraction study of the alloys of silver and mercury and described 3 separate phases:

1. α-phase - a silver mercury solid solution with a f.c.c. crystal structure. The limiting solid solubility of mercury in silver at room temperature was 50 wt. % (35 at. %).

2. β-phase - a h.c.p. structure with restricted composition of approximately 40 wt. % silver formed as a product of a peritectic reaction between α and liquid at 276°C.

3. γ-phase - b.c.c. structure formed as a product of a second peritectic reaction with a composition of 29-30 wt. % silver at 127°C.

(Note: the γ phase nomenclature is also used by Murphy to describe the orthorhombic phase of the silver-tin system).

Due to inadequacies in their experimental data, Murphy and Preston were unable to ascribe precise formulae to the β and γ phases but tentatively suggested that the γ phase might be either Ag_3Hg_4 or Ag_4Hg_5. Berman and Harcourt (1938) showed that this compound was, in fact Ag_2Hg_3. A full structural analysis of this γ phase of the silver mercury system was carried out much later by Fairhurst (1966) and Fairhurst and Cohen (1972) using single crystals and the precession X-ray diffraction technique. The space group was identified as the cubic I23 and the formula of the compound was shown to be Ag_2Hg_3. This result was confirmed by Baird and Muller (1969).

Attempts to determine the nature of the Sn-Hg system ran parallel to those of the Ag-Hg system but it would seem that severe experimental difficulties with X-ray and metallographic examinations of the alloys in this system have resulted in some uncertainty still existing. Simson (1924) identified a simple hexagonal γ tin-mercury phase which is stable at room temperature over the range 5-12 wt. % Hg. Gayler (1937 a) confirmed the existence of this phase and published a phase diagram for the Sn-Hg system which showed a γ+ liquid phase field adjacent to the peritectic γ at room temperature. However, Gayler (1937 a) also noted an anomalous thermal arrest during the casting of alloys with compositions lying in this γ+ liquid phase field and raised the possibility that this might indicate the presence of another phase which she called δ. Troiano (1938) arrived at similar conclusions to those of Gayler and the Sn-Hg phase diagram published by Hansen (1958) reflects the ambiguity which still persists about the possible existence of this δ phase.

There is, however, no doubt about the γ phase in the Sn-Hg system and its crystal structure was subsequently determined by Fairhurst and Ryge (1962) to be simple hexagonal with "c" values ranging from 2.995 to 2.984 and c/a = 0.931.

Interest in the Ag-Hg and Sn-Hg systems originated of course, from the desire to identify the products of the reaction between Ag_3Sn and Hg. Gayler (1937 a) went a step further and derived the Ag_3Sn-Hg phase diagram

(Figure 1.2). Using this equilibrium diagram, Gayler proposed (1937 b) that the phases formed on reaction of mercury with Ag_3Sn, in the proportions used in formulating dental amalgam, should be both the β and γ phases of the Ag-Hg system so that the setting reaction should be described by the equation:

$$Ag_3Sn + Hg \rightarrow \beta_{(Ag\text{-}Hg)} + \gamma_{(Ag\text{-}Hg)} + \gamma_{(Sn\text{-}Hg)}$$

Gayler's X-ray and metallographic observations of hardened amalgams were, however, internally inconsistent and the fact that in practice hardened amalgam existed in a state far removed from thermodynamic equilibrium raised serious doubts about the validity of applying the Ag_3Sn-Hg phase diagram to predict the reaction products contained in it. However, Gayler's work did allow predictions to be made of the way in which the final structure might be approached during the reaction of Ag_3Sn with mercury and Troiano (1938), observing that the $\beta_{(Ag\text{-}Hg)}$ phase could not be detected in hardened amalgam, suggested an alternative equation to Gayler's which involved an approach to equilibrium from the mercury rich corner of the phase diagram - i.e. in a direction opposite to that implied by Gayler's equation. Troiano's alternative proposal was as follows:

$$Ag_3Sn + Hg \rightarrow \gamma_{(Ag\text{-}Hg)} + \delta_{(Sn\text{-}Hg)} + Ag_3Sn \text{ (unreacted)}$$

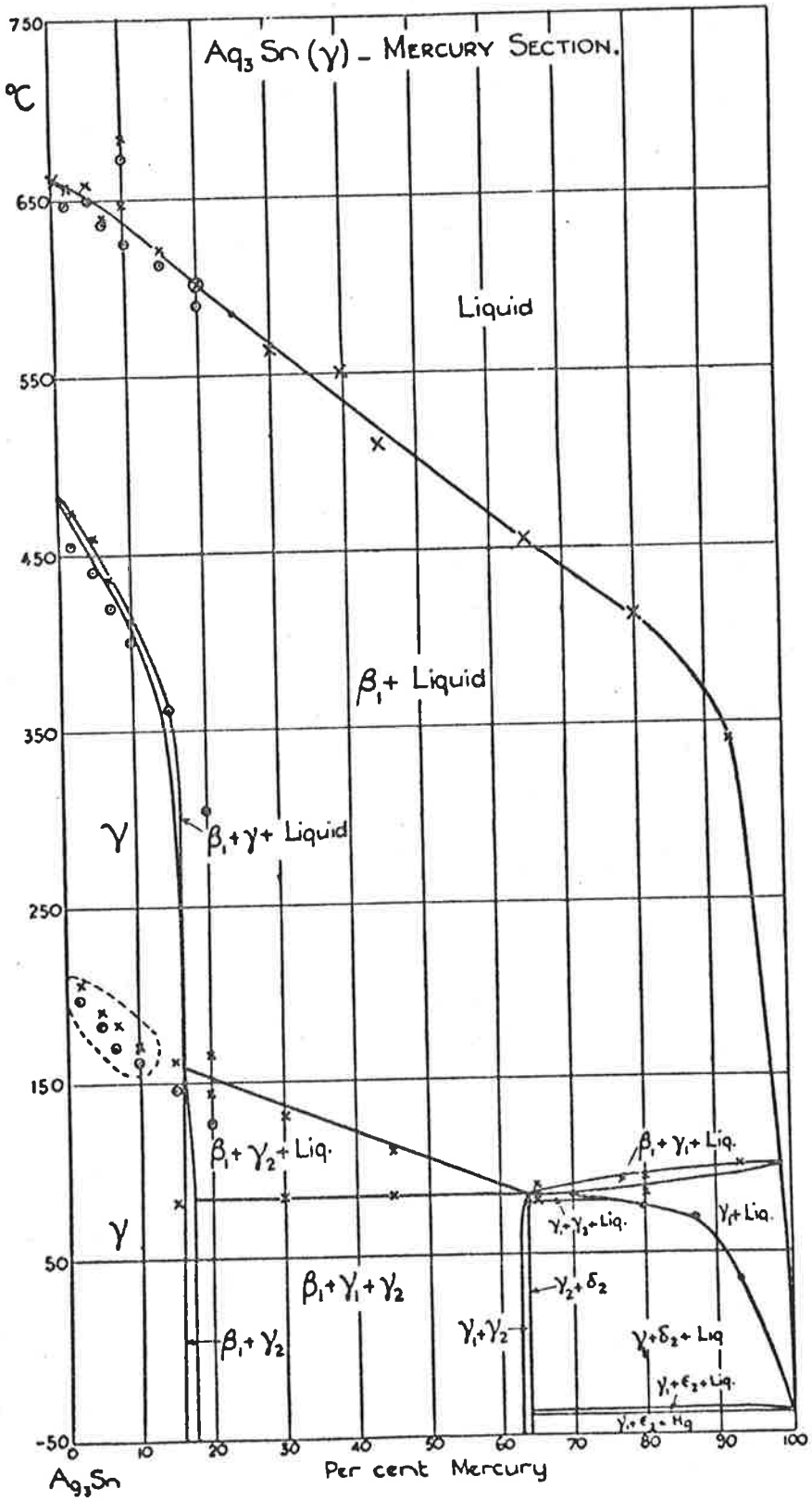

FIGURE 1.2 The equilibrium phase diagram of Ag_3Sn-Hg system as described by Gayler (1937 a).

As has already been pointed out, the question of the existence of the δ phase of the Sn-Hg system was highly controversial and a lively debate followed the publication of Troiano's proposed equation. The matter was not satisfactorily resolved until Ryge, Moffett and Barkow (1953) showed that there was no evidence of a $\delta_{(Sn-Hg)}$. Fairhurst and Ryge (1962) determined the structure of the $\gamma_{(Sn-Hg)}$ phase using X-ray techniques and showed that it was the only tin-mercury phase found in dental amalgam. Ryge, Moffett and Barkow using X-ray powder diffraction techniques showed that three main phases were present in dental amalgam - the γ phase of the Ag-Sn system (Ag_3Sn), the γ phase of the Ag-Hg system (which Fairhurst subsequently showed was Ag_2Hg_3), and the γ phase of the Sn-Hg system. Earlier, Stenbeck (1950) had obtained evidence which supported Gayler's assertion that dental amalgam contained also the β phase of the tin-mercury system. Ryge, Moffett and Barkow looked for it but could not find it in their alloys and were led to the conclusion that the $\beta_{(Ag-Hg)}$ phase, if present at all, must form long after the setting reaction was essentially complete. Subsequent work of Johnson (1967 a, b), Pihl and Beasley (1968), Otani (1970 a, b) and Vrijhoef and Driessens (1974) showed that indeed the $\beta_{(Ag-Hg)}$ phase, could be detected in dental amalgam but that it probably formed by the slow decomposition of the $\gamma_{(Ag-Hg)}$ phase to $\beta_{(Ag-Hg)}$ + free Hg. This decomposition, which can be detected (Reynolds) after the amalgam has been stored at room temperature for a period of some two years, (or after 2 days at 60°C (Otani 1970 a, b)) appears to initiate at the

boundary between the $\gamma_{(Ag-Hg)}$ phase and the remaining unreacted Ag_3Sn so that the free mercury liberated by the transformation would immediately react with Ag_3Sn. The clinical significance of the decomposition has not been established and although Johnson (1967a) felt that it may have an adverse effect on the mechanical properties of an amalgam restoration, Otani (1970a) suggested that the decomposition would not proceed to any marked extent because the $\gamma_{(Ag-Hg)}$ phase would tend to be stabilized by mercury released during the in vivo corrosion of $\gamma_{(Sn-Hg)}$. Both suggestions must, however, be considered to be speculative.

The determination of the structure of dental amalgam was seriously impeded by the absence of metallographic studies of sufficient quality to enable the phases present to be distinguished and identified. In their review of the mechanism of the setting of dental amalgam, Ryge, Fairhurst and Fischer (1961) made reference to a thesis submitted in 1958 by K. Schnuck in which the presence of three separate phases was demonstrated by relief polishing and to the work of Schmitt (1960) who used a selective etching technique to distinguish these three phases, which he identified from their relative resistance to chemical attack as probably $\gamma_{(Ag-Hg)}$, $\gamma_{(Sn-Hg)}$ and the original Ag-Sn alloy. On the basis of this metallographic evidence and the very extensive X-ray data available at that time, Ryge, Fairhurst and Fischer (1961) concluded that the products of the setting reaction of dental

amalgam were $\gamma_{(Ag-Hg)}$, $\gamma_{(Sn-Hg)}$ and unreacted Ag_3Sn. The setting reaction, which was soon to be confirmed by optical and electron-optical metallographic observations by the phases present (see 1.5 below) could then be written

$$Ag_3Sn + Hg \rightarrow \gamma_{(Ag-Hg)} + \gamma_{(Sn-Hg)} + \text{unreacted } Ag_3Sn$$

i.e.
$$\gamma + Hg \rightarrow \gamma_1 + \gamma_2 + \gamma$$

where $\gamma_1 = Ag_2Hg_3$; $\gamma_2 = Sn_{7-8}Hg$; $\gamma = Ag_3Sn$

1.5 THE METALLOGRAPHY OF SILVER-TIN DENTAL AMALGAM

Although a number of early attempts had been made to determine the microstructure of dental amalgam, these proved largely unsuccessful. Ryge, Dickson, Smith and Schoonover (1952), for example, were able to identify particles of unreacted Ag_3Sn in a hardened amalgam using a nitric acid etchant but the matrix in which these particles existed appeared merely as a rather structureless background. As has already been pointed out, Schnuck (1958) and Schmitt (1960) showed the way to the development of metallographic etchants which enabled the microstructure of the matrix to be revealed. The major contribution, however, was that of Wing (1965) who developed a double etching technique in which the polished amalgam was etched first with KCN and iodine and then NH_4OH and potassium ferricyanide. With this technique Wing demonstrated the

existence of unreacted (i.e. Ag_3Sn) in a two phase matrix which he assumed to be γ_1 (i.e. Ag_2Hg_3) and γ_2(Sn_7Hg). These assumptions were shown to be valid in later studies by Wing (1966) in which the identity of the three phases was determined using electron probe microanalysis. A typical example of the microstructure of a dental amalgam prepared from a spherical particle amalgam alloy (manufactured by an atomization process) and etched using Wing's double etching technique, is shown in Figure 1.3.

Several other etching techniques for revealing γ_1 and γ_2 have been proposed. Alan, Asgar and Peyton (1965) for example, used a triple etch procedure involving $K_2Cr_2O_7$, iodine and $Na_2S_2O_3$ to reveal the three phases in amalgam which they identified using electron probe micro-analysis; Otani (1970c) suggested that exposing a polished surface of amalgam to mercury vapour was effective in showing the presence of γ_1 and γ_2. More recently Abbott and Makinson (1978) published an etching procedure using NaOH and iodine which can be used to reveal the micro-structures of dental amalgam prepared from more complex ternary and quaternary amalgam alloys such as the commercial alloys "INDILOY", which contains 5% indium, "SYBRALOY" (containing 40% Ag, 30% Sn and 30% Cu), "TYTIN" (containing 60% Ag, 25% Sn, 15% Cu), "SPHERIPHASE S" (containing spherical ternary alloy particles of approximate composition 60% Ag, 25% Sn, 15% Cu plus spherical Ag_3Sn), etc.

FIGURE 1.3 Spherical dental amalgam etched using Wing's (1965) double cyanide technique.

Note: $\gamma_1(Ag_2Hg_3)$, $\gamma_2(Sn_{7-8}Hg)$ and $\gamma(Ag_3Sn)$ - the spherical particles being only nominally single phase γ. X 26,000.

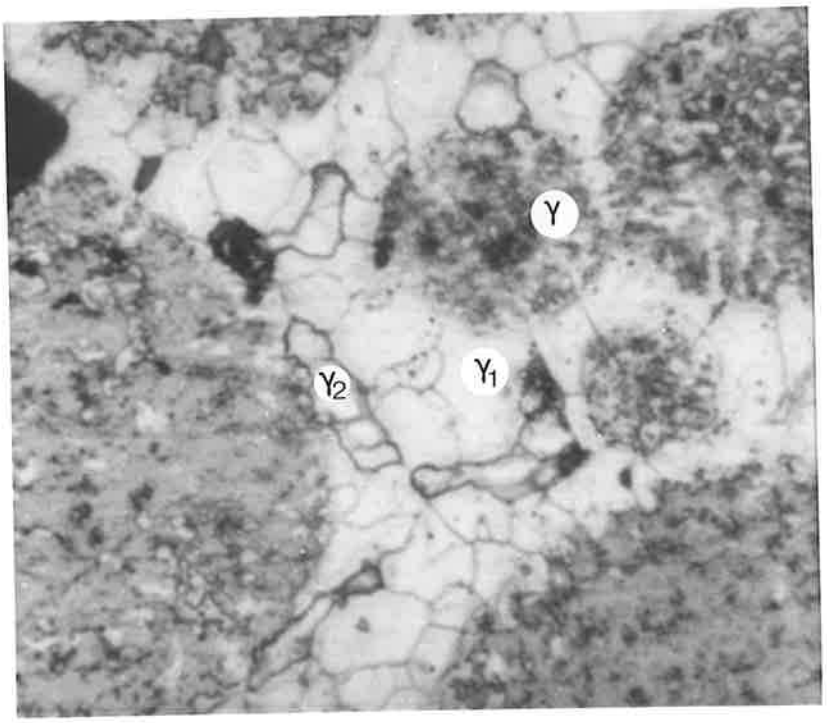
γ
γ1
γ2

The other important aspect of the observation of the microstructure of dental amalgam which was revealed by the modern metallographic techniques was that, in general, dental amalgam contained voids which were shown (Wing 1965, Taylor 1972, Reynolds, Warner and Wilsdorf 1975) to originate from inadequate condensation, lack of amalgamation during trituration or the long term absorption of small amounts of residual liquid mercury into the hardened amalgam.

These voids were shown by Asgar and Sutfin (1965) and Wing (1975) to have a detrimental effect on the mechanical properties of a restoration and as a consequence should be kept to a minimum by correct trituration, by the addition of small, carefully condensed increments of amalgam during the packing of the cavity and by the use of optimum mercury to alloy ratio in the original mixture.

CHAPTER 2

ALLOY PREPARATION AND METALLOGRAPHIC PROCEDURES

2.1 MANUFACTURE AND EXAMINATION OF SILVER-TIN ALLOYS

High purity silver and tin (composition given in Appendix 1) were degassed by vacuum melting. The appropriate quantities of silver and tin to formulate the required alloy composition were vacuum melted at 1000°C at a pressure of less than 2×10^{-4} torr in a continuously evacuated silica tube. The alloys were rapidly solidified by water quenching to ensure a fine initial grain size and were then sealed in silica capsules under a pressure of 0.5 atmosphere of argon before being subjected to an homogenizing heat treatment at 430°C for 72 hours. The loss in mass during melting and heat treatment was monitored at each stage of alloy preparation and provided that adequate care was exercised, was found to not exceed 0.003 g for a 20 g ingot. Alloys having a single phase γ structure were to be of major importance in the investigation and in order to obtain independent confirmation of the alloy composition the NATA registered Australian Mineral Development Laboratories carried out chemical analyses. The silver component was analysed by a thiocyanate titration while the tin component was analysed by an extremely sensitive titration method which involved the oxidation of stannous

to stannic ions. An alloy with a nominal composition of 73.5 wt. % Ag and 26.5 wt. % Sn was shown by the Amdel analysis to have an actual composition of 73.35 wt. % Ag and 26.55 wt. % Sn which indicates that the alloy preparation techniques employed enabled target alloy compositions to be satisfactorily attained.

Metallographic specimens were prepared by embedding the silver-tin alloys in cold setting resin and polishing with 600 and 1200 grades of silicon carbide paper followed by 6 and 1 μm diamond abrasives. For alloys containing less than 26.8 wt. % Sn, i.e. the ($\beta+\gamma$) and (γ) phases, some metallographic examination was carried out on materials prepared by electropolishing using an electrolyte of 90% ethanol and 10% perchloric acid at a temperature of -20°C. (Stainless steel electrodes, V = 5v, I = 20 mA, current density = 10^3 amp/m^2). Electropolishing was unsuitable for alloys containing (γ+Sn) and these were chemically polished with an aqueous solution of sodium hydroxide (5 wt. %) and iodine (20 wt. %).

Metallographic examination was carried out using light microscopy (Ultraphot II, Carl Zeiss), scanning electronmicroscopy (Siemens "Autoscan" with EDAX (Energy Dispersive Analysis of X-rays) analytical facility), and transmission electronmicroscopy (JEOL 120 CX with scanning attachment).

2.2 PREPARATION OF SPECIMENS FOR ELECTRONMICROSCOPY

The silver-tin alloys were spark machined to rods 3 mm in diameter which were then cut with a high speed slitting disc into slices 1.5 mm thick. These slices were reduced to 0.8 mm thickness by grinding on 1200 grade silicon carbide paper. To prepare specimens suitable for electronmicroscopy the 3 mm diameter slices were inserted into a Fischione jet polishing machine and electropolished in a solution comprising 90% ethanol and 10% perchloric acid under the following conditions, T = -70°C, I = 2 mA V = 21v, current density = 290 amp/m^2. Following perforation, the thin foils were removed from the polishing bath with the potential still applied and quickly washed in cold high purity ethanol and then dried in a warm air flow.

With a little experience foils which were likely to be transparent to electrons in the electronmicroscope could be identified by the distribution and intensity of light transmitted through the foil when examined using an optical microscope. Specimens which were inadequately thinned around the margins of a perforation were ion beam thinned ("Microlap", Ion Tech Ltd.) for 2-3 hours using the following conditions:- ion current 0.5 mA, voltage = 5 kV, angle of incidence of ion beam = 15°. A careful comparison in the electronmicroscope of specimens prepared with and without ion beam thinning failed to reveal evidence of ion induced damage to thin foils prepared using the above conditions.

2.3 METALLOGRAPHY OF Ag-Sn ALLOYS

It is immediately apparent from the Ag-Sn equilibrium diagram proposed by Murphy (Figure 1.1) that the range of composition over which a single phase γ structure is formed is very narrow. The more recent phase diagram prepared by Hansen (1958) on the basis of work published up to 1958, a very narrow range of composition is again indicated although the precise limits of stability of the γ phase appear not to have been accurately defined (it should be noted that Hansen departs from the more generally adopted nomenclature proposed by Murphy and uses ε to denote the phase which is normally designated γ). Since it was desirable in the present investigation to avoid ambiguities arising from the use of two phase alloys, it was necessary at the outset to determine more precisely the extent of the γ phase field.

A range of silver-tin alloys with compositions spanning the γ phase field as delineated in the phase diagram Figure 1.1 was therefore prepared for detailed metallographic and X-ray examination. The compositions of these alloys are listed in Table 2.1 along with their nominal structures derived on the basis of the previously published phase diagrams and the actual microstructures observed in the present investigation.

The results of this metallographic examination on carefully homogenized specimens can be summarized in terms of the three observed microstructures as follows:-

TABLE 2.1

Ag-Sn Alloy Compositions

Composition (wt. %)		Nominal Structure	Observed Microstructure
Ag	Sn		
85.0	15.0	β	β
76.1	23.9	β + γ	β + γ
74.4	25.6	β + [1]	β + [1]
74.0	26.0	γ	γ
73.8	26.2	γ	γ
73.5	26.5	γ	γ
73.4	26.6	γ	γ
73.3	26.7	γ	γ
73.2	26.8	γ	γ + Sn
73.0	27.0	γ + Sn	γ + Sn
72.5	27.5	γ + Sn	γ + Sn

(a) Two phase ($\beta+\gamma$)

Alloys containing 23.9 and 25.6 wt. % Sn were two phased and displayed regions in which alternate lamellae of β and γ phases could be clearly seen. A typical microstructure of the 23.9 wt. % Sn alloy is shown in Figure 2.1. In the 25.6 wt. % Sn alloy similar lamellae of β and γ were observed but as would be expected the proportion of β phase was substantially lower.

(b) Single phase (γ)

The five alloys with compositions lying in the range 26.0 to 26.7 wt. % Sn all displayed single phase γ microstructures. In Figure 2.2 an optical micrograph of the 26.5 wt. % Sn alloy is shown and this microstructure is typical of alloys in this composition range. During the examination of the alloys toward the upper end of this range special care was taken to detect the presence of any tin rich phase which may be present but even when examined by transmission electronmicroscopy (Figure 2.3), they appeared to be uniformly single phase.

(c) Two phase (γ+Sn)

The two alloys containing 26.8 and 27.0 wt. % Sn respectively had a duplex structure in which the second phase was present in a clearly delineated

FIGURE 2.1 Microstructure of the 23.9 wt. % Sn alloy showing grain boundaries of the γ phase with lamellae of β phase. Electropolished and etched surface.

X 900

FIGURE 2.2 Microstructure of the 26.5 wt. % Sn alloy showing single phase γ. Electropolished and etched surface.

X 900

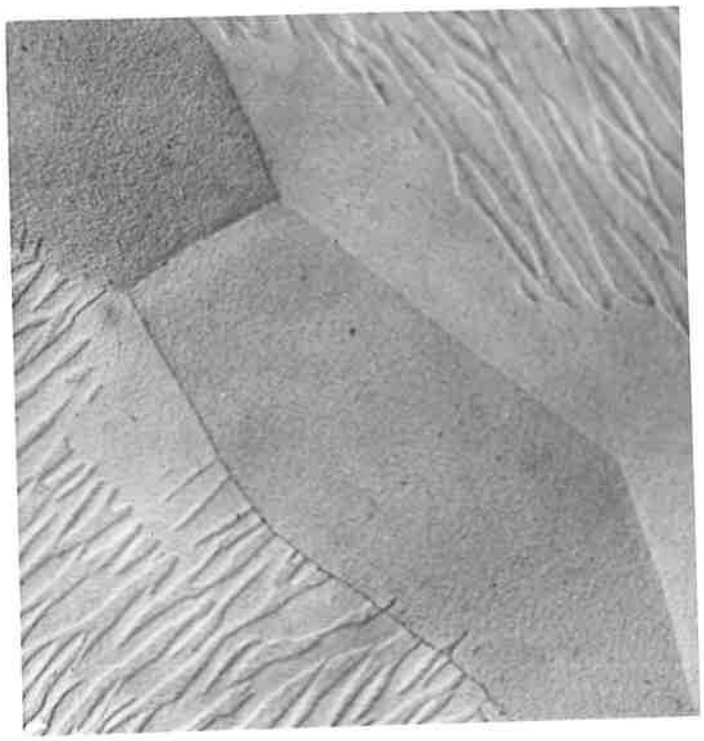

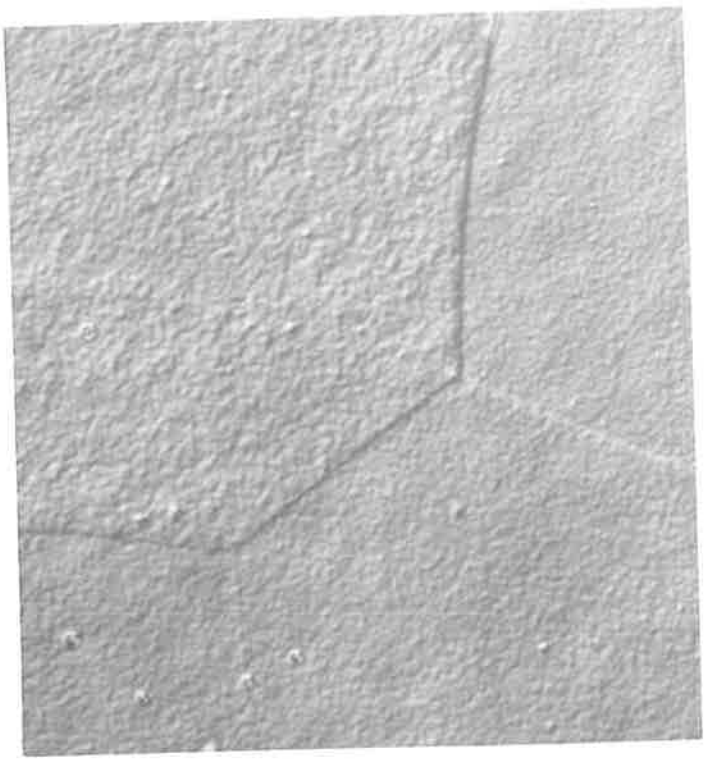

FIGURE 2.3 Transmission electron micrograph of the 26.5 wt. % Sn alloy showing a γ phase grain boundary.

X 64,000

zone around the grain boundaries of the first. An optical micrograph of this grain boundary structure obtained from the specimen containing 26.8 wt. % Sn is shown in Figure 2.4. It would be expected from the nature of the equilibrium diagram that if a second phase were present in an alloy of this composition it would probably be the terminal solid solution based on tin. Since the solid solubility of silver in tin at RT has been shown (Hanson et al., 1934) to be <0.02 wt. % the grain boundary phase would therefore be almost pure tin. Confirmation of this view was obtained by examining mechanically polished specimens in the scanning electronmicroscope where, with the assistance of the EDAX facility, an indication of the relative abundance of the two components (Ag and Sn) in each of the phases present in the alloy could be obtained. The results of this analysis is shown in Figure 2.5 (a), (b) and (c). In Figure 2.5 (a) the presence of the grain boundary phase can be seen in an image formed using back scattered electrons. The corresponding elemental X-ray map from this area using tin $L\alpha_1$ radiation (Figure 2.5 (b)) indicates qualitatively that the tin content of this grain boundary phase is higher than that of the adjacent γ phase while the silver $L\alpha_1$ map (Figure 2.5 (c)) shows that its silver content is lower than that of the γ phase.

FIGURE 2.4 Tin lying along γ grain boundaries of the 26.8 wt. % Sn alloy.

X 1200

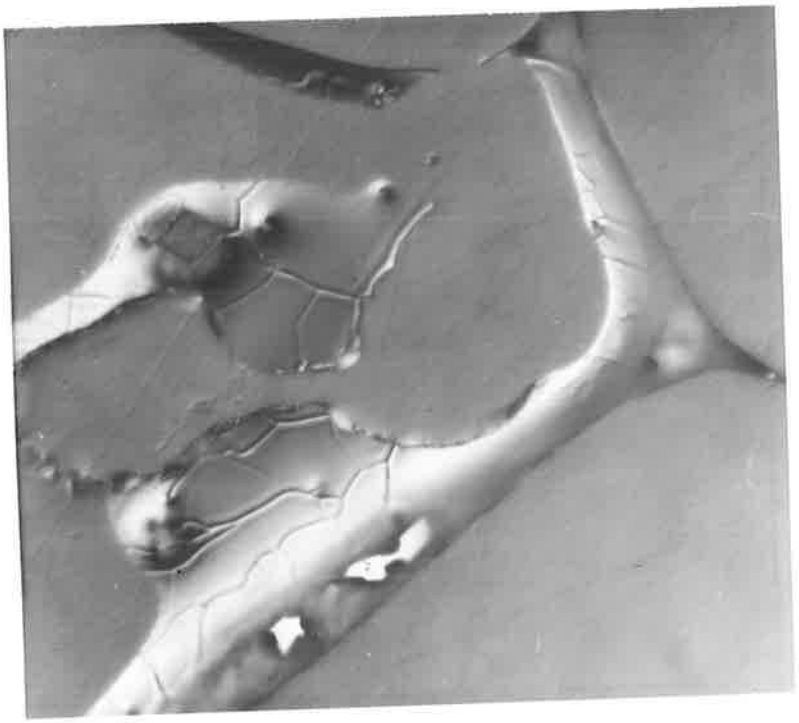

FIGURE 2.5 (a) Scanning electron micrograph of 26.8 wt. % Sn Alloy.

Note that the grain boundary phase is extensively pitted.

X 1000

FIGURE 2.5 (b) Elemental X-ray map using tin $L\alpha_1$ radiation.

FIGURE 2.5 (c) Elemental X-ray map using silver $L\alpha_1$ radiation.

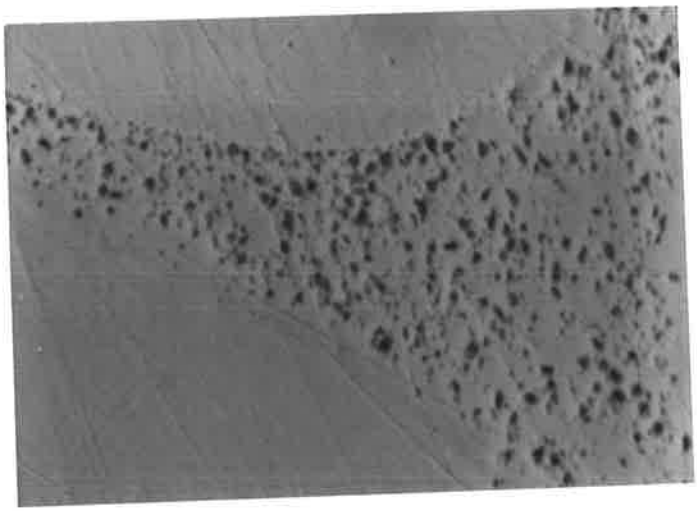

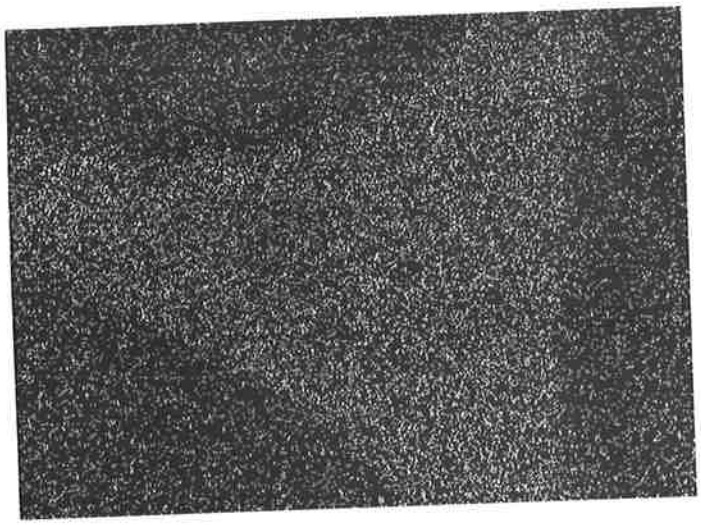

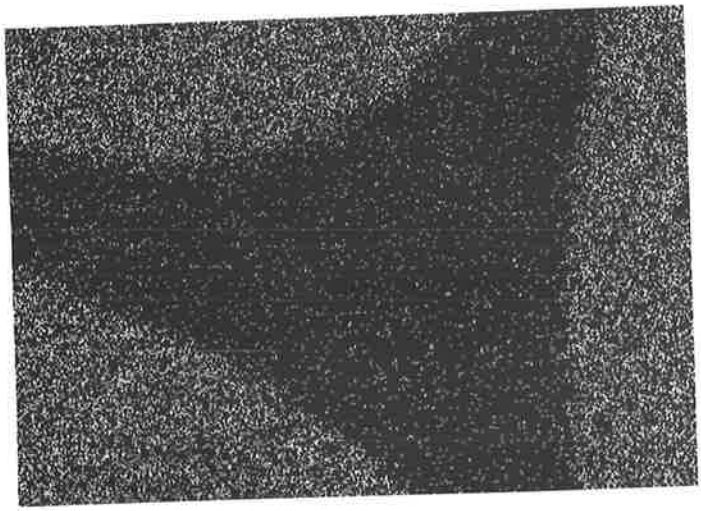

It will be noted in Figure 2.5 (a) that although care was exercised during the mechanical polishing of this specimen to the 1 μm diamond stage, the scanning electronmicroscope revealed that the tin rich phase along the grain boundaries was extensively pitted, suggesting that its resistance to abrasion was lower than that of the γ phase. If the polishing process using the 1 μm diamond abrasive is allowed to continue, substantial removal of the narrow zone of tin rich material may occur, particularly, when the diamond abrasive is carried on a pad such as "selvyt" which has a fairly long nap. When viewed in the optical microscope the grain boundaries of the specimen then appear to be unusually "broad". The association of this "broadening" of the grain boundaries with the removal of the tin rich grain boundary phase is illustrated in Figure 2.6.

A similar effect to that illustrated in Figure 2.6 can be observed on duplex alloys of (γ+Sn) structure after electropolishing or etching with a reagent (e.g. dilute HCl) which preferentially attacks the tin rich grain boundary phase.

X-ray diffraction examinations, using the Debye-Scherrer technique, were carried out on alloys selected from Table 2.1 to have structures which lay well within the β, β+γ, γ, and γ+Sn phase fields. While this proved useful in identifying the individual phases, and as will be described in Chapter 3 in obtaining important

FIGURE 2.6 Scanning electron micrograph showing a "broad" grain boundary produced by partial removal of tin rich material during metallographic polishing.

X 1000

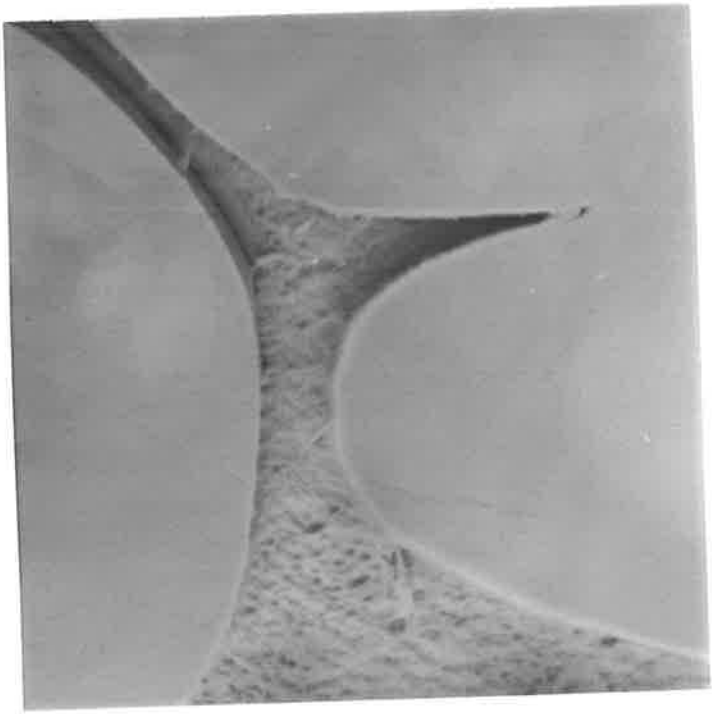

crystallographic information on the structure of the γ phase, the X-ray technique proved to be less sensitive than optical microscopy in establishing the location of the phase boundaries. For example, although the diffractometer trace for the 27.5 wt. % Sn alloy showed the presence of Sn as well as the γ phase, diffraction lines from tin were not able to be detected on the 26.8 wt. % Sn alloy even though as shown in Figure 2.4 a thin layer of the tin rich phase was present.

2.4 DISCUSSION

The present investigation has clearly established that the γ phase in the Ag-Sn system exists not as the single stoichiometric compound Ag_3Sn, the composition of which would be 73.15 % Ag, 26.85 wt. % Sn, but as a solid solution, the composition limits of which have been more precisely delineated than previously. On the silver rich side the limit of the γ phase field would appear now to be within the range 25.6 to 26.0 wt. % Sn, while on the tin rich side the upper limit of solubility of Sn in the γ phase is between 26.7 and 26.8 wt. % Sn. In this respect the present work is at variance with the early proposal of Petrenko (1907) whose phase diagram showed a phase of invariant composition corresponding to Ag_3Sn and also with Murphy's conclusion that the γ phase existed over a narrow range (not more than 0.9 wt. % Sn) of composition around 26.85 wt. % Sn. In the published

discussion of Murphy's paper on which the generally accepted phase diagram is based, the question of the extent of the γ phase field was raised by Dr. D. Hanson. Murphy reported that he had observed the 27 wt. % Sn alloy to be duplex while the 26 wt. % Sn alloy could be made "homogeneous", and that this led him to conclude (in a way which is by no means obvious!) that the range of solubility of tin in the γ phase was less than 0.9 wt. % Sn. Hume-Rothery in published correspondence on the paper, noted the "thick" grain boundaries in the micrographs of the polished and etched alloys containing 26.85 wt. % Sn which Murphy had observed as being homogeneous γ phase, and suggested that "the thick grain boundaries may quite well hide traces of a second constituent." This possibility was not, however, accepted by Murphy who ascribed the appearance of the grain boundaries to "fissures caused by partial disintegration of the brittle alloy." In the light of the present investigation it would seem that Hume-Rothery was correct for in the alloy containing 26.8 wt. % Sn the presence of a thin film of a second, tin-rich, phase around the grain boundaries of the γ phase was unequivocally established. This was not detected in alloys containing 26.7 wt. % Sn which were homogeneous γ phase, so it may be concluded that the upper limit of solid solubility of tin in the γ phase must lie between 26.7 and 26.8 wt. % Sn. The lower limit of solid solubility of tin in the γ phase has now been shown to lie between

25.6 and 26.0 wt. % Sn, so that the width of the γ phase field at room temperature is at least 0.7 wt. % Sn although it must be less than 1.2 wt. % Sn.

As mentioned in Section 2.3, X-ray diffraction was less sensitive than optical microscopy in establishing tin along the γ grain boundaries. Likewise, Johnson and Carwile (1978) observed tin in the microstructure of an alloy corresponding to stoichiometric Ag_3Sn but could not detect this film of tin by X-ray diffraction. It is interesting to note that it is clear that an alloy of composition corresponding to the stoichiometric compound Ag_3Sn, i.e. 25 at % Sn or 26.85 wt. % Sn lies outside the single phase γ field and within the (γ+Sn) two phase region of the phase diagram. For this reason the use of the formula Ag_3Sn to denote the γ phase of the silver tin system is a misnomer. More important however, is the fact that if the formula Ag_3Sn (i.e. 26.85 wt. % Sn) is used as the basis for formulating an alloy in the expectation that it will be of homogeneous γ phase structure, a two phase alloy will, in fact, result. As has been described above, the detection of a very thin film of the tin-rich grain boundary phase requires carefully controlled metallographic techniques, in the absence of which the second phase may be entirely overlooked. This is specially significant because the major interest in silver-tin alloys of these compositions arises from their use as dental amalgam alloys where a reaction

of the alloys with mercury takes place. In common with many alloy-liquid metal systems (Kamdar 1973, Nicholas and Old 1979, Old 1980) the grain boundaries constitute zones of high reactivity towards mercury so that the presence of a thin grain boundary film of a second phase would tend to assume disproportionate meaning particularly in a fundamental study of such a reaction. Several of the more recently published studies of the reaction between silver-tin alloys and mercury would now appear to have involved these duplex (γ+Sn) alloys rather than single phase γ alloys. For example, Ryge, Moffett and Barkow (1953) used an alloy of composition 26.85 wt. % Sn for a study of the formation and nature of the products of reaction of what they believed to be a homogeneous γ phase alloy with mercury. The published optical micrograph of this alloy, however, quite clearly shows the presence of "wide" grain boundaries. This micrograph was subsequently reproduced in one of the standard text books on dental amalgam (Skinner's Science of Dental Materials by R.W. Phillips 7th ed. 1973) where the misconception relating to the significance of "wide" grain boundaries has been further compounded (p. 307) by the implication that they are in some way indicative of an homogeneous structure. Wing and Ryge (1965) likewise used an alloy containing 26.85 wt. % Sn for a study of the reaction with mercury and once again, an examination of the published optical micrograph of the alloy reproduced here in Figure 2.7 showed the presence of "wide" grain boundaries. Wing and

FIGURE 2.7 Published photomicrograph from Wing and Ryge (1965).

Original caption: "Homogeneous structure with wide grain boundaries; annealed Ag_3Sn."

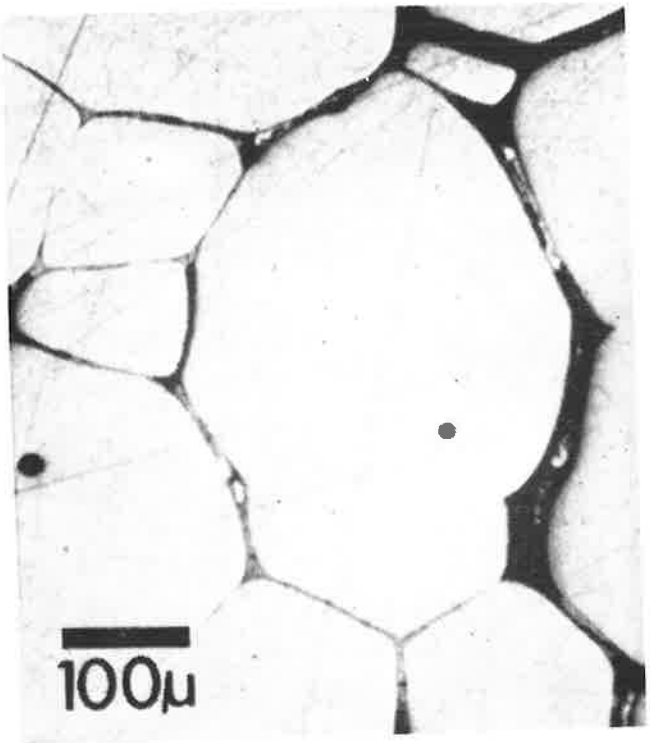
100μ

Ryge observed preferential grain boundary attack by mercury and put forward the suggestion that the explanation of this result may be that the "wide" grain boundaries of their alloy may contain a second phase of high tin content. Although no experimental evidence in support of this suggestion was presented by Wing and Ryge, it is clear from the present investigation that their interpretation was probably correct.

Wing and Ryge's investigation (1965) into the reaction with mercury covered silver-tin alloys with a wide range of composition and they showed that changes in microstructure were of great importance. This has practical implications for the manufacture of dental amalgam alloys. One of the recent developments in this field involves rapidly solidified alloys produced for example, by atomisation from the liquid state (e.g. "Sphericon", manufactured by Southern Dental Industries) and by the use of higher cooling rates produced by the process of "splat quenching". The precise nature of the microstructure developed by these rapid solidification techniques has not yet been satisfactorily determined and substantial departures from the equilibrium microstructures would be expected. The problems of predicting the microstructure of rapidly solidified peritectic alloys have recently been reviewed by Hillert (1979) and it appeared surprising that Wood and his co-workers (1976, 1978), and Johnson et al. (1974) claim to have generated

single phase alloys by these techniques. The conclusions of Wood et al. were reached mainly on the basis of X-ray diffraction studies which as mentioned in Section 2.3 above are comparatively insensitive. To throw further light on this matter a specimen of "splat quenched" alloy kindly supplied by Dr. J.V. Wood, University of Cambridge, was examined using the metallographic procedures described in Section 2.1. As can be seen in photomicrograph Figure 2.8 the alloy prepared by this technique contains at least three immediately discernible phases. A full analysis of this microstructure has not been undertaken as the interpretation is complicated by the fact that the alloy contains 4 wt. % Cu. It is clear however, that in spite of Wood's assertion to the contrary, this "splat quenched" material does not have a homogeneous single phase γ structure, and indeed the task of producing such a structure using the splat quenched technique would appear to be a formidable one.

FIGURE 2.8 "Splat quenched" alloy supplied by Dr. J.V. Wood, University of Cambridge. The alloy has at least 3 discernible phases.

X 700

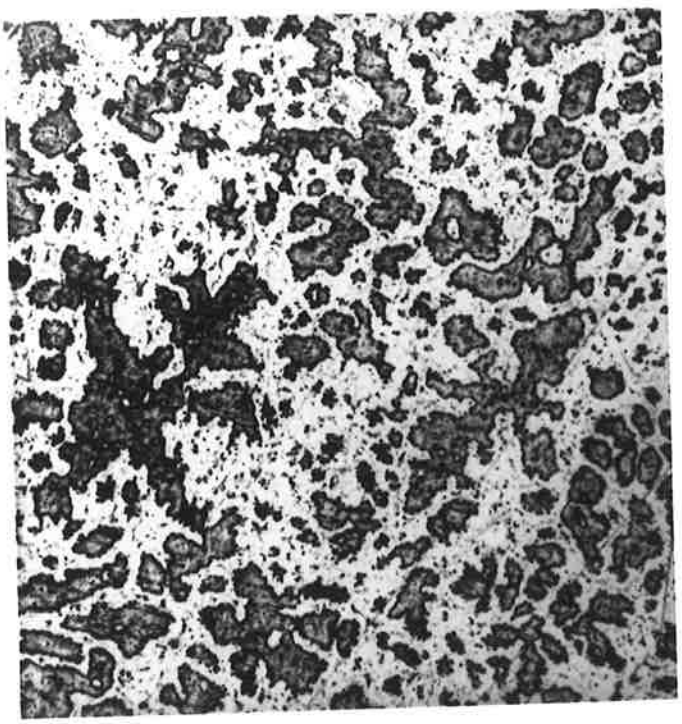

CHAPTER 3

CRYSTALLOGRAPHIC STUDY OF THE γ PHASE OF THE Ag-Sn SYSTEM

3.1 INTRODUCTION

As has been pointed out in the introductory chapter (Section 1.3) although it is now widely accepted that the crystal structure of the γ phase of the silver-tin system can be described in terms of an orthorhombic unit cell, two different orthorhombic cells have been proposed. On one hand, Nial et al. (1931) suggested a unit cell (Figure 3.1 a) with lattice constants a = 2.989 Å, b = 5.149, c = 4.771 whereas on the other, Fairhurst (1966) and Fairhurst and Cohen (1972) proposed a unit cell (Figure 3.1 b) which conformed to the orthorbombic Pmmn - D_{2h}^{13} No. 59 with lattice constants a = 5.968 Å, b = 4.780 and c = 5.184. It will be noted that apart from small differences in the unit cell dimensions (which presumably arise from differences in experimental technique, specimen preparation etc.) and the use of a different nomenclature by the two groups, so that the b and c dimensions of one cell must be interchanged to make them equivalent to the corresponding dimensions in the other, the essential difference between the two is that the Fairhurst unit cell has twice the a dimension of the Nial cell.

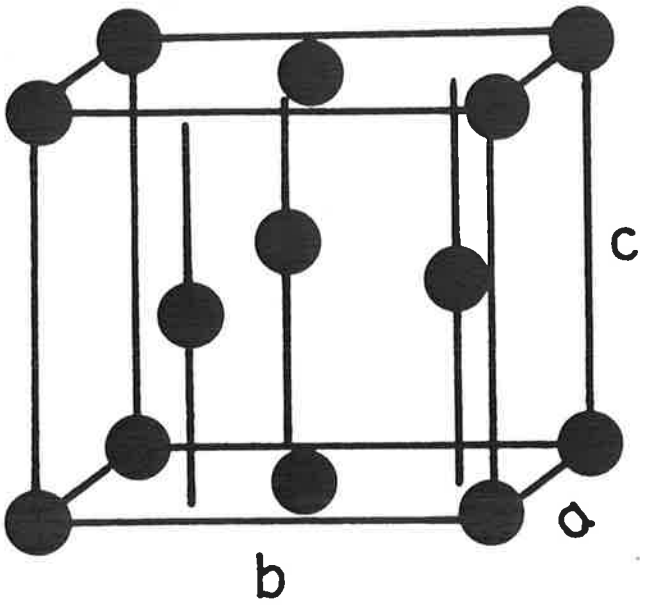

FIGURE 3.1 (a) The unit cell proposed by Nial et al. (1931).

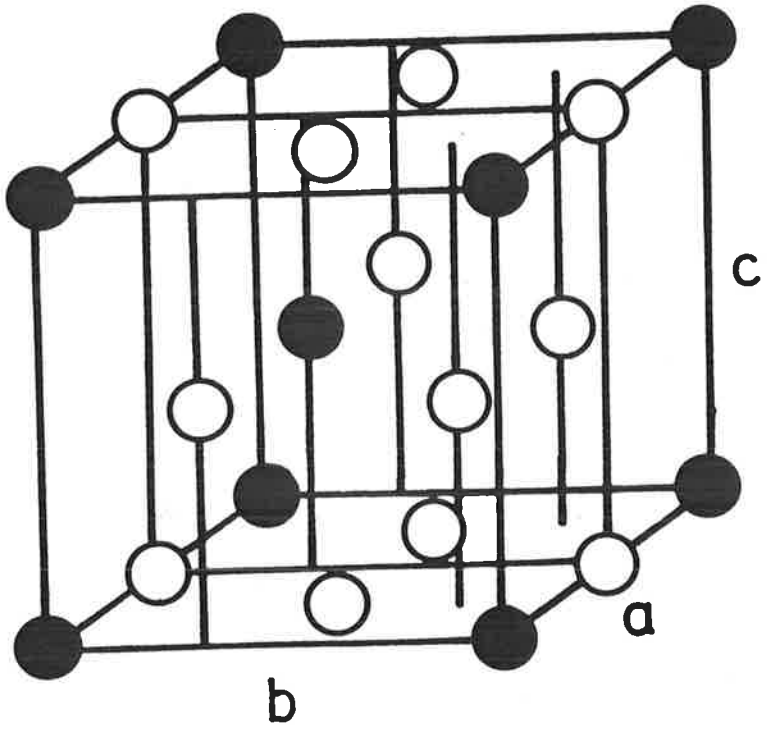

FIGURE 3.1 (b) The unit cell proposed by Fairhurst (1966). (Black atoms represent Sn, white atoms represent Ag.)

Fairhurst arrived at his unit cell after obtaining X-ray intensity data which could be interpreted only on the assumption that the material was ordered. By using extremely long exposure times (3-5 days) with single crystals and a precession camera, Fairhurst was able to observe a very weak X-ray reflection which on the basis of his unit cell was assigned 200 indices. The corresponding reflection was apparently not detected by Nial et al. on their Debye-Scherrer photographs. (This is perhaps understandable in view of Fairhurst's observation that the relative intensity of the 200 reflection and the strong 400 reflections was 483:11441). Fairhurst was able to account for this and several other weak reflections by assuming that the structure was ordered and that planes at $x = \frac{1}{4}$ and $x = \frac{3}{4}$ contained all silver atoms while the intermediate planes at $x = \frac{1}{2}$ contained half silver and half tin atoms. The difficulty in detecting the ordering was accentuated by the fact that the atomic scattering factors for X-rays for silver and tin are very close.

From an inspection of Figure 3.1 (b) it will be realised that if instead of being ordered, the material is disordered so that the probability of finding each of the sites occupied by one of the atom species is proportional to the atomic concentration of that atom in the alloy, then the $x = \frac{1}{2}$ plane in the Fairhurst model is exactly equivalent to the $x = 0$ and $x = 1$ planes and hence

no 200 reflection would occur. In this event it would then appear more logical to describe the structure in terms of the Nial unit cell to which the Fairhurst model would reduce. As has already been pointed out Fairhurst's experimental evidence, however, established the presence of a weak 200 reflection (or the equivalent 100 on Nial's model) which would be totally forbidden (zero intensity) on Nial's model.

In spite of the publication of Fairhurst and Cohen's evidence, support for the model of Nial et al. contained in the literature (Malhotra and Lawless 1975, Wood and Jacombs 1976, Wood and King 1978) has persisted so that further evidence relating to this dichotomy is clearly needed. Moreover, as will be seen from the nature of the research presented in Chapters 4 and 5 it was essential in the present investigation to resolve this controversy over the dimensions of the orthorhombic unit cell in order to calculate, with the assistance of accurate measurements of interplanar spacings, crystallographic data such as the intensities of X-ray and electron beams diffracted from the material, structure factor parameters, stereographic projections, angles between planes, angles between directions and other information required for the interpretation of metallographic observations.

3.2 X-RAY DIFFRACTION TECHNIQUES AND ANALYSIS

Precision measurements of the interplanar spacings of selected alloys were obtained using X-ray diffraction techniques. (Siemens Kristalloflex 4 with Type F diffractometer). Powder of 325 mesh size (∿50 μm) was sealed in silica capsules and annealed under a pressure of 0.5 atmosphere of argon at 300°C for 15 hours. Prior to the X-ray analysis a Au standard was used to align the diffractometer in the forward and reverse modes and for internal calibration silicon powder was mixed with the powder of the alloy under examination. A diffractometer scan speed of 1/10°/minute was used with Fe filtered Co radiation at 30 kv, 14 mA with an aperture diaphragm of ½° and a detector aperture of 0.1 mm.

To assist with the determination of the lattice parameters and unit cell dimensions the generalised computer program developed by Appleman et al. (1972) was found to be useful. This program which can be applied to all crystal systems provides successive least square approximations of observed and theoretical values of 2θ for each of the diffraction maxima. The output yields a tabulation of the indices of the diffracting planes, their observed and theoretical interplanar spacings and the unit cell dimensions of the crystal under examination.

For the theoretical calculation of the intensities of each of the diffraction maxima the standard computer

program "LAZY PULVERIX" prepared by Yvon et al. (1977) was employed. With the aid of this program and the sub-routine of Böhm et al. (1975) which is incorporated into it, tables of theoretical values of normalized X-ray intensity, (along with other diffraction data such as structure factor parameters, multiplicity, Lorentz-Polarization parameters etc.) can be produced. The atoms within the unit cell may be specified both by type (i.e. in terms of atomic scattering factor) and position. The program also has the facility of presenting the intensity data in a graphical form similar to that of a diffractometer trace. This proved convenient when making comparisons between theoretical and experimental diffraction data.

3.3 CRYSTALLOGRAPHY OF THE γ PHASE

3.3.1 X-ray line intensity calculations

Confirmation of the conclusion referred to in Section 3.1 that if the material is considered to be disordered the Fairhurst and Nial unit cells are equivalent, was obtained from the fact that calculations of the X-ray line intensity made on the basis of each of the two models gave identical results. Calculations were also carried out to compare the X-ray line intensities from ordered and disordered crystals using Fairhurst and Cohen's unit cell and the ordered structure which they proposed (1972). The results of these calculations are shown in Table 3.1 where differences in

TABLE 3.1

X-ray line intensities for ordered and disordered crystals using Fairhurst and Cohen's unit cell

Disordered			Ordered	
d	hkl	I	hkl	I
5.968	100	0.0		
5.184	001	0.0	001	0.5*
4.780	010	0.0		
3.914	101	0.0	101	0.3*
3.731	110	0.0	110	0.5*
3.514	011	0.0	011	1.2*
3.028	111	0.0	111	0.4*
2.984	200	0.0	200	0.1*
2.592	002	118.3	002	119.8
2.586	201	234.6	201	236.8
2.531	210	0.0		
2.390	020	372.1	020	375.1
2.378	102	0.0	102	0.3*
2.279	012	482.7	012	484.3
2.775	211	960.9	211	968.4
2.219	120	0.0		
2.171	021	0.0	021	0.1*
2.129	112	0.0	112	0.0
2.039	121	0.0	121	0.1*
1.989	300	0.0		
1.957	202	0.0	202	0.9*
1.866	220	0.0	220	0.1*
1.857	301	0.0	301	0.1*
1.837	310	0.0	310	0.1*
1.811	212	0.0	212	0.1*
1.757	022	69.9	022	70.3
1.755	221	139.0	221	138.8
1.731	311	0.0	311	0.1*

theoretical line intensity for the ordered and disordered states are indicated with an asterisk. Although this table reveals that over the range of d values some 15 "critical" lines could be expected to be present in the ordered state, (and could therefore provide ready evidence of ordering), a close examination indicates that each of these lines have extremely low intensities (<1.2). For example, it will be seen in Table 3.1 that one of these "critical" lines is the 200 which has an intensity of 0.1. By comparison, the intensity of the "noncritical" lines, e.g. 211, 020 etc. are several orders of magnitude higher (e.g. 968, 375 respectively). This table highlights the problem of detecting evidence of ordering in the material by X-ray diffraction - a problem which Fairhurst and Cohen met by using very long exposures with their precession camera.

X-ray facilities of the kind used by Fairhurst and Cohen were not available for the present investigation so an alternative approach involving the use of electron diffraction rather than X-ray diffraction was adopted. This had the benefit of enhancing the differences in scattering efficiency of Ag and Sn atoms. Of greater importance, however, was the fact that a thin foil of material could be manipulated in the goniometer stage of an electronmicroscope into such an orientation that low intensity electron diffraction spots corresponding to the critical reflections could be expected if the material

were ordered whereas if the material were disordered, these "critical" reflections would again be forbidden and the "critical" diffraction spots would not be recorded on the electron diffraction pattern.

3.3.2 Electron diffraction observations

A table of kinematic electron structure factors for the Fairhurst ordered and disordered structures was kindly prepared by Mr. D.J. Netherway (1979) on the basis of the electron scattering factors of Doyle and Turner (1968). A portion of this table is shown in Table 3.2 where it can again be seen that the reflections indexed with an asterisk constitute "critical" reflections in the sense that they will be present (albeit weak) if the structure is ordered but will have zero intensity if the structure is disordered. The possibility then arises of being able to establish whether or not the material is ordered on the basis of the presence or absence of one of these "critical" reflections in a single crystal electron diffraction pattern. In so doing care must of course be taken to eliminate the possibility that extra ("forbidden") reflections didnot arise from other sources such as double diffraction, which are not related to the presence or absence of ordering. From an understanding of the above factors and the diffraction process in the orthorhombic γ phase, the [001] orientation was selected as being an appropriate one for an experiment to establish the presence or absence of a critical reflection and hence

TABLE 3.2

Kinematic electron structure factors for the Fairhurst ordered and disordered structures

Disordered			Ordered	
d	hkl	$\|F\|^2$	hkl	$\|F\|^2$
5.968	100	0.000	100	0.000
5.184	001	2.369	001	0.108
4.780	010	0.000	010	0.000
3.914	101	0.035	101	5.098*
3.731	110	0.000	110	6.899*
3.514	011	0.571	011	8.034*
3.023	111	0.089	111	1.468*
2.984	200	0.000	200	3.367*
2.592	002	750.438	002	752.022
2.586	201	743.071	201	742.312
2.531	210	0.000	210	0.000
2.390	020	2682.785	020	2682.785
2.378	102	0.099	102	1.583*
2.279	012	1873.426	012	1872.459
2.275	211	1877.495	211	1878.025
2.219	120	0.000	120	0.000
2.171	021	0.949	021	0.279
2.129	112	0.205	112	0.001
2.039	121	0.016	121	0.273
1.989	300	0.000	300	0.000
1.957	202	3.211	202	4.447
1.866	220	0.000	220	0.329
1.857	301	0.013	301	0.144
1.837	310	0.000	310	0.301
1.811	212	0.961	212	0.269
1.757	022	416.959	022	417.376
1.755	221	413.335	221	413.135
1.731	311	0.039	311	0.179

to provide independent evidence as to whether or not the γ phase is ordered in the manner proposed by Fairhurst and Cohen.

The electron diffraction pattern from a single crystal in a thin foil with an orientation [001] would, if the ordered unit cell of Fairhurst is considered, be expected to provide an electron diffraction pattern of the following kind:

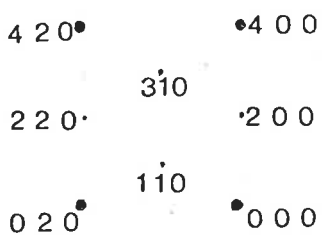

Foil orientation [001]
Ordered structure

If, on the other hand, the material was disordered then the reflections of the kind 110, 200, 220 will, as shown in Table 3.2 be forbidden (zero intensity). The electron diffraction pattern for an [001] zone would be as follows:

Foil orientation [001]
Disordered structure

The experimental electron diffraction pattern, illustrated in Figure 3.2 is clearly of the former kind, i.e. the superlattice reflections 110, 200 etc., characteristic of the ordered structure can be clearly seen. An examination of this diffraction pattern reveals that the weak reflections indexed as 110, 200 etc. cannot be

FIGURE 3.2 Electron diffraction pattern of the [001] zone containing low intensity superlattice reflections.

(See text for indexing.)

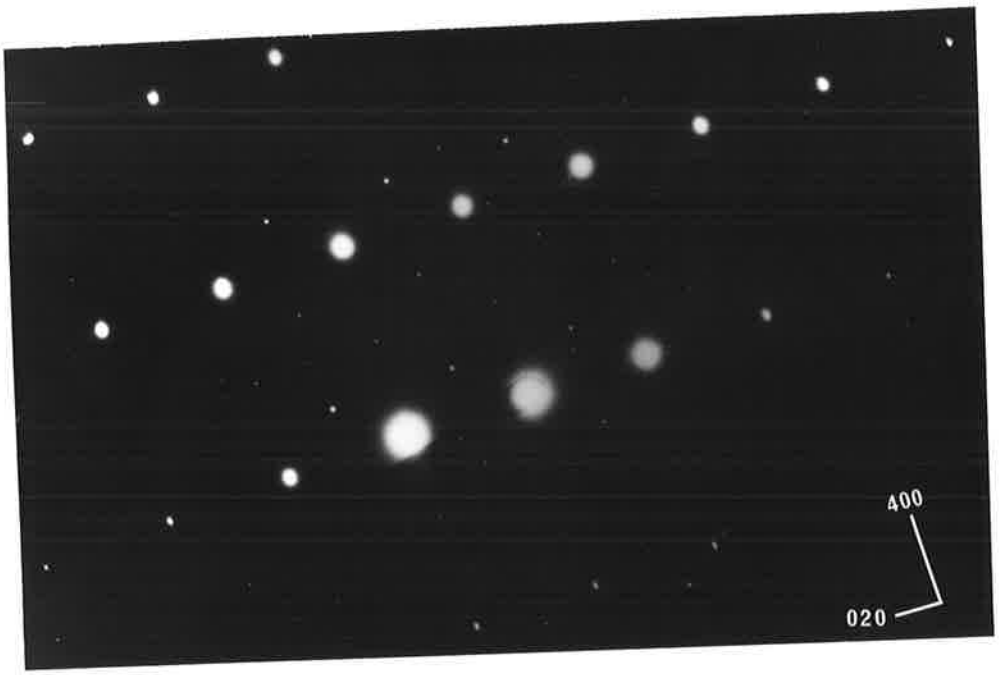
400
020

accounted for by double diffraction. It should be pointed out in passing that the electron diffraction pattern which has been indexed according to a unit cell based on the disordered Fairhurst model, may as discussed in Section 3.1 be indexed according to the Nial unit cell. In this event the 400 spot, for example, would be indexed 200 etc. However, the general argument relating to the significance of the additional reflections shown in Figure 3.2 still applies.

The conclusion derived from studies of this kind is that the electron diffraction patterns can be fully interpreted on the basis of an ordered structure with a unit cell as specified by Fairhurst and Cohen. The results are not consistent with the material having a disordered structure (i.e. a unit cell which can be shown to reduce to the Nial model).

3.3.3 Determination of interplanar spacings for the γ phase

To provide data for the interpretation of electron diffraction and electron channelling patterns to be discussed in Chapters 4 and 5, interplanar spacings for the γ phase were required. Having obtained independent evidence in support of the work of Fairhurst and Cohen, X-ray diffraction data obtained from diffractometer traces was interpreted on the basis of the Fairhurst and Cohen (1972) structure. The conditions for diffraction were:

$h00 : h = 2n$ $\quad$ $hk0 : h + k = 2n$ $\quad$ $0k0 : k = 2n$

These conditions are consistent with Pmmn - D_{2h}^{13} (No. 59) (International Tables for X-ray Crystallography, Volume 1). Table 3.3 lists the hkl's associated with the experimentally observed d values. The refinement of these experimental values produced orthorhombic lattice constants of a = 5.967 Å, b = 4.781 and c = 5.183.

The results tabulated in Table 3.3 were obtained using a silver-tin alloy containing 26.5 wt. % Sn and as discussed in Chapter 2 represents a composition towards the midpoint of the range of stability of the γ phase. This alloy composition was used for the studies to be reported in Chapters 4 and 5 where it was desirable to ensure that the material was of an homogeneous γ phase structure, i.e. that neither β phase or tin were present in the alloy. The variation in lattice parameters across the narrow range of stability of the γ phase has not been investigated.

3.4 DISCUSSION

The controversy surrounding the determination of the crystal structure and lattice parameters of the γ phase appears to have lingered on for well over half a century. From the earliest work by Preston (1926) to the latest by Wood and King (1979) there appears to be doubt as to its true nature. The question of ordering in the lattice was considered as early as 1926 when Hume-Rothery suggested to Preston that the γ phase could not have a

TABLE 3.3

Experimental d spacings for 26.5 w% % Sn γ phase.

h k l	d_{exp}
002	2.589
201	2.587
020	2.388
012	2.277
400	1.491
014	1.251
412	1.248
040	1.195
024	1.139
034	1.005
440	0.933

Lattice Parameters a = 5.967 Å
b = 4.781
c = 5.183

simple hexagonal unit cell as this crystal structure would require the γ phase to be disordered, as with only two atoms per unit cell the stoichiometry could not be satisfied. Indeed, Hume-Rothery proposed that the unit cell could be formed by ordering within each layer so that an hexagonal super lattice is formed with 8 atoms per unit cell (Figure 3.3). Fairhurst (1966) considered a structure which was essentially equivalent to that proposed by Hume-Rothery although Fairhurst described it in terms of an orthorhombic unit cell. However, Fairhurst noted that the unit cell would be double in the c direction, a result he could not account for from his experimental work. Because of this 'incompatability' with the experimental observations the model was discarded. Further evidence against the Hume-Rothery model was obtained in the present investigation by carrying out X-ray line intensity calculations for this model using the procedures of Section 3.3.1. The results are shown in Table 3.4. On the basis of the model seven reflections of moderate intensity should be observed with a d spacing > 2.592 A°. No such reflections are observed experimentally.

The relatively short X-ray exposure times employed with the Debye-Scherrer technique does not allow the detection of weak superlattice reflections, the detection of which are essential to enable the ordered and disordered structures to be differentiated. This clearly provides an

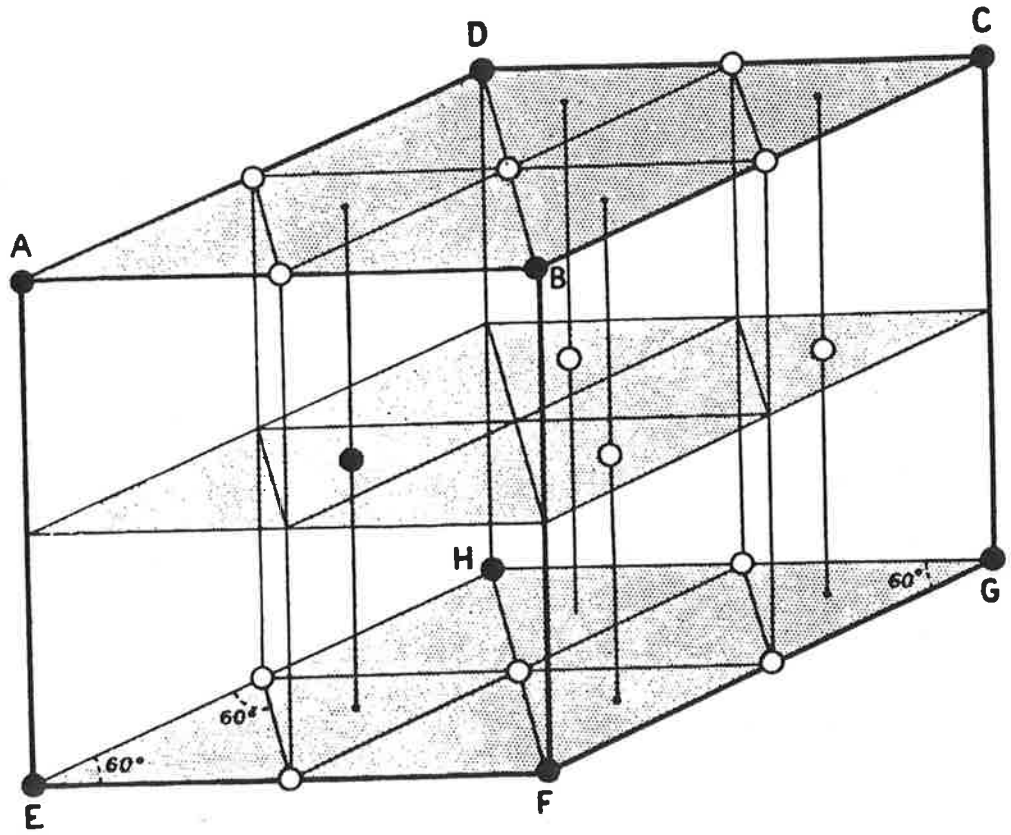

FIGURE 3.3 The hexagonal super lattice proposed by Hume-Rothery (1926).

TABLE 3.4

Theoretical intensity calculations for Hume-Rothery's Multiple Hexagonal unit cell.

d	hkl	I	F_{hkl}
4.781	010	53	92
4.342	011	85	91
3.731	110	58	89
3.514	012	43	83
3.511	111	86	80
3.028	112	67	85
2.801	013	27	84
2.592	004	161	314
2.586	202	320	314
2.535	113	41	81
2.531	210	20	81
2.459	211	37	81
2.391	020	507	613
2.278	014	500	457
2.274	212	995	455
2.129	114	24	77
2.042	213	21	76
1.902	015	9	74
1.836	310	8	73
1.812	115	12	67

explanation of the fact that Wood and Jacombs (1976) and Wood and King (1978) were led to the false conclusion that their Debye-Scherrer X-ray results provided evidence in support of a disordered structure with lattice parameters close to those of Nial et al. These difficulties are however, put to one side by the use of electron diffraction techniques. The weak superlattice reflections observed as electron diffraction patterns from single crystals of the γ phase alloy in the [001] orientation can be accounted for only on the basis of an ordered orthorhombic structure. This evidence therefore constitutes unequivocal and independent confirmation of the structure proposed earlier by Fairhurst and Cohen.

CHAPTER 4

THE REACTION OF γ PHASE Ag-Sn ALLOY WITH MERCURY

4.1 INTRODUCTION

The nature of the products of the reaction between a Ag-Sn alloy containing a substantial amount of γ phase and mercury was established by Wing (1966) from studies using optical metallography and electron probe micro-analysis of amalgams prepared from commercial spherical particle alloys. A typical microstructure of an amalgam prepared using Wing's techniques was shown in Figure 1.3 where the silver rich product phase Ag_2Hg_3 designated γ_1 and the tin rich produce phase $Sn_{7-8}Hg$ designated γ_2 were identified on the basis of Wing's analysis. What is not clear from Wing's study of the reaction however, is the mechanism by which the reaction of mercury with the γ phase Ag-Sn alloy actually proceeds. The significance of gaining an understanding of the mechanism of the reaction as well as the nature of the reaction products arises from the opportunity which such information may provide to control or modify the reaction in such a way that the properties of the dental amalgam are optimised.

As background to a more fundamental study involving the use of laboratory prepared alloys, some preliminary experiments were undertaken using a commercial spherical

particle dental amalgam alloy and standard clinical procedures for preparing dental amalgam. In Section 4.2 below these observations will be reported and some evidence suggesting a crystallographic dependence of mercury attack will be shown. As can be seen in Figure 1.3 this commercial spherical particle alloy had a microstructure which was far removed from single γ phase. The interpretation of the reaction of this complex alloy with mercury would therefore be difficult.

To overcome these difficulties, filings of a laboratory alloy of exactly γ phase structure (26.5 wt. % Sn) were produced and amalgams were prepared from this, again using standard clinical techniques. The results obtained with laboratory prepared material are reported in Section 4.3. A crystallographically dependent mercury attack was then apparent and to throw further light on this, experiments involving the reaction of mercury initially with bars of polycrystalline γ phase material and then with single crystals were carried out. These are reported in Sections 4.3 and 4.5.

4.2 STUDIES INVOLVING A COMMERICAL SPHERICAL PARTICLE ALLOY

The material used for the preparation of the amalgam, the microstructure of which was shown in Figure 1.3, was "Sphericon" (Southern Dental Industries) and the manufacturer's recommendations for the clinical

preparation of dental amalgam from this alloy were adopted (alloy: Hg ratio 10:9.0, trituration time 8 seconds using the "Ultramat" high energy mechanical amalgamator, condensation pressure 7MPa).

It was established by experiment that two hours after the condensation had been completed the amalgam was sufficiently hard to enable a satisfactory metallographic finish to be obtained by mechanical polishing. Immediately following such treatment the surface of the material was essentially flat and when examined in the SEM displayed only a series of fine scratches originating from the 1 μm abrasive, used as the final polishing medium. At this stage, however, the alloy reaction was by no means complete for after a further 30 minutes the surface contained evidence of the development of additional reaction products which, as shown in Figure 4.1 (a), appear to have well defined crystallographic morphology. An EDAX analysis of these reaction products indicated that they were essentially Ag-Hg crystals and were presumably the γ_1 phase (Ag_2Hg_3). The γ_2 reaction product ($Sn_{7-8}Hg$) was not detected on the surface of the specimen until much longer times had elapsed. In Figure 4.1 (b) for example, a long plate-like extrusion of high tin content (presumably γ_2) can be seen to have emerged from the area shown in Figure 4.1 (a) 19 hours after Figure 4.1 (a) had been taken.

FIGURE 4.1 (a) Metallographically polished amalgam 2½ hours after condensation. Silver-mercury crystals are visible on the surface.

X 2000

FIGURE 4.1 (b) Same area as 4.1 (a) but 21½ hours after condensation. A plate-like extrusion of tin-mercury has emerged from the surface.

X 2000

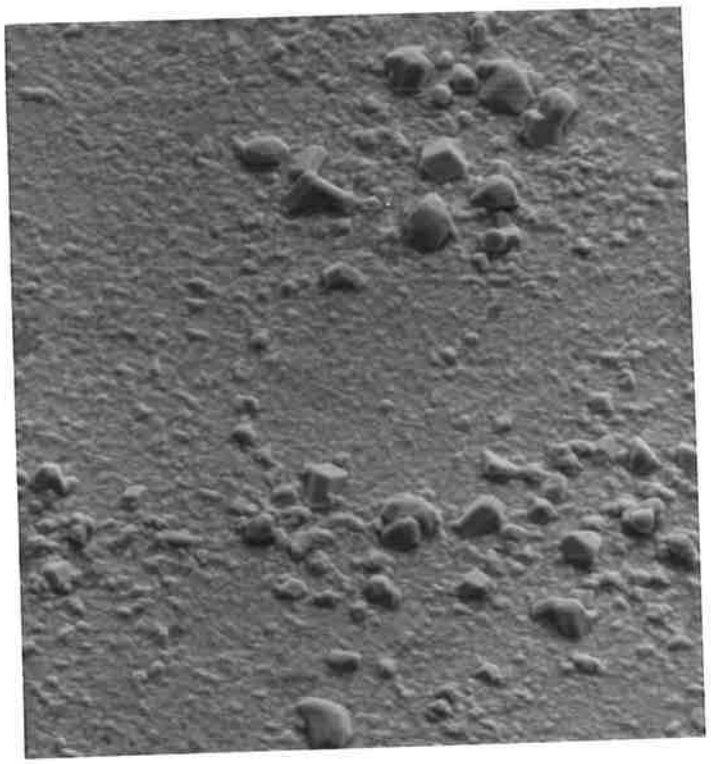

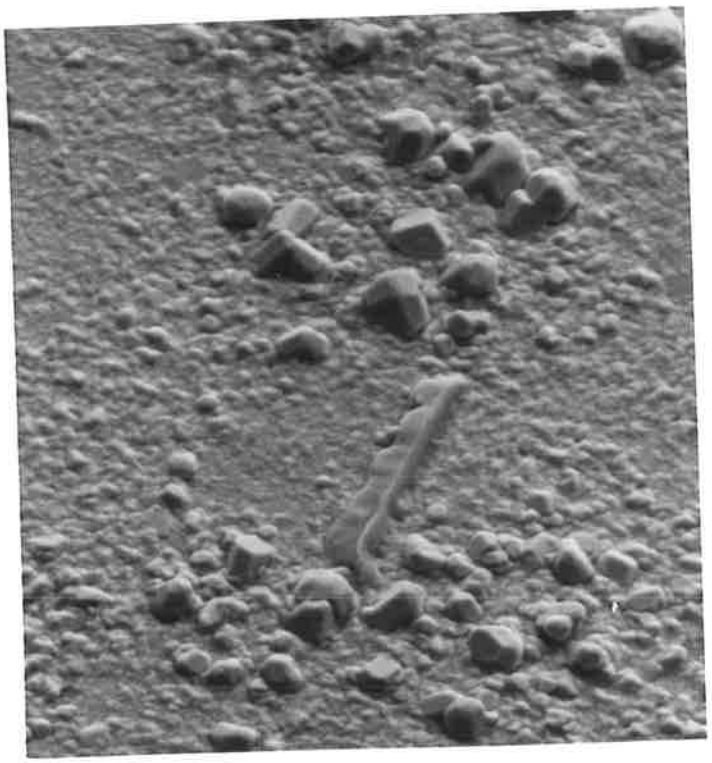

The interpretation of Figures 4.1 (a) and 4.1 (b) is open to the criticism that the metallographic polishing procedures may have resulted in the smearing of unreacted mercury across the surface of the specimen so that further reaction may have initiated from this surface layer. However, after heavily etching to reveal the structure beneath the surface, plates of γ_2 similar to those observed on the surface (e.g. at A in Figure 4.2) were detected particularly around the circumference of the spherical particles.

Another difficulty in interpreting observations made on commercial alloys arises from the fact that, in general, they contain other alloying elements, e.g. copper, which introduce additional phases into the microstructure. Moreover, because of the way in which the alloys are prepared, substantial departures from equilibrium microstructures would be expected. These non-equilibrium effects can be minimized by subjecting the spherical particles to an homogenizing anneal (e.g. 72 hours at 430°C) before reacting them with mercury. One of the consequences of this additional annealing treatment was to increase the γ grain size in spherical particles and this in turn enabled evidence of grain boundary reaction to be detected as well as revealing evidence which suggested that preferential attack by mercury may occur along well defined crystal planes in the γ phase (Figure 4.3).

FIGURE 4.2 "Sphericon" amalgam showing a spherical particle containing plates of γ_2 and crystals of γ_1.

X 2000

FIGURE 4.3 "Sphericon" amalgam containing homogenised alloy particles which show evidence of mercury attack along grain boundaries as well as along crystal planes.

X 3750

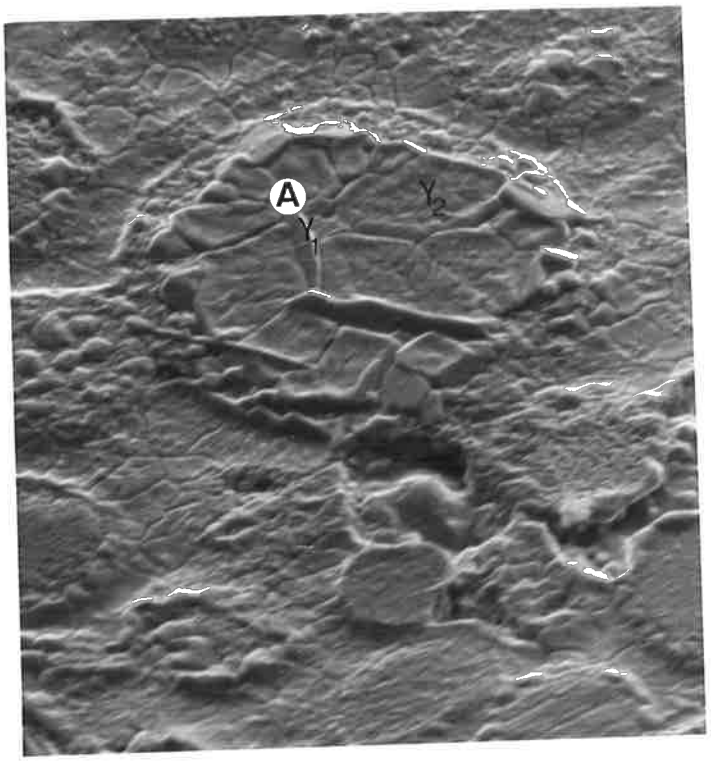
A
Y_1
Y_2

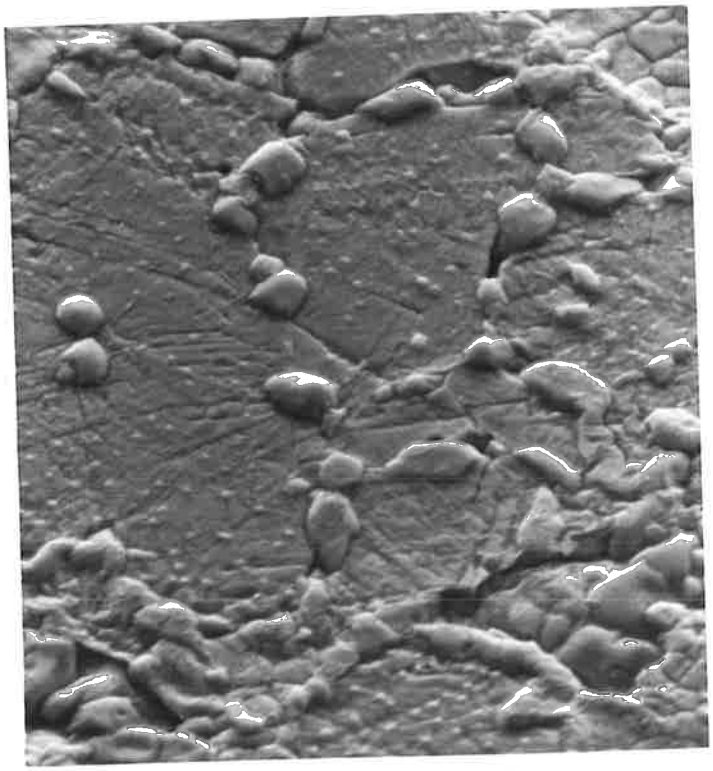

4.3 STUDIES INVOLVING SINGLE PHASE γ ALLOY

The possibility that the reaction between mercury and the γ phase may occur preferentially along some crystal planes in the γ phase was of particular interest. The interpretation of observations made on commercial alloys was complicated by the fact that the alloys did not possess a homogeneous single phase γ structure and to overcome these difficulties a laboratory prepared alloy with a composition designed to yield a homogeneous structure was used to prepare lathe cut filings. As shown in Figure 4.4 striking evidence (e.g. at A) of a crystallographic preference for mercury attack on the γ phase material was found. In order to eliminate uncertainties arising from the trituration, mechanical polishing and metallographic etching procedures, a more fundamental approach was adopted which involved studies of mercury attack on freshly fractured surfaces of tensile specimens of a polycrystalline γ phase alloy.

The material was extremely brittle and displayed characteristic intercrystalline and cleavage fracture. As shown in Figure 4.5, prior to application of mercury numerous deformation markings were observed on the newly exposed fracture surfaces, the nature of which will be discussed below. The application of a small quantity of mercury to these surfaces resulted in the immediate wetting by the mercury so that most of the surface detail of individual crystals was masked by a liquid film

FIGURE 4.4 An amalgam prepared from a lathe cut single γ phase alloy. The γ phase labelled A demonstrates mercury attack along well defined crystallographic planes.

X 1600

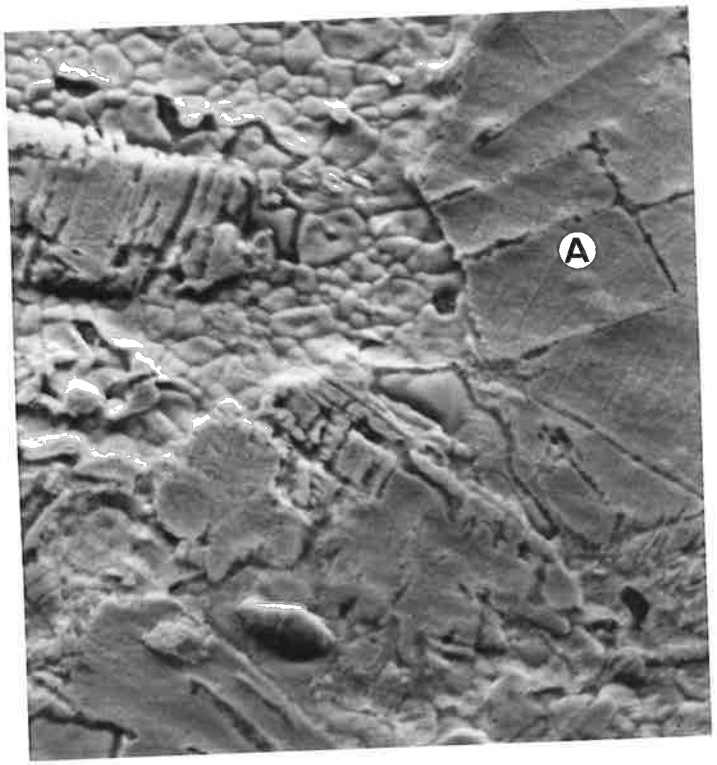
A

FIGURE 4.5 Deformation markings visible on the surface of tensile fractured polycrystalline γ phase.

X 4000

FIGURE 4.6 Masking of the γ crystalline surface by mercury.

X 1600

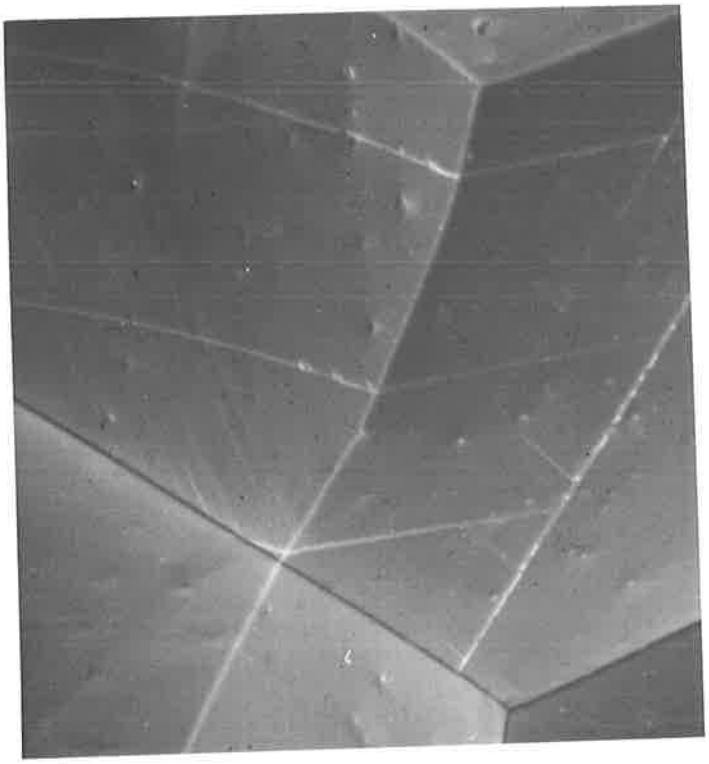

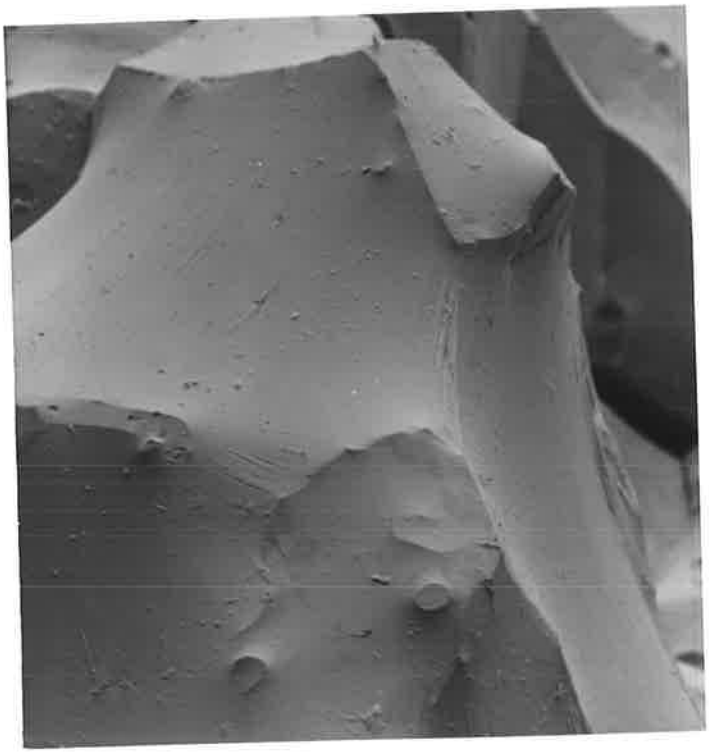

(Figure 4.6). However, after the elapse of a period between one and two hours, the reaction between mercury and the γ phase proceeded to the stage at which the mercury film was no longer visible. It was quite apparent that the reaction had produced a dramatic change in the surface features of the γ crystals. Notably there was a change from the crystalline surface of Figure 4.5 to a surface which was no longer smooth but instead displayed evidence of reaction along crystal planes together with crack development within γ crystals. For example, in Figures 4.7 and 4.8, the γ surface demonstrates attack along well defined crystal planes with greatest penetration of mercury at the intersection of these planes. Another feature of this attack as shown in Figure 4.9, were cracks within γ crystals, which appear to have developed from the initial penetration of mercury along crystal planes. The dissolution of silver and tin atoms from the crystallographic reaction meant of course, that reaction products must be produced. In fact, Figures 4.8 and 4.9 show reaction products lying on reacted γ crystal surfaces. An EDAX analysis of the crystal of well defined morphology (labelled A) in Figure 4.8 revealed the presence of silver and mercury in the reaction product, suggesting this to be the silver-mercury phase (usually designated γ_1) of the silver-tin-mercury system. In other areas, long plate-like crystals of the tin-mercury phase (usually designated γ_2) were also observed.

FIGURE 4.7 The γ surface demonstrating preferential attack by mercury along crystal planes. Note enhanced reaction at the intersection of crystal planes.

X 2750

FIGURE 4.8 The crystal labelled A consists of silver-mercury while the γ surface B contains evidence of preferential attack along crystal planes.

X 1600

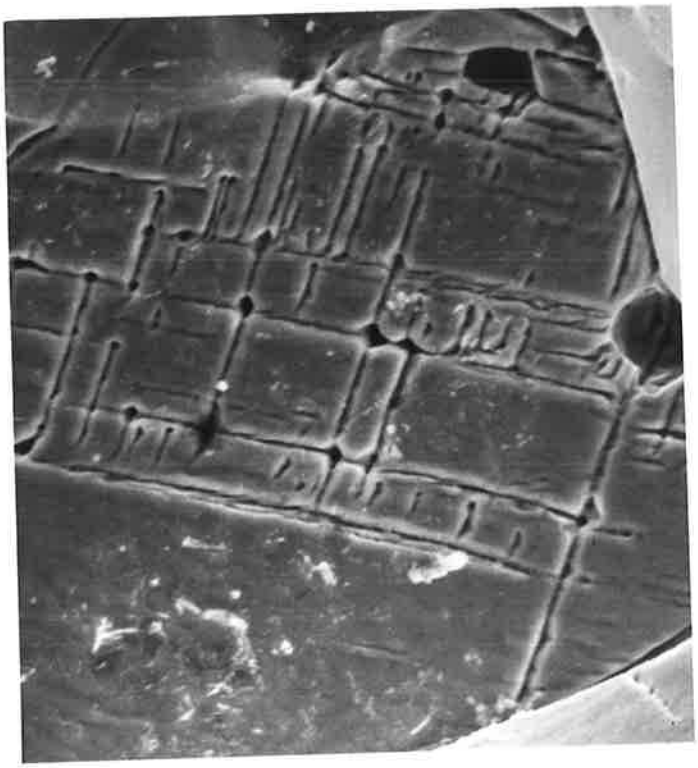

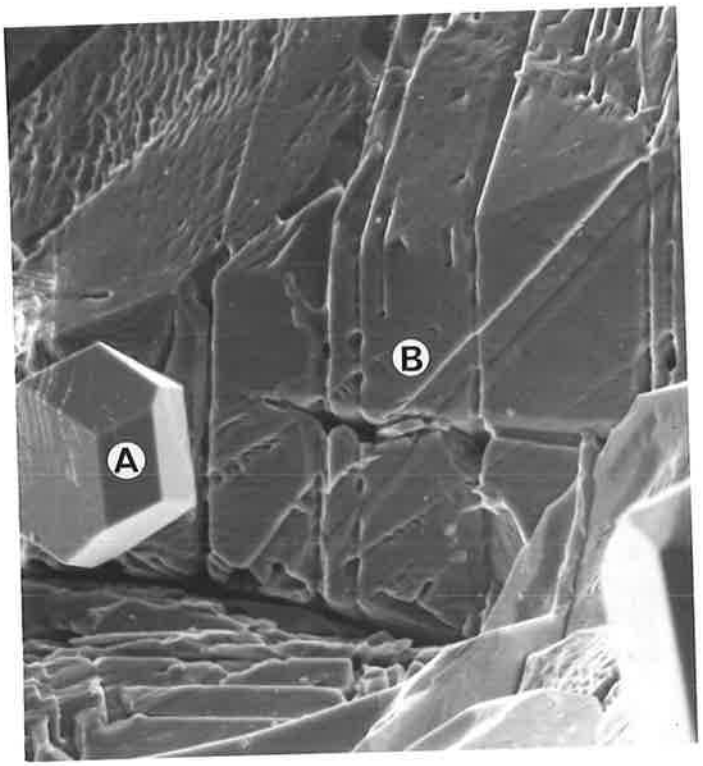
A
B

FIGURE 4.9 Mercury attack on the γ phase showing cracks within the γ crystal and the formation of reaction product (A).

X 4800

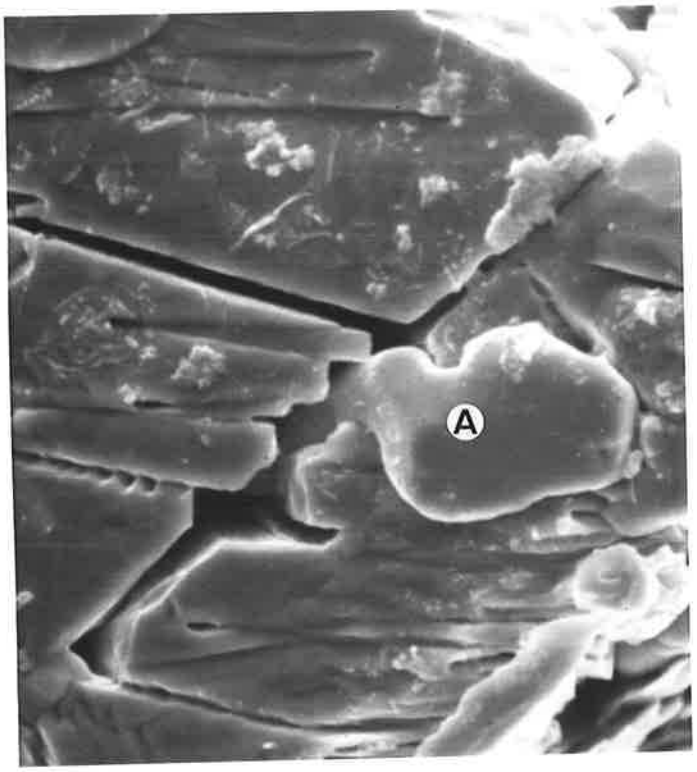
A

To obtain precise information on the nature of the markings such as those shown in Figure 4.7, experiments involving mercury attack on single crystals of γ phase of known orientation were undertaken. The single crystals required for these studies were able to be extracted from the fracture surfaces of polycrystalline specimens with the aid of a dissecting microscope, a scalpel and a pair of fine tweezers. These single crystals had dimensions which were typically of the order 0.4 - 0.6 millimetres so that determination of their crystallographic orientation could not conveniently be carried out using X-ray diffraction techniques. On the other hand, the thickness of the crystals was, in general, too great to enable transmission electronmicroscopy to be used. However, the comparatively recent technique of Electron Channelling (Hren, Goldstein and Joy 1979, Grundy and Jones 1976) was ideally suited to the determination of the orientation of single crystals of these dimensions. The JEOL 120CX electron microscope was equipped with a scanning facility which was able to be operated in a mode which enabled electron channelling patterns to be generated. A brief account of this technique is presented below.

4.4 ELECTRON CHANNELLING

Kikuchi patterns are formed in the transmission mode by inelastic scattering of electrons to produce an

angular distribution of electrons which are incident on crystal planes at angles which satisfy the Bragg criteria. These electrons then undergo diffraction to produce the familiar Kikuchi lines. In the case of Electron Channelling on the other hand, use is made of the variation of the intensity of inelastically scattered electrons with angular deviation from the Bragg condition. Here, a range of incident angles is produced by rocking the incident beam through a known solid angle while the microscope is in the scanning mode. The intensity of back scattered secondary electrons produced during the inelastic collisions of the incident electrons is detected. This is related to the inelastic scattering intensity which in turn is dependent on angular deviation from the exact Bragg condition. Hence a crystallographically dependent distribution of electrons is produced in which an array of linear discontinuities corresponding to the exact fulfilment of the Bragg diffraction conditions of the incident electron beam is generated. The image formed by the backscattered electron detector contains an array of crystallographically dependent lines which make up the Electron Channelling Pattern (E.C.P.). The symmetry of the arrays of lines on these E.C.P.'s is, like that of Kikuchi patterns, determined by the conditions of diffraction in the crystal and can, in a similar way, be used to determine the crystallographic orientation of the crystal.

In the context of the present research the fundamental advantage of Electron Channelling is that this crystallographic information can be obtained from the surface of a comparatively massive specimen of the kind required for metallographic observations. A typical E.C.P. from a single crystal of the γ phase and illustrating the [001] zone axis is shown in Figure 4.10.

4.5 CRYSTALLOGRAPHIC ANALYSIS OF SINGLE CRYSTAL DEFORMATION MARKINGS

An S.E.M. micrograph of a crystal of homogeneous γ phase which was subjected to investigation in this manner is shown in Figure 4.11 (a), and a sketch of the crystal on which specific features are identified in Figure 4.11 (b). The crystallographic orientation of the crystal is also indicated in Figure 4.11 (b). This polyhedral crystal was selected for crystallographic analysis because the adjacent faces of the crystal were reasonably planar and were traversed by deformation markings which could be followed from one crystal face to the next so that trace analyses were made relatively easy. The procedure adopted to determine the orientation of this crystal was as follows:-

1. The crystal, mounted on a high angle goniometer stage, was oriented with Face A normal to the incident beam. An Electron Channelling Pattern and corresponding S.E.M. photomicrograph were

FIGURE 4.10 An electron channelling pattern from the γ phase of the [001] zone axis.

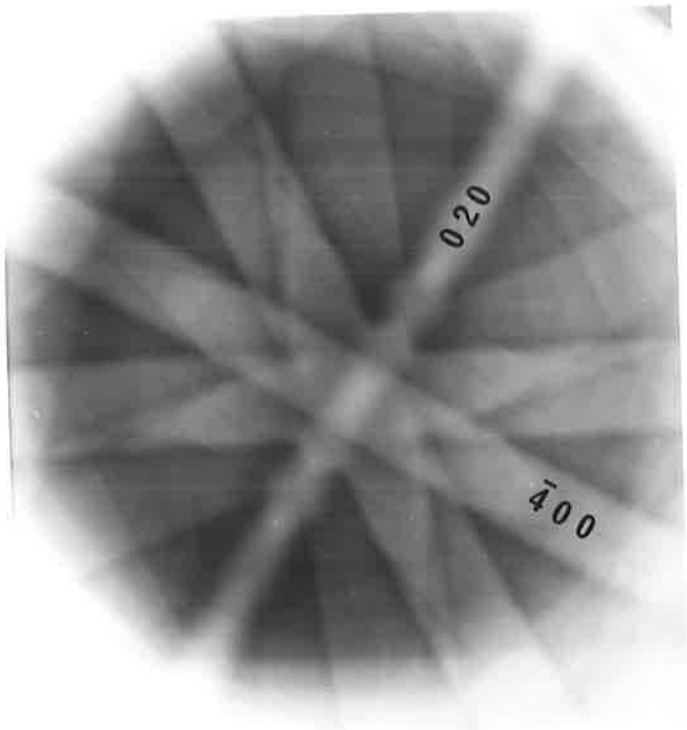
020
$\bar{4}00$

FIGURE 4.11 (a) A crystal of γ phase displaying deformation markings.

X 200

FIGURE 4.11 (b) Interpretation of Figure 4.11 (a).

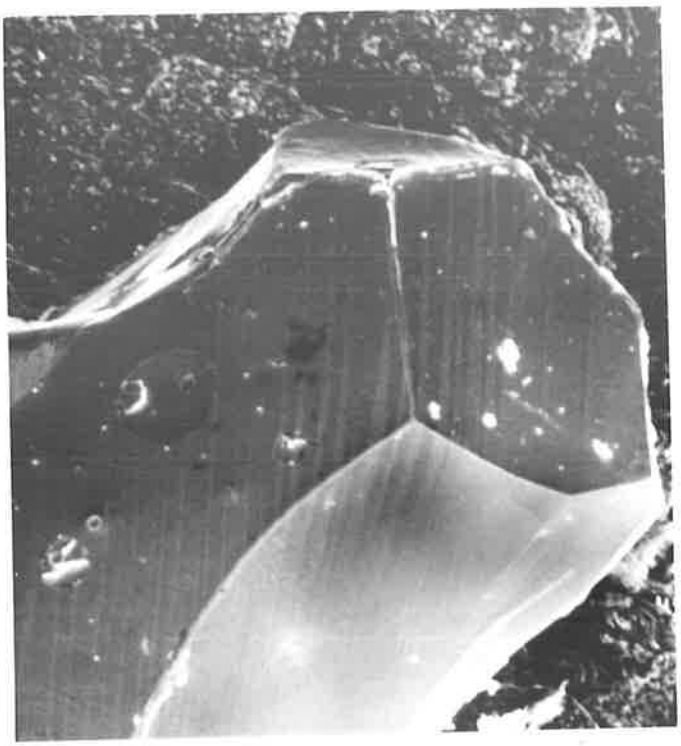

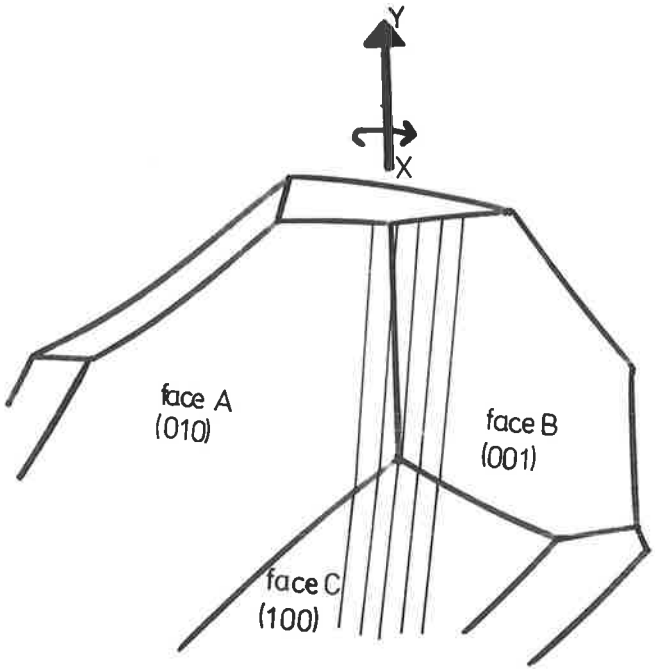
Y
X
face A
(010)
face B
(001)
face C
(100)

taken to enable the E.C.P. to be correctly oriented relative to the crystal surface.

2. The crystal was then rotated about an axis corresponding to the direction X-Y in Figure 4.11 (b) until Face B was normal to the incident beam and the orientation of Face B was obtained from an E.C.P. as described above.

3. The orientation of Face C was determined by using the double tilt stage and tilting the crystal face until it was normal to the incident beam.

4. The direction of the three principle crystallographic axes in the crystal were obtained from an analysis of this information. For the specimen shown in Figure 4.11 (a) the crystal faces A, B and C although not exactly planar, were very close to the low index planes (010), (001) and (100) respectively. Measurements made in the microscope using the calibrated goniometer and tilt rotation stages confirmed that the angles between the faces were close to 90° as would be expected.

The goniometer stage proved useful in providing confirmatory evidence for the validity of the crystallographic analyses. For example, during the rotation from Face A to Face B about the axis XY (which corresponded approximately to the direction [001]), a succession of poles was observed on the E.C.P.'s. The progress of the

tilting operation was also followed by reference to the corresponding map of the most intense diffracting planes (see Appendix 2). An example of an intermediate E.C.P. is shown in Figure 4.12. Here, at a tilt of 45° from Face A, the electron beam was incident in the [01$\bar{1}$] direction. This orientation is of particular relevance because as can be seen in Figure 4.11 the traces of the deformation markings in faces A, B and C all lay approximately parallel to the axis of rotation XY. As can be seen from the standard projection of Face A (Figure 4.13), these features lay parallel to the (01$\bar{1}$), suggesting that the deformation markings under examination lay on the (01$\bar{1}$) plane. Further confirmation of this interpretation was obtained from a determination of the orientation of Face C and the direction in which the traces of the features lay on this surface.

4.6 SINGLE CRYSTALS AND THEIR REACTION WITH MERCURY

The objective of this investigation was to react mercury with a single crystal of known orientation, so that a precise determination of the preferentially attacked crystal planes could be made. The crystal described in Section 4.5 was exposed to mercury and following the reaction it was observed that not only had attack occurred along the previously determined (01$\bar{1}$) planes, but had also proceeded along additional sets of markings (Figure 4.14). These deformation markings are

FIGURE 4.12 Electron channelling pattern of the $[01\bar{1}]$ zone axis.

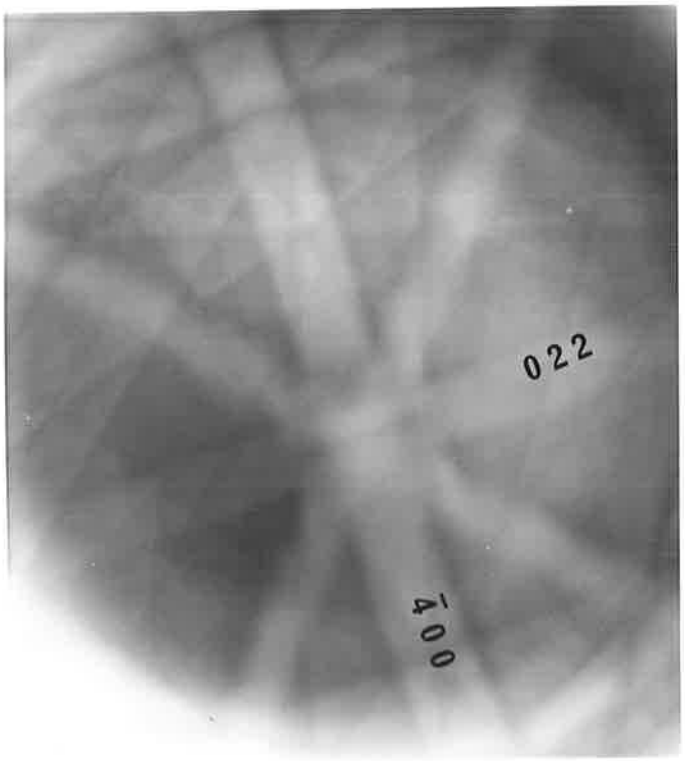
022
400

FIGURE 4.13 The (010) standard projection.

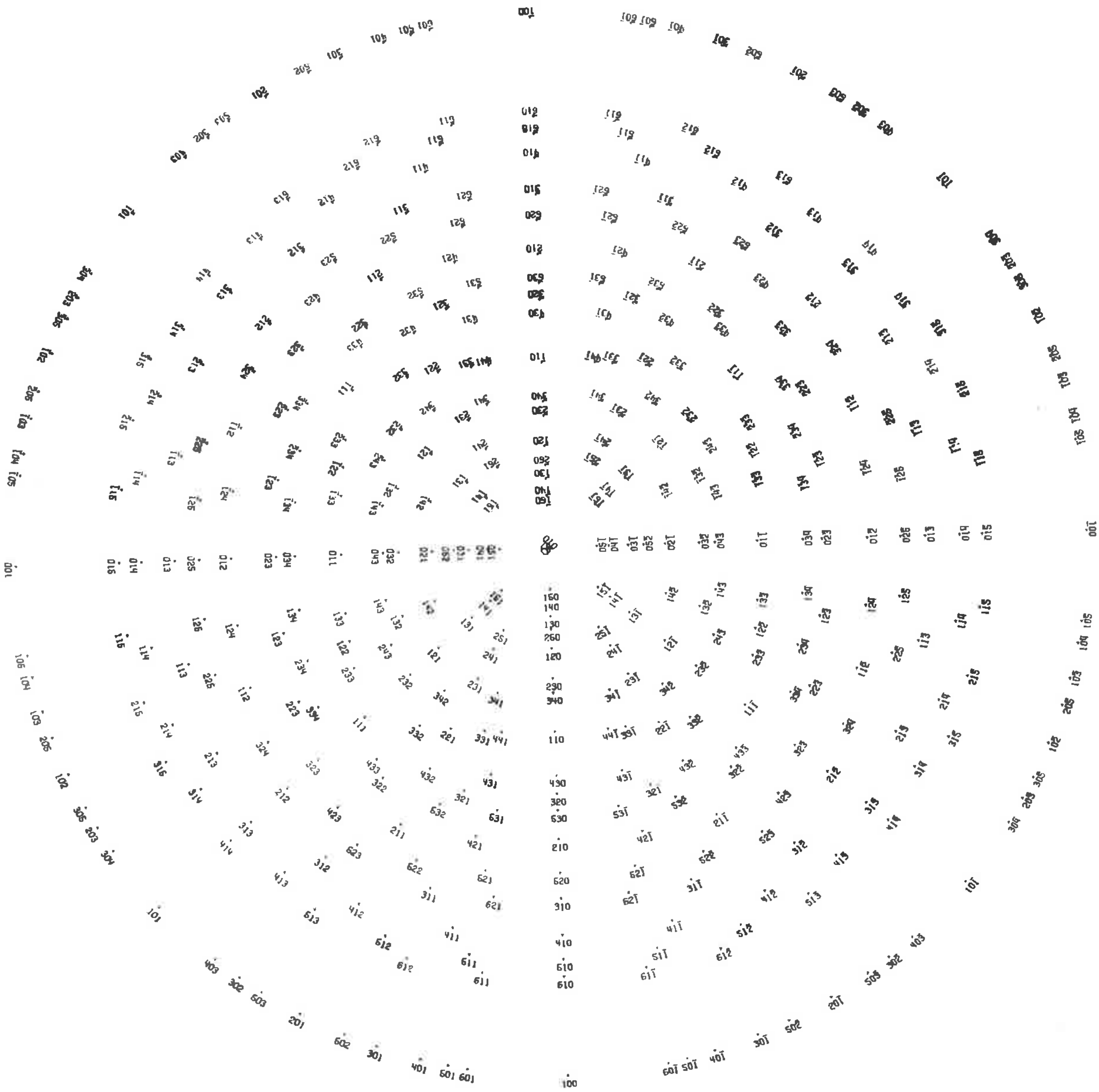

FIGURE 4.14 The [100] crystal face displaying markings lying along (011), (01$\bar{1}$) and (010) planes.

X 2000

from Face C of the crystal and intersect at approximately 90° the $(01\bar{1})$ markings. The crystallographic information derived earlier together with a stereographic analysis on the [100] surface revealed that the intersecting plane was (011). Markings at 45° to (011) and $(01\bar{1})$ can be seen in Figure 4.14 and these were analysed as lying parallel to the (010) plane.

The intersection of (011) and $(01\bar{1})$ deformation markings constitutes a highly reactive region where a vigorous reaction with mercury is initiated. This is illustrated in Figures 4.15 (a) and (b) where at the intersection of the (011) and $(01\bar{1})$ there has been a deep penetrating reaction resulting in deep planar intrusions of notches within γ crystals. Moreover, as shown in Figure 4.15 (b) substantial reaction has also occurred along the boundary between the deformation markings and the matrix. The significance of this mode of attack as a liquid metal embrittlement pathway will be discussed in Chapter 6.

The nucleation of crystalline reaction products is observed to initiate within the mercury film covering the γ crystal. Studies of the nucleation and growth of the reaction products and of the rate of reaction were made difficult by the fact that the temperature of the specimen was not able to be precisely determined. This is because the proximity of the anticontamination plates to the specimen stage results in the specimen being significantly

FIGURE 4.15 (a)

X 2000

Preferential mercury attack occurring at the intersection of (011) and (01$\bar{1}$) planes.

FIGURE 4.15 (b)

X 4000

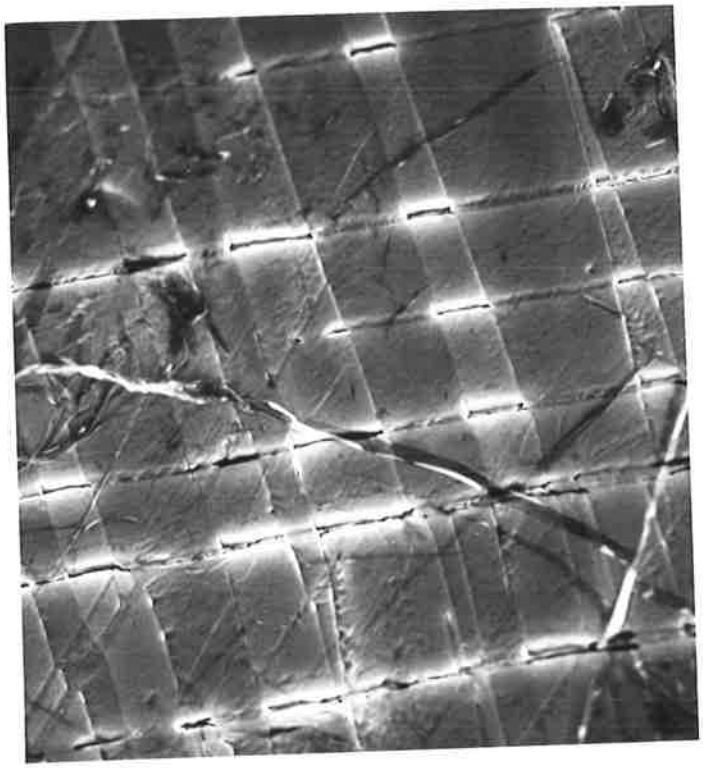

cooled, thereby slowing down the reaction. In some instances however, evidence of nucleation of the reaction products could be observed after the reaction had essentially gone to completion. On one specimen for example, after the film of liquid mercury had disappeared, a small cluster of particles of reaction products was observed on the surface of the γ phase crystal. Following the application of a second droplet of mercury to the crystal, the initial cluster of reaction products was seen to lie on the surface of a number of large well defined crystals (Figure 4.16) which were subsequently identified by EDAX analysis to be γ_1. This suggested that the nucleation of the large crystals occurred from nuclei present in the initial cluster of reaction product. Figure 4.16 not only shows these nuclei and nucleation products but also displays numerous examples of the crystallographic nature of the reaction with mercury.

While the work so far has delineated the planes along which mercury preferentially attacked, it was necessary to confirm the nature of these deformation markings by transmission electronmicroscopy. This information is presented in Chapter 5 and will be followed by a discussion on the reaction of the γ phase with mercury in Chapter 6.

FIGURE 4.16 Crystals of the silver-mercury phase lying over the γ surface. The cluster of nucleation material is labelled A.

X 1600


A

CHAPTER 5

TRANSMISSION ELECTRONMICROSCOPY OF THE γ PHASE

5.1 THE ORTHORHOMBIC SYSTEM

The special features of this system can best be discussed by making a comparison between the cubic and orthorhombic system. In the case of cubic crystals, of course, the indices of a direction in the crystal are the same as those of the plane to which that direction is normal and the angles between directions and angles between planes can be calculated quite easily. This is not generally the case with orthorhombic (or with hexagonal close packed crystals) where the indices of a direction are not simply related to the indices of the plane to which that direction is normal. In these cases of lower crystal symmetry a double stereographic technique can often be used with advantage to assist in the analysis of diffraction patterns where the directional indices are superimposed on the planar indices. At all times when carrying out these procedures great care must be exercised to differentiate clearly between indices of directions and the indices of planes.

The formulae shown in Table 5.1 for angles between plane normals and angles between directions in orthorhombic crystals involves the lattice parameters a, b and c so that

TABLE 5.1

Formulae for determination of interplanar angles and interzonal angles in cubic and orthorhombic crystals

1. Angle ϕ between $(h_1k_1l_1)$ and $(h_2k_2l_2)$

Cubic

$$\cos\phi = \frac{h_1h_2 + k_1k_2 + l_1l_2}{\sqrt{[(h_1^2 + k_1^2 + l_1^2)(\ _2^2 + k_2^2 + l_2^2)]}}$$

Orthorhombic

$$\cos\phi = \frac{\frac{1}{a^2}\,h_1h_2 + \frac{1}{b^2}\,k_1k_2 + \frac{1}{c^2}\,l_1l_2}{\sqrt{\left[\left(\frac{1}{a^2}h_1^2 + \frac{1}{b^2}k_1^2 + \frac{1}{c^2}l_1^2\right)\left(\frac{1}{a^2}h_2^2 + \frac{1}{b^2}k_2^2 + \frac{1}{c^2}l_2^2\right)\right]}}$$

2. Angle ρ between $[u_1v_1w_1]$ and $[u_2v_2w_2]$

Cubic

$$\cos\rho = \frac{u_1u_2 + v_1v_2 + w_1w_2}{\sqrt{[(u_1^2 + v_1^2 + w_1^2)(u_2^2 + v_2^2 + w_2^2)]}}$$

Orthorhombic

$$\cos\rho = \frac{a^2u_1u_2 + b^2v_1v_2 + c^2w_1w_2}{\sqrt{[(a^2u_1^2+b^2v_1^2+c^2w_1^2)(a^2u_2^2+b^2v_2^2+c^2w_2^2)]}}$$

in contrast to the situation with cubic crystals, in general, the calculated value of the angle between two plane normals in an orthorhombic material will apply uniquely to that particular material so that widely applicable tables of crystallographic data of this kind are not available. The same difficulty arises with standard projections which must be produced individually for different materials.

Moreover, since interplanar spacings and angles between plane normals are dependent on the lattice parameters a, b, c the (h k l) plane is no longer the same kind as the (h l k) plane. For example, the {123} have quite different interplanar spacings to the {321}, so that no longer can the orientation of a crystal be referred to a standard triangle (as is the case for cubic crystals). In both cubic and orthorhombic crystals, each quadrant of the stereographic projection contains six triangles. However, in the cubic system each of these triangles is equivalent, i.e. a diffraction pattern can be indexed in any one of the six triangles. Whereas, in the orthorhombic case the six triangles are not equivalent so that a quadrant of the stereographic projection must be used to index a diffraction pattern.

5.2 KIKUCHI MAP CONSTRUCTION

The implication of using a reference quadrant is that the Kikuchi map must also extend over a whole

quadrant of the standard projection rather than a standard triangle (or two of them) as in the cubic case. Kikuchi patterns in conjunction with Kikuchi maps enhance the ease of carrying out crystallographic manipulations in the electron microscope. Besides being able to tilt from one zone to another along a Kikuchi pair it is possible to precisely determine the beam direction without the 180° ambiguity associated with spot patterns (Thomas 1966).

A manually drawn Kikuchi map centred on the $[\bar{1}11]$ projection is reproduced in Appendix 2 where it can be seen that the map is based on a reference quadrant bound by (001), (010) and $(\bar{1}00)$ and contains poles of the form $\bar{h}kl$. A computer program was devised to determine which planes passed through the quadrant and to calculate the angles between planes whose zone axes lie within the bounds of the quadrant.

5.3 COMPUTER PROGRAMS

The author in collaboration with Dr. D.J. Netherway developed two computer programs specifically for the orthorhombic system. A very brief account of the operation of these two programs is given below, but full details on how to use them, together with the source listings are given in Appendices 3 and 4.

The first program is called ORTHEX and calculates the zone axis of an array of spots from a spot diffraction

pattern. The basic input data consists of the distances in millimetres from the central spot to three other spots and the angles between these spots. By knowing λL the computer calculates d spacings from each measurement and compares calculated angles with measured angles. Finally a vector addition test is performed and a zone axis generated.

The other program is known as KORTHU and calculates the beam direction from a Kikuchi pattern. It requires as input several Kikuchi spacings together with the angles between them. When an acceptable match between input and calculated distances and angles is obtained the beam direction is calculated.

Stereographic projections of both planes and directions which were used in the analysis of the twin and slip planes, were plotted by computer using the program of Johari and Thomas (1969). with modifications by Pearce (1972).

5.4 DETERMINATION OF SLIP PLANES

Plastically deformed bars of γ phase were prepared for thin foil transmission electronmicroscopy as described in Section 2.2. Slip bands such as that shown in Figure 5.1 (a) were observed in numerous foils and the procedure adopted to determine the slip plane was as follows:-

FIGURE 5.1 (a) A : trace of (010) slip band.
B : trace of ($\bar{1}$00) slip band.
Beam Direction [$\bar{1}$42].
X 33,400

FIGURE 5.1 (b) Selected area diffraction pattern of [$\bar{1}$42] zone axis.

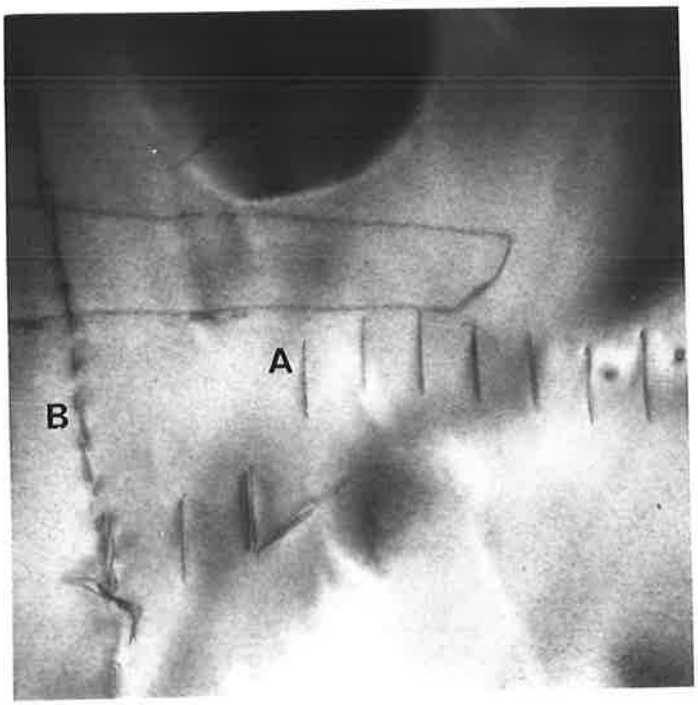
A
B

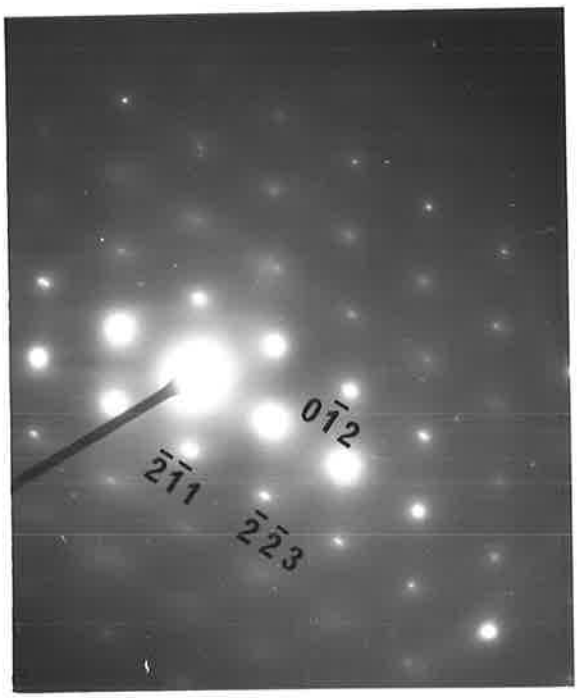
$0\bar{1}2$
$\bar{2}\bar{1}1$
$\bar{2}\bar{2}3$

1. The foil was mounted in the tilt-rotating stage and rotated until the slip band was lying along the tilt axis.

2. To determine the orientation as well as the projected width of the slip band, a bright field micrograph and corresponding diffraction pattern were taken at one tilt setting. The foil was then tilted a known number of degrees before taking another bright field and associated diffraction pattern. From this information a crystallographic analysis of the slip plane could be made.

The indexed diffraction pattern corresponding to the zone axis $[\bar{1}42]$ is shown in Figure 5.1 (b). The directional indices were converted into planar indices $(\bar{3}.56, 9.14, 5.37)$ and a stereographic projection for this orientation computed. After correcting for the angle of rotation between the micrograph and the diffraction pattern and taking into account the projected width calculation, the trace of slip band A was found to lie along (010) while the trace of B was found to correspond to the $(\bar{1}00)$.

Another slip band showing paired and multiple dislocations is shown in Figure 5.2. From the work presented in Chapter 3 it was established that the γ phase consists of an ordered lattice of silver and tin atoms. The pairing of the dislocations in Figure 5.2 is not unexpected, because as will be discussed later, such pairs of dislocations are often observed in ordered structures.

FIGURE 5.2 Slip band showing pairs of dislocations.
X 43,400
Foil orientation [023].
Diffraction vector g($\bar{4}$00).

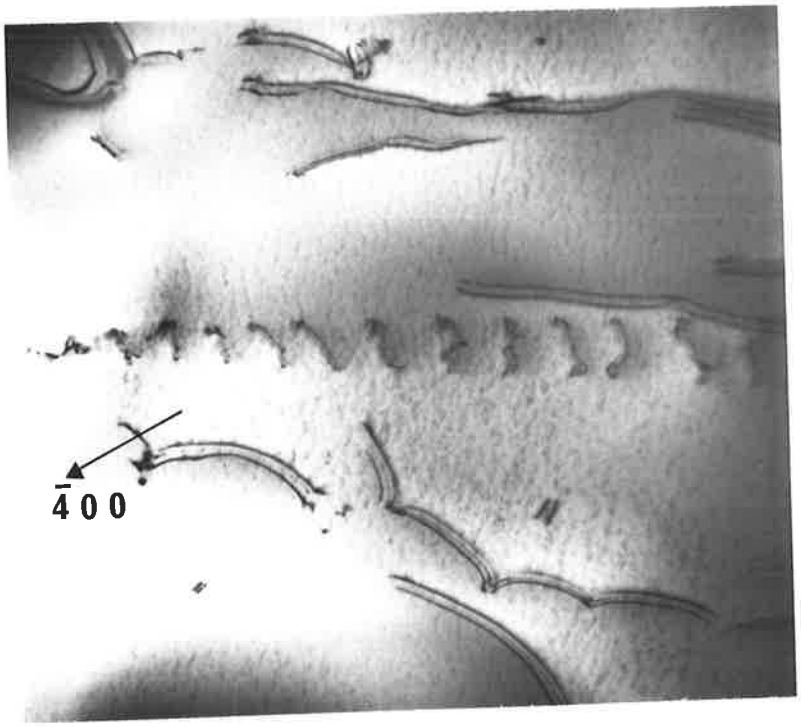
$\bar{4}00$

5.5 DETERMINATION OF TWINNING PLANES

The twinning planes in the γ phase were determined using similar procedures to those outlined in Section 5.4 except that microbeam diffraction was also used. Microbeam diffraction enables a very small portion of the specimen to be illuminated, so that the technique is particularly useful for determining the orientation of fine twins. Figure 5.3 (a) shows a γ phase twin that has been analysed by microbeam diffraction. The [102] matrix and twin orientation superimposed on the same pattern is shown in Figure 5.3 (b) with its analysis in Figure 5.3 (c). Both the matrix and twin reflections contain $(\bar{2}01)$, (010) and $(\bar{2}11)$ with the forbidden (010) produced as a result of double diffraction. By slightly altering the tilt angle and specimen position it was possible to obtain twin and matrix diffraction patterns separately. The twin Kikuchi pattern (Figures 5.3 (d) and (e)) has a beam direction of [0.036, 0.086, 0.171] or in planar indices (1.28, 1.96, 4.59), while the matrix orientation (Figure 5.3 (f)) is [302] or (1.07, 0, 0.54). A stereographic analysis was carried out for both the matrix and twin orientations, and the trace of the twin in both cases was found to be consistent with a $(\bar{2}11)$ twinning plane. The twin in Figure 5.3 (a) also contains stacking faults and these were observed to lie on the (010) plane. Similar markings are seen within the twins of Figures 5.4 (a) and 5.4 (b). The twinning plane in these photomicrographs is also $(\bar{2}11)$. From the analysis of several foils it is

FIGURE 5.3 (a) $(\bar{2}11)$ twin with (010) stacking faults.
(Note: contamination of foil in the electron beam obscured the clarity of the photomicrograph.)
X 86,500

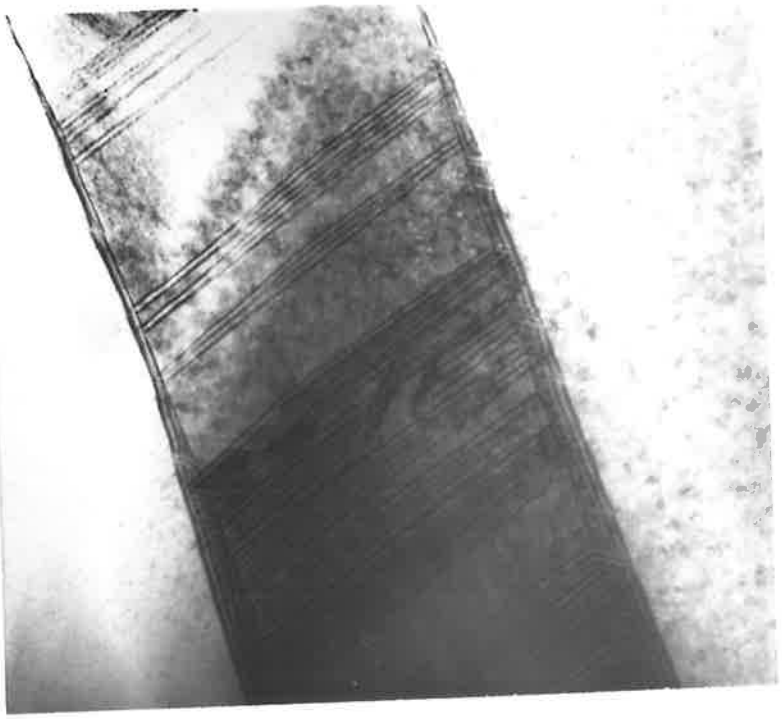

FIGURE 5.3 (b) Microbeam diffraction : Twin and Matrix orientiation both [102].

FIGURE 5.3 (c) Analysis of Figure 5.3 (b). (Open circles represent matrix spots.)

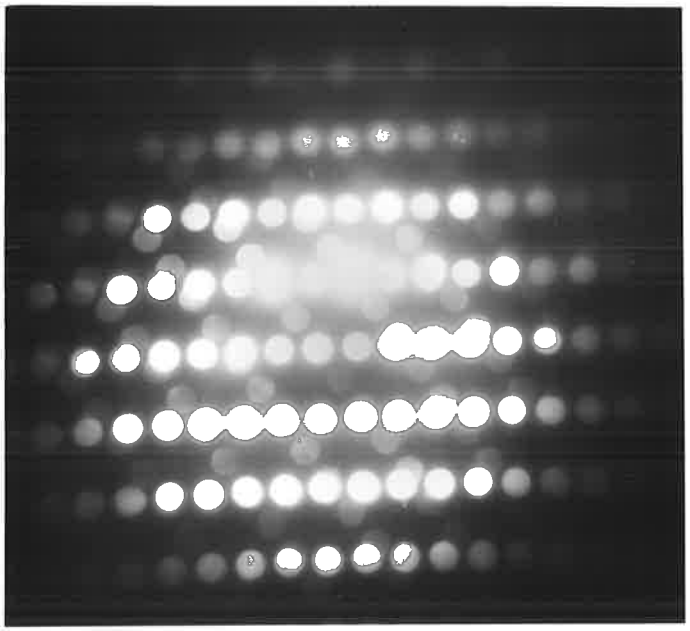

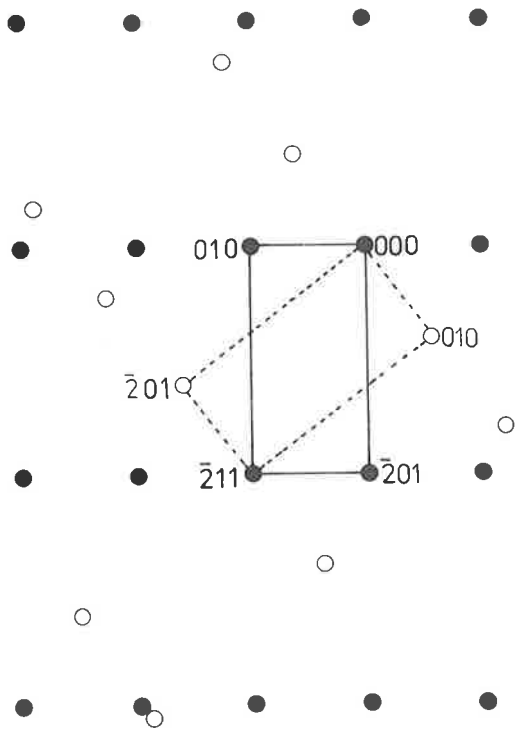
010
000
010
$\bar{2}01$
$\bar{2}11$
$\bar{2}01$

FIGURE 5.3 (d) Twin orientation [0.036, 0.086, 0.171].

FIGURE 5.3 (e) Analysis of Kikuchi pattern of 5.3 (d) (not reproduced at the same scale as 5.3 (**d**)).

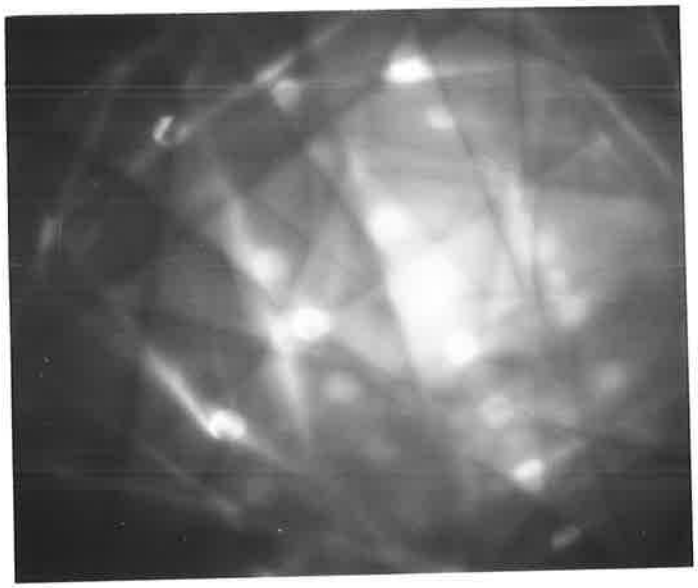

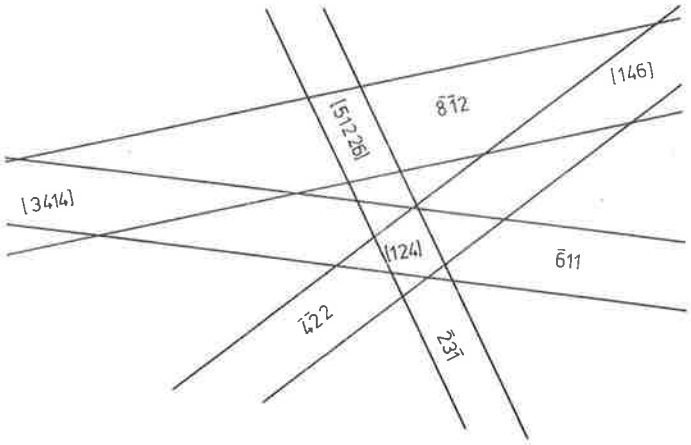
[3414]
[51226]
8̄12
[146]
[124]
6̄11
4̄22
2̄31

FIGURE 5.3 (f) Matrix orientation [302].

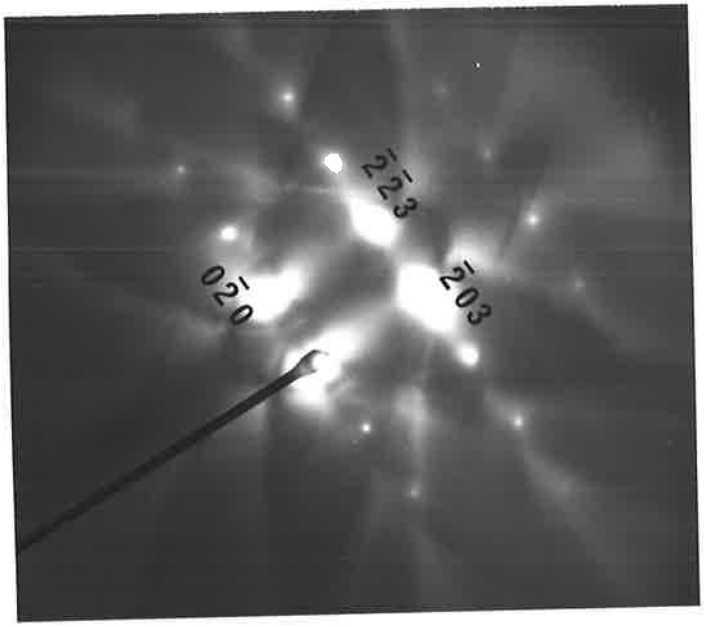
$2\bar{2}3$
$0\bar{2}0$
$20\bar{3}$

FIGURE 5.4 (a) A thin foil of γ phase showing twins lying along the $(\bar{2}11)$ plane.

X 26,000

FIGURE 5.4 (b) Twins containing markings similar to 5.3 (a).

X 64,000

apparent that the other twinning planes in the γ phase are (011) and (0$\bar{1}$1). A micrograph of a typical (011) twin under dark field is shown in Figure 5.5.

The discussion on the findings of this chapter together with their relevance to the reaction mechanism is presented in Chapter 6.

FIGURE 5.5 Dark field twin lying along $(0\bar{1}1)$ plane. X 64,000

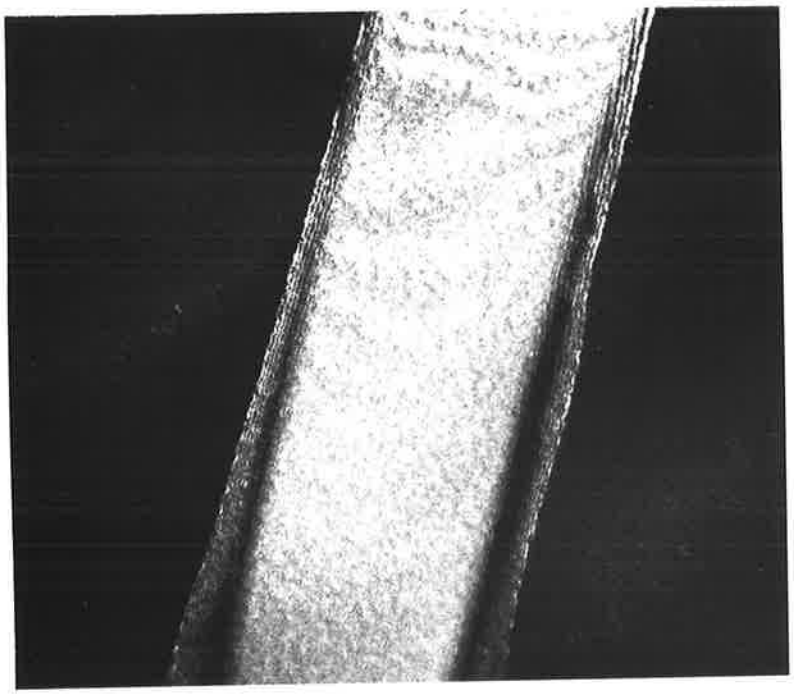

CHAPTER 6

DISCUSSION, CONCLUSIONS AND SUGGESTIONS FOR FUTURE INVESTIGATION

The objective of the present investigation was to examine the reaction mechanism between the γ phase of the silver-tin system and mercury. From the optical and electron-metallography presented in Chapters 2, 3, 4 and 5, it is possible for the first time to explain the effect of factors such as heat treatment, amount of plastic deformation etc., on the alloy and its subsequent reaction with mercury. The potential significance of this work is that if the influence of these factors can be controlled, then it may be possible to optimize the nature and distribution of reaction products, and in this way improve the clinical performance of dental amalgam.

The present study has shown that previous work (e.g. Ryge, Moffett and Barkow 1953, Wing and Ryge 1965) on the reaction of dental amalgam alloy with mercury was not carried out on a single phase γ alloy but on a duplex structure containing γ and Sn. In the present work an alloy of composition towards the midpoint of the range of stability of the γ phase (i.e. 26.5 wt. % Sn) at room temperature was selected for crystallographic and electron-optical studies on the reaction mechanism. The

crystallographic investigation involved both X-ray and electron diffraction and provided unequivocal evidence that the γ phase consisted of an ordered orthorhombic crystal lattice.

The transmission electronmicroscope study presented in Chapter 5 revealed important structural information about the deformation characteristics of the γ phase. Earlier work by Wood and Jacombs (1976) on a splat quenched alloy of nominal Ag_3Sn composition was hampered by their lack of computerised crystallographic facilities, which are undoubtedly required for this type of study. As a result these workers did not analyse any structural information. Moreover, as mentioned in Chapter 2 the alloy that Wood and Jacombs were examining was by no means a single phase γ structure, with the result that the analysis and interpretation of electron diffraction patterns would have been unduly complicated.

On the other hand, the present investigation developed a technique of producing thin foils from a single phase homogeneous alloy. Moreover, the determination of beam directions from electron diffraction patterns was derived by rigorous computer analysis, so that consistent indexing was achieved. Additionally, crystallographic tilting experiments in the electron microscope were carefully controlled by reference to the Kikuchi map of the γ phase. Without these important crystallographic aids, the determination of structural information by transmission

electronmicroscopy would be extremely difficult to pursue. The development of these techniques represents a great advancement for future electronmicroscope studies of the γ phase.

The analysis of electron diffraction patterns presented in Chapter 5 showed that the (010) plane was a slip plane. It is apparent from the ball model of Figure 3.1b that the (010) is the closest packed plane, which of course, makes the (010) slip plane a not unexpected result. It will be noted from Figure 5.2 that in this ordered alloy, the dislocations normally occurred in pairs, which suggests that they may be superlattice dislocations, comparable with those reported by Marcinkowski et al. (1961) in ordered $AuCu_3$.

Evidence was also obtained that deformation twinning occurred in the $(\bar{2}11)$, $(0\bar{1}1)$ and (011) planes. Bearing in mind that the γ phase crystal structure is very close to being hexagonal, then the equivalent plane to the $(0\bar{1}1)$ in the hexagonal system is $(10\bar{1}2)$. In fact, this is a common twinning plane in hexagonal materials as Cd, Zn, Mg, Ti and Be all have $(10\bar{1}2)$ as a twinning plane. From a two surface analysis of single crystals of Ag_3Sn, Fairhurst and Cohen (1972) determined that $(0\bar{1}1)$ was a twinning plane, and this is in agreement with the present work. These authors examined the question of a possible change of order brought about by the twinning process, and concluded that because only small atomic movements

were involved, and that the initial atom neighbours were not disrupted by the twinning process, then no change in order would be observed. This view was supported by Vanderschaeve and Sarrazin (1977) who studied the influence of deformation twins in ordered Ni_3V. In the present investigation the twins were heavily deformed and contained large numbers of stacking faults. This observation supports work reported by Partridge (1967) that heavily faulted twins are commonly observed in hexagonal metals. Similar results were obtained by Poirier et al. (1967).

One of the more important findings of the present investigation is that twins and slip planes are areas of high reactivity where a preferential reaction with mercury takes place. It will be noted that previous observations into this reaction have not revealed this path of attack, although Wing and Ryge (1965) have reported grain boundary penetration of mercury. Grain boundaries undoubtedly play an important part in this reaction; however, the question of grain boundary attack has, because of time constraints remained outside the scope of the present investigation. Subsequent work by the Materials Engineering Group has indicated the importance of grain boundary attack (Abbott, Miller and Netherway 1981) and will be reported elsewhere.

Other workers have tried to explain the reaction in terms of grain boundary diffusion of silver and tin atoms (Okabe et al. 1974), thermodynamical considerations (Reynolds and Barker 1975), etc. A study by Reynolds et

al. (1975) reported scanning electron microscope observations of mercury attack on amalgam specimens that were fractured 13 minutes after condensation. As a consequence of their experimental method these workers observed reaction products covering the γ particles and, of course, completely missed the crystallographic nature of the reaction. In fact, Reynolds et al. acknowledged that it was impossible to observe the initial stages of reaction, so that they had reported on the next stage of the reaction which involved the nucleation and growth of phases.

In the present investigation the experimental design allowed the early stages of wetting the alloy particles by mercury to be monitored, and hence, it was possible to observe the initial stages of the reaction mechanism.

As mentioned previously, it is recognized that the grain boundaries are sites of preferential attack as proposed by Wing and Ryge (1965). In this respect the reaction between mercury and the γ phase appears to have a great deal in common, as Wing and Ryge pointed out, with the well established phenomena of the embrittlement of brass by mercury. Although the phenomena of liquid metal embrittlement (LME) has been known for well over sixty years the mechanism of LME is still not well understood (Old and Trevena 1979). This subject has recently been reviewed by Old (1980) who divides LME into a number of

categories, and the reaction between the γ phase and mercury clearly falls into the category described by Old as a "reactive system", i.e. a chemical compound is formed between the liquid metal and the alloy system. The example of this, cited by Old, was that of the copper-lithium system, in which following intergranular fracture crystals of a copper lithium compound formed on the fracture face. This reaction would be comparable to the formation of Ag-Hg crystals on the surface of the γ phase.

In addition to the "reactive system" Old defines three other processes which constitute mechanisms of liquid metal embrittlement. These processes are:

(a) classical LME, in which a pure metal or alloy can suffer fast brittle fracture when strained in contact with a liquid metal,

(b) grain boundary penetration of the solid by the liquid,

(c) selective attack of phases or precipitates in the solid.

It is now clear that grain boundary attack is by no means the unique characteristic of a reactive system, and that from the present work it is now seen that preferential attack along these other crystallographic features is of major importance in the reaction. The question arises as to why these crystallographic features

undergo preferential attack and indeed of course, why it is that grain boundary attack occurs. It is possible to speculate that while grain boundaries are regions of high stress, the other crystallographic features probably represent areas of large dislocation concentrations, which could account for the vigorous penetrating reaction at those sites. While the present study has involved a preliminary investigation into the nature of the deformation characteristics of the γ phase by transmission electronmicroscopy, the above speculation is clearly an issue which needs to be resolved by further investigation.

The development of cracks within the embrittled γ phase alloy as observed in Figure 4.9 is of interest, as it may constitute a reaction path by which mercury can penetrate the alloy for further reaction. Various theories have been proposed to explain the development and propagation of cracks which appear in the embrittled material. One of the more recent theories proposed by Lynch (1977) explains crack development on the basis of the nucleation and movement of dislocations being facilitated by chemisorption of liquid metal atoms. When crack growth eventually occurs it is by the tensile separation of atoms at atomically sharp crack tips (Lynch 1981). As the crack propagates the metal or alloy may fracture intergranularly, although some cases of transgranular fracture have been reported, e.g. Zircalloy-2 embrittled by cadmium (Nicholas and Old (1979).

Although a careful examination of photomicrographs of dental amalgams published by a number of workers, e.g. Okabe et al. (1979), suggests that preferential attack along well defined crystallographic planes similar to that reported in the present study has occurred, the significance of this attack has apparently not been recognized in the past. For example, Okabe et al. (1979) in a study of the setting reaction of dispersed phase amalgams published a photomicrograph (Figure 4, Page 1090 of the paper by Okabe et al.) of the γ phase surrounded by reaction products. It is evident from this photomicrograph that mercury has reacted along specific crystal planes. Likewise as mentioned above, no evidence of any crystallographic dependence of the reaction with mercury was reported by Reynolds et al. (1975). However, in a schematic diagram on the reaction between mercury and the γ phase, Dubois et al. (1981) proposed that mercury not only attacked grain boundaries but also reacted with heavily faulted regions in the γ phase. While these authors had no evidence to support their proposition, it is clear from the present work that there is a preferred crystallographic attack between mercury and the γ phase.

It is from this type of mercury attack that it is now possible to understand why the manufacturing process of annealing plays such an important part in producing a controlled setting reaction. During the formation of the alloy filings, e.g. by lathe cutting and in the subsequent

milling process to further reduce the particle size, the alloy is heavily plastically deformed by slip and twinning. The manufacturer employs an annealing treatment of 100°C for a few hours which would result in a lowering of the dislocation density and internal stress by conventional recovery mechanisms. As the present work has shown that the reaction with mercury is markedly influenced by the presence of slip and twinning, then an annealing treatment would be expected to reduce the reactivity the alloy with mercury to an extent dependent on the temperature and duration of the annealing process.

The trituration and condensation processes which come under the direct control of the dentist, are likewise recognized as having an important influence on the hardening reaction. During trituration and condensation, the amalgam alloy particles are undoubtedly subjected to further plastic deformation, the result of which would be increased amounts of slip and twinning and enhanced reactivity.

The further consequence of the present investigation relates to the implication which the newly observed reaction mechanism has for the clinical performance of amalgam restorations. It is clear that the reaction results in the formation of deep planar intrusions or notches within the partially reacted alloy particles. These planar intrusions must have important implications for the mechanical and corrosive behaviour of stressed dental amalgam restorations.

The present investigation has opened the way for further studies into the reaction of the γ phase with mercury. The resolution of some of the issues raised in the present work is already underway, while others clearly form the basis of further work to be carried out in an extension of this project. For example, transmission electronmicroscopy has already revealed some of the deformation characteristics of the γ phase; however, additional work needs to be carried out to establish the Burgers vectors of the dislocations. It would also be of considerable interest to confirm that the pairs of dislocations observed in the deformed γ phase alloy were of the superlattice type.

The dislocation density in regions in which high reactivity with mercury occurs, e.g. at the intersection of deformation twins, needs to be investigated. Further information on the nature of the stress fields in the vicinity of the intersection can readily be obtained from appropriately sectioned single crystals. This will provide information that may well be relevant to the broader field of liquid metal attack in other alloy systems.

The importance of the observed preferential attack along deformation twins, slip bands and grain boundaries to the mechanical and corrosive properties of hardened amalgam are immediately apparent. This not only reflects on the behaviour of dental amalgam but may be relevant to

the understanding of the dimensional changes that occur. Therefore, the work should proceed in the direction of studying the dimensional changes that occur during setting as related to the reaction mechanism.

Appendix I

Silver and Tin Impurities

SILVER AND TIN IMPURITIES

1. Silver

Cu	0.001%
Fe	0.002%
Pb	0.002%

2. Tin

Fe	0.01%
Pb	0.01%
Cu	0.0025%
Bi	0.002%
Total Foreign Metals	0.04%
As	0.0005%
Sb	0.025%

Appendix 2

Kikuchi Map of the γ Phase

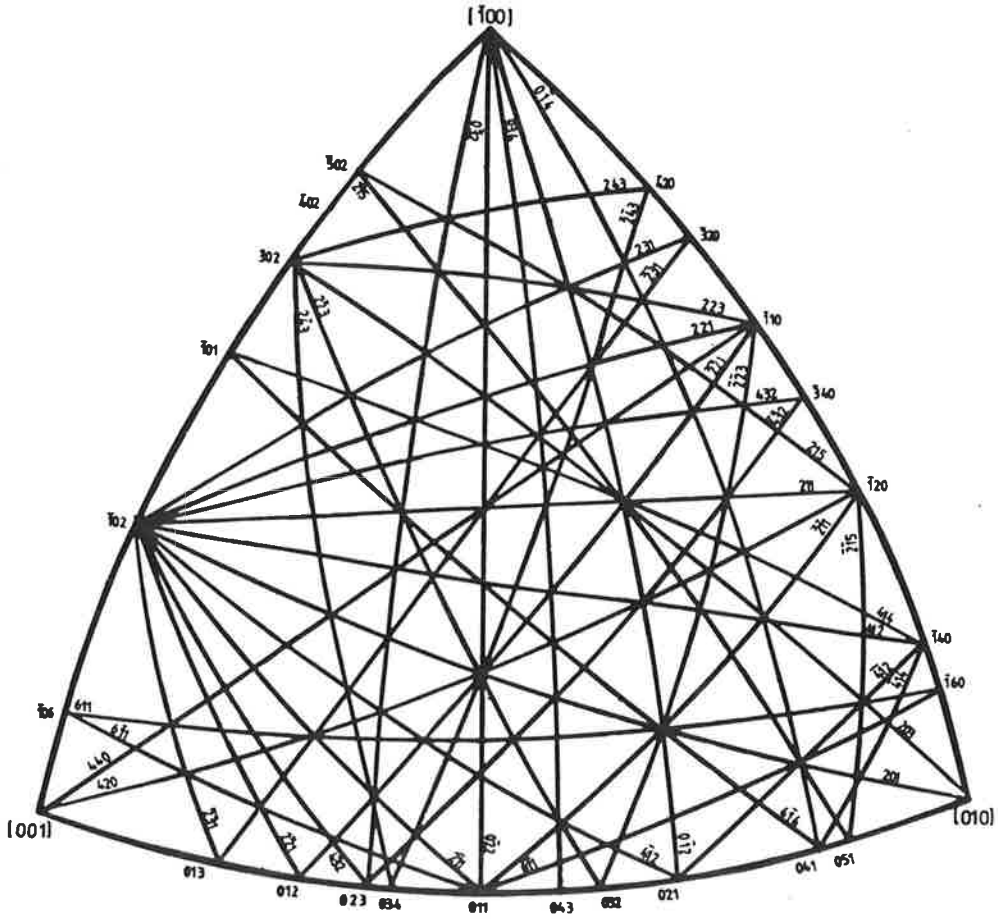
[100]
[001]
[010]

Appendix 3

Computer Program

ORTHEX

PROGRAM ORTHEX

```
      PROGRAM ORTHEX(INPUT,OUTPUT)

C          ORTHEX FINDS POSSIBLE SOLUTIONS TO ORTHORHOMBIC
C                       STRUCTURE ORIENTATIONS.


C       DATA CARDS
C       1      JOB IDENTIFIER                                        A10
C       2,3,4  LATTICE PARAMETERS                                    REAL
C       5      LAMDA*CAMERA LENGTH IN ANGSTROM*MM                    REAL
C       6      D SPACING A IN MMS AS MEASURED ON NEGATIVE            REAL
C       7      % TOLERANCE                                           REAL
C       8      D SPACING B              "                            REAL
C       9      % TOLERANCE                                           REAL
C       10     D SPACING C              "                            REAL
C       11     % TOLERANCE                                           REAL
C       12     ANGLE AB                                              REAL
C       13     ANGLE BC                                              REAL
C       14     ANGLE CA                                              REAL
C       15     TOLERANCE IN DEGREES FOR ANGLE MEASUREMENTS           REAL
C       16     1= VECTOR ADDITION TEST
C              0= NO VECTOR ADDITION TEST                          INTEGER
C


      DIMENSION MH(200,3),MK(200,3),ML(200,3),ALAM(3,200),DD(3)
     *,NEW(3,1000),J1(3,200),J2(3,200),J3(3,200),JZ(3,200),R(3)
      DIMENSION DSPAC(3),DTOL(3),ANG(3),ANGLE(3)
     *,NZ1(3),NZ2(3),ANGF(3,200),NB(4),NUM(3)


      PRINT100
  100 FORMAT('1')
C READ JOB NUMBER.
      READ (*,501,END=10000)JOBNO
  501 FORMAT(BZ,A10)

C READ LATTICE CONSTANTS.
10000 READ (*,* ,END=10001)A,B,C
10001 READ (*,*,END=10002)ALAML
C READ R FROM NEGATIVE IN MM AND TOLERANCES
10002 READ (*,*,END=10003)(R(I),DTOL(I),I=1,3)
C READ ANGLE BETWEEN PLANES AND TOLERANCE.
10003 READ (*,*,END=10004)ANG,ANGTOL
10004 READ (*,201, END=10005)IVECTA
  201 FORMAT(BZ,I1)
C PRINT JOB NUMBER HEADING.
10005 PRINT502,JOBNO,JOBNO,JOBNO
  502 FORMAT(//1X,3(5X,'NEGATIVE PLATE ',A10,5X)//)

      PRINT82
   82 FORMAT(/' EXPERIMENTAL DATA'/)
```

```
C PRINT LATTICE CONSTANTS.
      PRINT89,A,B,C
 89   FORMAT(/' A,B,C LATTICE DIMENSIONS ',3F10.5//)
      PRINT 160,ALAML
 160  FORMAT('0 LAMBDA BY L =',F8.3)
      PRINT162,R
 162  FORMAT('0 SPACING FROM NEGATIVE IN MM',3F14.2)
      DO 170 I=1,3
 170  DSPAC(I)=ALAML/R(I)
      PRINT 202,(DSPAC(I),DTOL(I),I=1,3),ANG,ANGTOL
 202  FORMAT(/' D SPACINGS : A=',F8.3,' +/-',F4.1,'%',5X,
     1 'B=',F8.3,' +/-',F4.1,'%',5X,'C=',F8.3,' +/-',F4.1,'%'/
     2 /' ANGLE AB =',F8.1,5X,'ANGLE BC =',F8.1,5X,'ANGLE CA =',
     3 F8.1,10X,'TOLERANCE =',F6.1,' DEGREES')
      IF(IVECTA) 110,110,120
 110  PRINT 112
 112  FORMAT(/'  NO VECTOR ADDITION TEST PERFORMED '/)
      GO TO 125
 120  PRINT 122
 122  FORMAT(/'  VECTOR ADDITION TEST PERFORMED '/)
 125  CONTINUE
C C CONVERT PERCENT TOLERANCES.
      DO 180 I=1,3
      DTOL(I)=DTOL(I)*DSPAC(I)/100.
 180  CONTINUE
C
C CALCULATE FORMING PLANES.
      CALL HKL(MH,MK,ML,NUM,A,B,C,DSPAC,DTOL)

C PRINT FORMING PLANES.
 3    CONTINUE
      PRINT91
 91   FORMAT(' PLANES TESTED')
      DO 94 I=1,3
      NU=NUM(I)
      PRINT 96
 96   FORMAT(/)
 94   PRINT92,(MH(M,I),MK(M,I),ML(M,I),M=1,NU)
 92   FORMAT(10(1X,3I2,1X))

C SET UP ELEMENTS OF GRID.
      NB(1)=0
      NUM2=0
      DO 150 L=1,3
      N=NUM(L)
      DO 140 I=1,N
      NOS=0
 130  CALL SIGN (MH(I,L),MK(I,L),ML(I,L),NOS)
      IF(NOS-5) 132,140,140
 132  IF(MAGICQ(MH(I,L),MK(I,L),ML(I,L),-1).EQ.1) GO TO 130
      NUM2=NUM2+1
      NEW(1,NUM2)=MH(I,L)
      NEW(2,NUM2)=MK(I,L)
      NEW(3,NUM2)=ML(I,L)
      GO TO 130
 140  CONTINUE
      NB(L+1)=NUM2
```

```
 150  CONTINUE
C NUM2 CONTAINS TOTAL OF ELEMENTS IN LIST.
      PRINT93,NUM2
 93   FORMAT(//' NO. OF ELEMENTS FORMED IS ',I3//)
C      PRINT 95,((NEW(I,M),I=1,3),M=1,NUM2)
 95   FORMAT(/' LIST OF POSSIBLE ELEMENTS '//9(1X,3I2,1X))


C START ANALYSIS


      INZS=0
      NU2=NB(2)
      NU3=NB(2)+1
      NU4=NB(3)
      NU5=NB(3)+1
      NU6=NB(4)
      DO 800 K=1,NU2
      DO 800 L=NU3,NU4
      CALL FI(A,B,C,NEW(1,K),NEW(2,K),NEW(3,K),NEW(1,L),NEW(2,L),
     *NEW(3,L),ANGLE(1))
      IF(ABS(ANGLE(1)-ANG(1)).GT.ANGTOL)GOTO 800
      DO 700 M=NU5,NU6
      CALL FI(A,B,C,NEW(1,L),NEW(2,L),NEW(3,L),NEW(1,M),NEW(2,M),
     *NEW(3,M),ANGLE(2))
      IF(ABS(ANGLE(2)-ANG(2))-ANGTOL) 205,205,700
 205  CALL FI(A,B,C,NEW(1,M),NEW(2,M),NEW(3,M),NEW(1,K),NEW(2,K),
     *NEW(3,K),ANGLE(3))
      IF(ABS(ANGLE(3)-ANG(3))-ANGTOL) 207,207,700
 207  CONTINUE
      CALL ZONE (NEW(1,K),NEW(2,K),NEW(3,K),NEW(1,L),NEW(2,L),
     *NEW(3,L),NZ1)
      IF(MAGICQ(NZ1(1),NZ1(2),NZ1(3),1)) 700,700,210
 210  CALL ZONE (NEW(1,M),NEW(2,M),NEW(3,M),NEW(1,L),NEW(2,L),
     *NEW(3,L),NZ2)
      IF(MAGICQ(NZ2(1),NZ2(2),NZ2(3),1)) 700,700,240
 240  CALL REDUCE(NZ1(1),NZ1(2),NZ1(3))
      CALL REDUCE(NZ2(1),NZ2(2),NZ2(3))
      DO 260 I=1,3
      IF(NZ1(I)-NZ2(I)) 700,260,700
 260  CONTINUE
      IF(IVECTA.EQ.0) GO TO 330
      DO 270 I=1,3
      IF(NEW(I,K)+NEW(I,L)-NEW(I,M))280,270,280
 270  CONTINUE
      GO TO 330
 280  DO 290 I=1,3
      IF(NEW(I,K)+NEW(I,L)+NEW(I,M)) 300,290,300
 290  CONTINUE
      GO TO 330
 300  DO 305 I=1,3
      IF(NEW(I,K)-NEW(I,L)-NEW(I,M)) 310,305,310
 305  CONTINUE
      GO TO 330
 310  DO 315 I=1,3
      IF(NEW(I,K)-NEW(I,L)+NEW(I,M)) 700,315,700
 315  CONTINUE
 330  CONTINUE
```

```
C     WE NOW HAVE A SOLUTION

      INZS=INZS+1
      IF(INZS-200) 338,338,336
 336  PRINT 337
 337  FORMAT('0 NO. OF SOLNS GREATER THAN ARRAY SIZE')
      GO TO 700
 338  DO 360 I=1,3
      J1(I,INZS)=NEW(I,K)
      J2(I,INZS)=NEW(I,L)
      J3(I,INZS)=NEW(I,M)
      ANGF(I,INZS)=ANGLE(I)
      JZ(I,INZS)=NZ1(I)
 360  CONTINUE
 700  CONTINUE
 800  CONTINUE
      IF(INZS) 311,311,345
 345  CONTINUE
      PRINT100
      PRINT830
 830  FORMAT(//17X,' FINAL SOLUTION(S) '//
     * 5X,'PLANE A',13X,'PLANE B',13X,'PLANE C',16X,'ZONE AXIS',8X,'ANG
     *AB'       ,8X,'ANGBC',9X,'ANG CA'//)
      DO 3000 N=1,INZS
      CALL SPAD(A,B,C,J1(1,N),J1(2,N),J1(3,N),DD(1))
      CALL SPAD(A,B,C,J2(1,N),J2(2,N),J2(3,N),DD(2))
      CALL SPAD(A,B,C,J3(1,N),J3(2,N),J3(3,N),DD(3))
      DO 347 I=1,3
 347  ALAM(I,N)=R(I)*DD(I)
      PRINT 312,(J1(I,N),I=1,3),ALAM(1,N),(J2(I,N),I=1,3),ALAM(2,N),
     ,(J3(I,N),I=1,3),ALAM(3,N),(JZ(I,N),I=1,3),(ANGF(I,N),I=1,3)
 312  FORMAT(3(3X,3I3,3X,F5.2),7X,3I3,3(8X,F6.2)/)
 3000 CONTINUE
      GO TO 900
 311  PRINT 890
 890  FORMAT('0 NO SOLUTIONS FOUND')
 900  PRINT 72
 72   FORMAT(///10X,' BYE BYE ORTHEX.')
      STOP
      END

      SUBROUTINE ZONE (M1,M2,M3,N1,N2,N3,NZ)
      DIMENSION NZ(3)
      NZ(1)=M2*N3-M3*N2
      NZ(2)=M3*N1-M1*N3
      NZ(3)=M1*N2-M2*N1
      IF(NZ(3)) 10,20,20
 10   DO 15 I=1,3
 15   NZ(I)=-NZ(I)
 20   RETURN
      END
      SUBROUTINE SPAD(AA,BB,CC,NH,NK,NL,ANS)
C A,B,C LATTICE CONSTANTS.
C H,K,L INDICES OF PLANE
C ANS IS D SPACING

      IF((AA.LE.0.01).OR.(BB.LE.0.01).OR.(CC.LE.0.01))GOTO1
```

```
      GOTO2

 1    PRINT3
 3    FORMAT(' PROG. STOPPED.  LATTICE CONSTANT(S) NEAR ZERO)')
      STOP

 2    CONTINUE
      AH=FLOAT(NH)
      AK=FLOAT(NK)
      AL=FLOAT(NL)
      X=AH*AH/(AA*AA)
      Y=AK*AK/(BB*BB)
      Z=AL*AL/(CC*CC)
      ANS=1.0/SQRT(X+Y+Z)
      RETURN
      END

      SUBROUTINE FI(AA,BB,CC,MH,MK,ML,NH,NK,NL,FY)
C CALCULATES ANGLE PHI.
      PI=3.1415926
       A2=AA*AA
       B2=BB*BB
       C2=CC*CC
      ANUM1=FLOAT(MH*NH)/A2
      ANUM2=FLOAT(MK*NK)/B2
      ANUM3=FLOAT(ML*NL)/C2
      ANUM=ANUM1+ANUM2+ANUM3
      DEN1=FLOAT(MH*MH)/A2
      DEN2=FLOAT(MK*MK)/B2
      DEN3=FLOAT(ML*ML)/C2
      DEN4=FLOAT(NH*NH)/A2
      DEN5=FLOAT(NK*NK)/B2
      DEN6=FLOAT(NL*NL)/C2
      DEN=(DEN1+DEN2+DEN3)*(DEN4+DEN5+DEN6)
      DEN=SQRT(DEN)
      ANS=ANUM/DEN
      FY=ACOS(ANS)*180.0/PI
      IF(FY.GT.90.) FY=180.-FY
      RETURN
      END

      SUBROUTINE SIGN(NH,NK,NL,NSIGN)
      IF((NH.EQ.0).AND.(NK.EQ.0))GOTO70
      IF((NK.EQ.0).AND.(NL.EQ.0))GOTO70
      IF((NH.EQ.0).AND.(NL.EQ.0))GOTO70
      IF(NH.EQ.0)GOTO71
      IF(NK.EQ.0)GOTO72
      IF(NL.EQ.0)GOTO71
      GOTO60

 70   IF(NSIGN.EQ.0)GOTO50
      NSIGN=5
      RETURN
 71   IF(NSIGN-1) 50,12,74
 72   IF(NSIGN-1) 50,13,74
 74   NSIGN=5
      RETURN
```

```
60    IF(NSIGN.EQ.0)GOTO50
      IF(NSIGN.EQ.1)GOTO13
      IF(NSIGN.EQ.2)GOTO12
      IF(NSIGN.EQ.3)GOTO13
      IF(NSIGN.EQ.4)GOTO50
      IF(NSIGN.GE.5)RETURN


12    NK=-NK
      GOTO50

13    NH=-NH

50    NSIGN=NSIGN+1
      RETURN
      END

      FUNCTION MAGICQ (IA,IB,IC,MUMMY)
C     MAGICQ ACCEPTS OR REJECTS THE PLANE (POLE)
C     IA,IB,IC WITH FOLLOWING CONSTRAINTS.
C     ACCEPT -IA,IB,IC  ALL .GT. 0
C REJECT OR ACCEPT (MUMMY=-1 OR 1 RESPECT.)
C OOL
C -HOO
C OKO
C -HKO
C -HOL
C OKL
C REJECT ALL ELSE.
C     MAGICQ=1  IA,IB,IC FITS MAGIC QUADRANT.
C     MAGICQ=0  IA,IB,IC, DOES NOT FIT MAGIC QUADRANT.

      IF((IA.EQ.0).AND.(IB.EQ.0).AND.(IC.LT.0))IC=-IC
      IF((IA.GT.0).AND.(IB.EQ.0).AND.(IC.EQ.0))IA=-IA
      IF((IB.LT.0).AND.(IC.EQ.0))GOTO4
      GOTO5
 4    CONTINUE
      IA=-IA
      IB=-IB
 5    CONTINUE
      IF((IA.LT.0).AND.(IB.GT.0).AND.(IC.GT.0))GOTO1
      IF(MUMMY.EQ.-1)GOTO2
      IF((IA.LE.0).AND.(IB.EQ.0).AND.(IC.GT.0))GOTO1
      IF((IA.LT.0).AND.(IB.GE.0).AND.(IC.EQ.0))GOTO1
      IF((IA.EQ.0).AND.(IB.GT.0).AND.(IC.GE.0))GOTO1
      GOTO2
 1    MAGICQ=1
      RETURN
 2    MAGICQ=0
      RETURN
      END

      SUBROUTINE REDUCE (IA,IB,IC)
C REDUCES POLE INDICES TO LOWEST ORDER.
C IT IS PRESUMED NO PRIME NUMBER .GT. 17 WILL BE A COMMON FACTOR.

      DIMENSION NOB(3),NPRIME(7)
      DATA NPRIME/2,3,5,7,11,13,17/
```

```
      NOB(1)=IA
      NOB(2)=IB
      NOB(3)=IC

      DO 50 K=1,7
10     DO 20 I=1,3
      IF(MOD(NOB(I),NPRIME(K))) 50,20,50
20    CONTINUE
30    DO 40 I=1,3
40    NOB(I)=NOB(I)/NPRIME(K)
      GO TO 10
50    CONTINUE
      MIN=1000
      DO 100 I=1,3
      IF(NOB(I)) 60,100,70
60    JERK=-NOB(I)
      GO TO 80
70    JERK=NOB(I)
80     IF(JERK-MIN) 90,100,100
90    MIN=JERK
100   CONTINUE
      IF(MIN-NPRIME(7)) 130,130,105
105   DO 110 I=1,3
      IF(MOD(NOB(I),MIN)) 130,110,130
110   CONTINUE
      DO 120 I=1,3
120   NOB(I)=NOB(I)/MIN
130   IA=NOB(1)
      IB=NOB(2)
      IC=NOB(3)
      END
      SUBROUTINE HKL(MH,MK,ML,NUM,A,B,C,DSPAC,DTOL)
C
C     CALCULATE H K L VALUES WHICH HAVE D SPACING WITHIN TOLERANCES
C
      DIMENSION DSPAC(3),DTOL(3),MH(200,3),MK(200,3),ML(200,3),NUM(3)
      DO 50 I=1,3
 50   NUM(I)=0
      DO 200 IH=1,16
      I=IH-1
      DO 200 IK=1,16
      J=IK-1
      DO 200 IL=1,16
      K=IL-1
      IF(K) 54,54,56
 54   IPJ=I+J
      IF(IPJ) 200,200,56
C     TO REMOVE FORBIDDEN REFLECTIONS CHANGE 56 TO 55 IN PREVIOUS LINE
 55   IF(MOD(IPJ,2)) 200,56,200
 56   D=1./SQRT((I/A)**2+(J/B)**2+(K/C)**2)
      DO 100 L=1,3
      IF(ABS(DSPAC(L)-D)-DTOL(L)) 60,60,100
 60   NUM(L)=NUM(L)+1
      N=NUM(L)
      MH(N,L)=I
      MK(N,L)=J
      ML(N,L)=K
 100  CONTINUE
```

```
200  CONTINUE
     RETURN
     END
```

Appendix 4

Computer Program

KORTHU

PROGRAM KORTHU

```
      PROGRAM KORTHU (INPUT,OUTPUT,TAPE5=INPUT,TAPE6=OUTPUT,TAPE7)
C          PROGRAM TO INDEX KIKUCHI PATTERNS
C
C      FILES TO BE ATTACHED
C
C              TAPE7 -  CONTAINS (HKL) VALUES
C
C                    -  FORMAT:  3 BLANK CARDS THEN (1X,3I3)
C
C      DATA CARDS
C
C      1        JOB IDENTIFIER                                    (A10)
C      2,3,4    LATTICE PARAMETERS                                (F10.3)
C      5        LAMBDA*L                                          (F10.3)
C      6        WAVELENGTH                                        (F10.3)
C      7        ANGLE TOLERANCE                                   (F10.3)
C      8        NUMBER OF KIKUCHI LINES EXCLUDING THE TWO
C               CHOSEN AS REFERENCE LINES - MAX. IS 6             (I1)
C      9        SPACING OF REF.1 LINE IN MMS                      (F10.3)
C      10       TOLERANCE OF SPACING                              (F10.3)
C      11       SPACING OF REF.2 LINE IN MMS                      (F10.3)
C      12       TOLERANCE OF SPACING                              (F10.3)
C      13       DISTANCE IN MMS FROM INTERSECTION OF THE TWO
C               REFERENCE LINES ("REFERENCE INTERSECTION")
C               TO BEAM STOP (THE TRANSMITTED BEAM)               (F10.3)
C      14       ACUTE ANGLE BETWEEN REFERENCE LINES IN DEGREES (F10.3)
C
C      15       SPACING IN MMS OF A KIKUCHI LINE                  (F10.3)
C      16       TOLERANCE OF THE SPACING                          (F10.3)
C
C               ALTERNATIVES FOR CARDS 17-21
C
C          (A) THE KIKUCHI LINE DOES NOT PASS THROUGH THE
C              REFERENCE INTERSECTION
C      17       DISTANCE FROM REFERENCE INTERSECTION TO THE
C               INTERSECTION OF THE K LINE WITH REF.1             (F10.3)
C      18       DISTANCE FROM K LINE/REF.1 INTERSECTION TO
C               BEAM STOP                                         (F10.3)
C      19,20    REPEAT 17,18 FOR INTERSECTION WITH REF.2
C      21       DISTANCE BETWEEN K LINE/REF1 INTERSECTION
C               AND K LINE/REF.2 INTERSECTION                     (F10.3)
C
C          (B) THE KIKUCHI LINE PASSES THROUGH THE REFERENCE
C              INTERSECTION
C      17       0.                                                (F10.3)
C      18       0.                          (F10.3)
C      19        0.
C      20        0.
C      21       0.
C
C      22       TOLERANCE APPLIED TO MEASUREMENTS 17-21           (F10.3)
C      23       ACUTE ANGLE BETWEEN K LINE AND REF.1              (F10.3)
C      24       ACUTE ANGLE BETWEEN K LINE AND REF.2              (F10.3)
```

```
C      25...   ACUTE ANGLES BETWEEN THIS K LINE AND
C              K LINE 1, K LINE 2,..., K LINE (THIS ONE -1)    (F10.3)
C
C              REPEAT DATA CARDS 15-22 FOR EACH ADDITIONAL
C              K LINE (MAXIMUM OF 6)
C
C   LAST       ANGLE OF OVERLAP INTO ADJACENT QUADRANTS
C                    IN DEGREES                                (F10.3)
C
C
C
      DIMENSION A(3),RTK(6),DIST(2,6),BS(2,6),LKHRF1(3,200),
     *LKHRF2(3,200),DPR1(200),DPR2(200),DTK(6),TEMP(200),NTH(6),
     *ITEM(3,200),DPT(200,6),ICPR(3),ICPR1T(3),IZP1(3,6),LOOP(6),
     *RD(6),DPMM1(6),DPMM2(6),ICPR2T(3),DISTT(6),IZP2(3,6)
     *,LKHTK(3,200,6),CL1(6),CL2(6),CL(6),U(3,3),ANGL(3,6)
      DIMENSION DPMM3(6),CL3(6),CAV(3),C(3),AC(3),BD(3),BP(3)
     *,AR(3),IP1(3),IP2(3),IP3(3),BETA(6),GAMMA(6),TOLKSP(6),TOLKD(6),
     *BETAT(6),GAMMAT(6),ANGKK(6,4),IP4(3)
      COMMON /OVERLP/ OVLP
C
      READ(5,100) JOB,A,ALAML,ALAMDA,ANGTOL
 100  FORMAT(BZ,A10,6(/F10.3))
10000 READ(5,103,END=10001) NTK
 103  FORMAT(BZ,I1)
10001 READ(5, 105,END=10002)REF1,TOLR1,REF2,TOLR2,BS0,ALPHA
 105  FORMAT(BZ,F10.3)
10002 DO 115 N=1,NTK
      READ(5, 110,END=10003)RTK(N),TOLKSP(N),(DIST(I,N),BS(I,N),I=1,2),D
     *ISTT(N),  TOLKD(N),BETA(N),GAMMA(N)
 110  FORMAT(BZ,F10.3)
10003 IF(N.EQ.1) GO TO 115
      NM1=N-1
      DO 114 K=1,NM1
      READ(5,105,END= 114 ) ANGKK(K,N)
 114  CONTINUE
 115  CONTINUE
      CAMLTH=ALAML/ALAMDA
      WRITE(6, 120)JOB,JOB,JOB,A,ALAML,ALAMDA,ANGTOL,CAMLTH
 120  FORMAT(1H1/3(5X,'NEGATIVE PLATE  ',A10,5X)//5X,'LATTICE PARAMETERS
     * ' ,3F10.3,'  ANGSTROMS'//5X,'LAMBDA BY L =',F10.3//5X,'WAVELENGTH
     * =',F10. 5,'  ANGSTROMS'//5X,'ANGLE TOLERANCE =',F9.1,'  DEGREES'/
     */            5X,'CAMERA LENGTH = ',F10.1,' MM')
      WRITE(6, 125) NTK
 125  FORMAT(/5X,'NO. OF LINES REFERRED TO REFERENCE',I5)
      DTORAD=3.14159/180.
      DO 144 I=1,3
 144  AR(I)=1./A(I)
C
      READ *,OVLP
      PRINT 121, OVLP
 121  FORMAT(/' ANGLE OF OVERLAP INTO ADJACENT QUADRANTS IS',F8.2,
     1 ' DEGREES')
      OVLP=SIN(OVLP*DTORAD)
C
C
      IER=0
      DO 162 N=1,NTK
```

```
      IF(DIST(1,N)-0.01) 146,151,151
  146 BS(1,N)=BS0
      BS(2,N)=BS0
      DISTT(N)=0.
      GO TO 162
  151 CA=ABS((DIST(1,N)**2+DIST(2,N)**2-DISTT(N)**2)/(2.*DIST(1,N)
     1 *DIST(2,N)))
      IF(CA-1.) 154,154,152
  152 WRITE(6,153)N,DIST(1,N),DIST(2,N),DISTT(N),ALPHA,BETA(N),
     1 GAMMA(N)
  153 FORMAT(/' ERROR IN DATA FOR K LINE',I3,5X,'TRIANGLE DISTANCES'
     1 ,'ARE',3F10.3,5X,'ANGLES ARE ',3F10.3)
      IER=1
      GO TO 162
  154 IF(ABS(ACOS(CA)/DTORAD-ALPHA)-ANGTOL) 157,157,152
  157 CB=ABS((DIST(1,N)**2+DISTT(N)**2-DIST(2,N)**2)/(2.*DIST(1,N)
     1 *DISTT(N)))
      IF(CB-1.) 158,158,152
  158 IF(ABS(ACOS(CB)/DTORAD-BETA(N))-ANGTOL) 159,159,152
  159 CG=ABS((DIST(2,N)**2+DISTT(N)**2-DIST(1,N)**2)/(2.*DIST(2,N)
     1 *DISTT(N)))
      IF(CG-1.) 161,161,152
  161 IF(ABS(ACOS(CG)/DTORAD-GAMMA(N))-ANGTOL) 162,162,152
  162 CONTINUE
      IF(IER.GT.0) STOP
C
      WRITE(6,127) REF1,TOLR1,REF2,TOLR2,BS0,ALPHA
  127 FORMAT(//' REF.1 SPACING',F8.1,' MM +/-',F5.1,'%',4X,'REF.2 SPACIN
     1G'     ,F8.1,' MM +/-',F5.1,'%'//' REFERENCE INTERSECTION : DIST.
     2TO'        ,' BEAM STOP',F8.1,'   ACUTE ANGLE',F8.1)
      DO 138 N=1,NTK
      WRITE(6,129) N,RTK(N),TOLKSP(N),TOLKD(N)
  129 FORMAT(//2X,'K LINE',I5,8X,'SPACING',F8.1,' MM  +/-',F5.1,'%',15X,
     *        'DEGREES PER MM TOLERANCE  +/-',F5.1,'%')
      WRITE(6,131) (IR,N,DIST(IR,N),BS(IR,N),IR=1,2)
  131 FORMAT(/' R',I1,'/K',I1,'  INTERSECTION :  DIST. TO REFERENCE'
     1    ,' INTERSECTION',F8.1,' DIST. TO BEAM STOP',F8.1)
      WRITE(6,133) N,DISTT(N)
  133 FORMAT(/8X,'DISTANCE BETWEEN INTERSECTIONS OF K LINE',I5,
     *  '  WITH REF. 1 AND REF. 2',F10.1)
      NM1=N-1
      IF(NM1) 134,134,136
  136 WRITE(6,137) BETA(N),GAMMA(N),(ANGKK(K,N),K=1,NM1)
  137 FORMAT(/8X,'ACUTE ANGLES BETWEEN THIS K LINE AND PREVIOUS '
     * ,'LINES IN DEGREES',8F8.1)
      GO TO 138
  134 WRITE(6,137) BETA(N),GAMMA(N)
  138 CONTINUE
C
C      CALCULATE PLANES TO BE TESTED FROM SPACINGS AND TOLERANCES
C
      DRF1=ALAML/REF1
      DRF2=ALAML/REF2
      CALL LKH(LKHRF1,NRF1,A,DRF1,TOLR1,DPR1)
      CALL LKH(LKHRF2,NRF2,A,DRF2,TOLR2,DPR2)
      DO 160 I=1,NTK
      DTK(I)=ALAML/RTK(I)
      CALL LKH(ITEM,NTH(I),A,DTK(I),TOLKSP(I),TEMP)
```

```
      N=NTH(I)
      DO 150 J=1,N
      DO 145 K=1,3
 145  LKHTK(K,J,I)=ITEM(K,J)
 150  DPT(J,I)=TEMP(J)
 160  CONTINUE
C
      DO 165 I=1,NTK
 165  TOLKD(I)=TOLKD(I)/100.
C
C      BEGIN TESTING POSSIBLE PLANES
C
      DO 800 N1=1,NRF1
      DO 170 I=1,3
 170  IP1(I)=LKHRF1(I,N1)
      DO 800 N2=1,NRF2
      DO 172 I=1,3
 172  IP2(I)=LKHRF2(I,N2)
C
C     TEST WHETHER THE POSSIBLE REFERENCE PLANES ,IP1IP2, HAVE
C     THE CORRECT ANGLE BETWEEN THEM WITHIN TOLERANCES
C
      ALPHAT=ZANG(IP1(1),IP2(1),AR(1))
      ALPHAT=ALPHAT/DTORAD
      IF(ALPHAT.GT.90.) ALPHAT=180.-ALPHAT
      IF(ABS(ALPHAT-ALPHA)-ANGTOL) 190,190,800
 190  CALL ICROSS(IP1,IP2,ICPR)
C
C     TEST TO SEE IF THE ZONE OF IP1,IP2 IS IN REFERENCE QUADRANT
C
      IF(IQUAD(ICPR(1),A(1))) 800,800,200
 200  DO 205 I=1,NTK
 205  LOOP(I)=0
      N3=1
 210  LN3=LOOP(N3)+1
      N4=NTH(N3)
      DO 400 N5=LN3,N4
      DO 212 I=1,3
 212  IP3(I)=LKHTK(I,N5,N3)
C
C     TEST ANGLE BETWEEN POSSIBLE REF.1 AND POSSIBLE K LINE
C
      BETAT(N3)=ZANG(IP1(1),IP3(1),AR(1))
      BETAT(N3)=BETAT(N3)/DTORAD
      IF(BETAT(N3).GT.90.) BETAT(N3)=180.-BETAT(N3)
      IF(ABS(BETAT(N3)-BETA(N3))-ANGTOL) 215,215,400
C
C     TEST ANGLE BETWEEN POSSIBLE REF.2 AND POSSIBLE K LINE
C
 215  GAMMAT(N3)=ZANG(IP2(1),IP3(1),AR(1))
      GAMMAT(N3)=GAMMAT(N3)/DTORAD
      IF(GAMMAT(N3).GT.90.) GAMMAT(N3)=180.-GAMMAT(N3)
      IF(ABS(GAMMAT(N3)-GAMMA(N3))-ANGTOL) 217,217,400
 217  CALL ICROSS(IP1,IP3,ICPR1T)
C
C     TEST TO SEE IF ZONE OF POSSIBLE REF.1 AND POSSIBLE K PLANE
C     ARE IN THE REFERENCE QUADRANT (BAR H K L)
C
```

```
      IF(IQUAD(ICPR1T(1),A(1))) 400,400,220
  220 ANGL(1,N3)=ZANG(ICPR(1),ICPR1T(1),A(1))
C
C     CHECK TO SEE IF K LINE INTERSECTS REFERENCE INTERSECTION
C
      IF(DIST(1,N3)-0.01) 222,230,230
C
C     TEST TO SEE IF ZONES ARE THE SAME (ANGLE BETWEEN THEM SMALL)
C
  222 IF(ANGL(1,N3)-1.E-3) 224,400,400
  224 CALL ICROSS(IP2,IP3,ICPR2T)
      ANGL(2,N3)=ANGL(3,N3)=0.
      GO TO 285
C
C     TEST TO SEE WHETHER ANGLE BETWEEN POSSIBLE REFERENCE ZONE  AND
C     ZONE OF POSSIBLE REF.1  K LINE IS CONSISTANT WITH GIVEN CAMERA
C     LENGTH AND WAVELENGTH
C
  230 IF(ABS(ANGL(1,N3)*CAMLTH/DIST(1,N3)-1.)-TOLKD(N3))240,240,400
  240 CONTINUE
      CALL ICROSS(IP2,IP3,ICPR2T)
C
C     TEST WHETHER ZONE OF POSS.  REF.2/K LINE IN CORRECT QUADRANT
C
      IF(IQUAD(ICPR2T(1),A(1))) 400,400,260
  260 ANGL(2,N3)=ZANG(ICPR(1),ICPR2T(1),A(1))
C
C     TEST ANGLE BETWEEN ZONES OF POSS. REF.2/KLINE AND REF. INTERSECT.
C
C
      IF(ABS(ANGL(2,N3)*CAMLTH/DIST(2,N3)-1.)-TOLKD(N3))280,280,400
  280 CONTINUE
      ANGL(3,N3)=ZANG(ICPR1T(1),ICPR2T(1),A(1))
C
C     TEST ANGLE BETWEEN ZONES OF POSS. REF.1/K LINE AND REF.2/K LINE
C
      IF(ABS(ANGL(3,N3)*CAMLTH/DISTT(N3)-1)-TOLKD(N3)) 285,285,400
C     TEST TO SEE IF ANGLES BETWEEN THIS K LINE AND OTHERS IS OK
  285 N3M1=N3-1
      IF(N3M1) 298,298,286
  286 DO 289 I=1,N3M1
      DO 287 J=1,3
  287 IP4(J)=LKHTK(J,LOOP(I),I)
      ANGKK(N3,I)=ZANG(IP3(1),IP4(1),AR(1))/DTORAD
      IF(ANGKK(N3,I).GT.90.) ANGKK(N3,I)=180.-ANGKK(N3,I)
      IF(ABS(ANGKK(N3,I)-ANGKK(I,N3))-ANGTOL) 289,289,400
  289 CONTINUE
  298 DO 300 I=1,3
      IZP1(I,N3)=ICPR1T(I)
  300 IZP2(I,N3)=ICPR2T(I)
      LOOP(N3)=N5
      IF(N3-NTK) 320,340,340
  320 N3=N3+1
      GO TO 210
  340 CONTINUE
C
C     WE NOW HAVE A POSSIBLE SOLUTION
C
```

```
      RD1=DPR1(N1)*REF1
      RD2=DPR2(N2)*REF2
      CLR1=RD1/ALAMDA
      CLR2=RD2/ALAMDA
      DO 350 I=1,NTK
      RD(I)=RTK(I)*DPT(LOOP(I),I)
      CL(I)=RD(I)/ALAMDA
      IF(DIST(1,I)-0.01) 345,346,346
345   CL1(I)=CL2(I)=CL3(I)=DPMM1(I)=DPMM2(I)=DPMM3(I)=0.
      GO TO 350
346   Z=ANGL(1,I)/DIST(1,I)
      CL1(I)=ALAMDA/Z
      DPMM1(I)=Z*180./3.14159
      Z=ANGL(2,I)/DIST(2,I)
      CL2(I)=ALAMDA/Z
      DPMM2(I)=Z*180./3.14159
      Z=ANGL(3,I)/DISTT(I)
      CL3(I)=ALAMDA/Z
      DPMM3(I)=Z*180./3.14159
350   CONTINUE
      WRITE(6,351)
351   FORMAT(//3X,'REFERENCE',4X,'RD',13X,'REFERENCE',6X,'RD',
     * 13X,'REFERENCE',12X,'R1/R2 ANGLE'/4X,'PLANE 1',31X,
     * 'PLANE 2',32X,'ZONE')
      WRITE(6,360)(LKHRF1(I,N1),I=1,3),RD1,(LKHRF2(I,N2),I=1,3)
     *,RD2,(ICPR(I),I=1,3),ALPHAT
360   FORMAT(/2(1X,3I3,F10.2,10X),3I4,F17.1)
      WRITE(6,361)
361   FORMAT(/3X,'K PLANE',8X,'INTERSECTION',3X,'D/MM',3X,'LL',5X,
     * 'INTERSECTION',2X,'D/MM',3X,'LL',6X,'D/MM',3X,'LL'/28X
     *                ,'WITH REF 1',19X,'WITH REF 2'/)
      DO 368 J=1,NTK
      JM1=J-1
      LOOPJ=LOOP(J)
      IF(JM1) 364,364,369
364   WRITE(6,365) (LKHTK(I,LOOPJ,J),I=1,3),RD(J),
     *(IZP1(I,J),I=1,3),DPMM1(J),CL1(J),(IZP2(I,J),I=1,3),DPMM2(J),
     *CL2(J),DPMM3(J),CL3(J),BETAT(J),GAMMAT(J)
      GO TO 368
369   WRITE(6,365) (LKHTK(I,LOOPJ,J),I=1,3),RD(J),
     *(IZP1(I,J),I=1,3),DPMM1(J),CL1(J),(IZP2(I,J),I=1,3),DPMM2(J),
     *CL2(J),DPMM3(J),CL3(J),BETAT(J),GAMMAT(J),(ANGKK(J,JJ),
     *JJ=1,JM1)
365   FORMAT(3I3,F7.2,2(3I4,F7.3,F7.2,2X),F5.3,F7.1
     *,7F6.1)
368   CONTINUE
C
C     NOW CALCULATE BEAM DIRECTION
C
      AVRD=RD1+RD2
      DO 366 I=1,NTK
366   AVRD=AVRD+RD(I)
      AVRD=AVRD/FLOAT(2+NTK)
      AVCL=0.
      NDP=0
      AVDPMM=0.
      DO 371 I=1,NTK
      IF(DIST(1,I).LT.0.01) GO TO 371
```

```
      NDP=NDP+3
      AVDPMM=AVDPMM+DPMM1(I)+DPMM2(I)+DPMM3(I)
  371 CONTINUE
      IF(NDP.GT.0) THEN
                        AVDPMM=AVDPMM/FLOAT(NDP)
                        AVCL=1./(AVDPMM*DTORAD)
                   ELSE
                        GO TO 401
      ENDIF
      DO 367 I=1,3
  367 CAV(I)=0.
      N=0
      DO 380 K=1,NTK
      IF(DIST(1,K).LT.0.01) GO TO 380
      DO 370 I=1,3
      U(1,I)=ICPR(I)
      U(2,I)=IZP1(I,K)
      U(3,I)=IZP2(I,K)
  370 CONTINUE
      C(1)=COS(BS0/AVCL)
      C(2)=COS(BS(1,K)/AVCL)
      C(3)=COS(BS(2,K)/AVCL)
      CALL BEAM (A,U,C)
      DO 372 I=1,3
  372 CAV(I)=C(I)+CAV(I)
      N=N+1
  380 CONTINUE
      IF(N) 401,401,381
  381 DO 382 I=1,3
  382 CAV(I)=CAV(I)/FLOAT(N)
      DO 395 I=1,3
      BD(I)=CAV(I)/A(I)
      BP(I)=CAV(I)*A(I)
      IF(ABS(CAV(I))-1.) 383,383,384
  383 AC(I)=180.*ACOS(CAV(I))/3.14159
      GO TO 395
  384 IF(ABS(CAV(I))-1.001) 386,386,385
  385 WRITE(6,387) CAV(I),I
  387 FORMAT(/' COS .GT. 1.001 , COS=',F12.4,'I=',I5)
  386 AC(I)=0.
  395 CONTINUE
      WRITE(6,397) CAV,BD,BP,AC
  397 FORMAT(/7X,14HBEAM DIRECTION//3X,18H DIRECTION COSINES,
     *11X,9HDIRECTION,17X,6HPLANAR,15X,' ANGLES TO  1 0 0   0 1 0    0 '
     *,'0 1'/3(3F8.4,2X),6X,3F9.1/)
      AVLL=ALAMDA*AVCL
  401 WRITE(6,398) AVRD,AVDPMM,AVLL
  398 FORMAT(/4X,'AVERAGE CAMERA LENGTH :   RD= ',F8.2,5X,
     1 'DPMM =',F8.3,5X,'LAMBDA/DPMM =',F8.2)
  400 CONTINUE
  405 N3=N3-1
      IF(N3) 800,800,410
  410 IF(LOOP(N3)-NTH(N3)) 420,405,405
  420 LOOP(N3+1)=0
      GO TO 210
  800 CONTINUE
C
      WRITE(6, 900)
```

```
900   FORMAT(//' BYE BYE KORTHU')
      STOP
      END
      FUNCTION IQUAD(ICPR,A)
C
C     RETURNS IQUAD=1 IF ZONE ICPR IS WITHIN 10 DEGREES OF THE
C     QUADRANT BAR H K L. IQUAD=0 OTHERWISE.
C
      DIMENSION ICPR(3),CPR(3),A(3)
      COMMON /OVERLP/OVLP
      DO 5 I=1,3
      IF(ICPR(I)) 7,5,7
 5    CONTINUE
      GO TO 400
 7    S=0.
      DO 10 I=1,3
      CPR(I)=ICPR(I)*A(I)
      S=CPR(I)**2+S
 10   CONTINUE
 50   S=SQRT(S)
      DO 60 I=1,3
 60   CPR(I)=CPR(I)/S
      IF(CPR(1)-OVLP) 70,70,150
 70   IF(CPR(2)+OVLP) 150,80,80
 80   IF(CPR(3)+OVLP) 150,300,300
 150  IF(CPR(1)+OVLP) 400,160,160
 160  IF(CPR(2)-OVLP) 170,170,400
 170  IF(CPR(3)-OVLP) 200,200,400
 200  DO 250 I=1,3
 250  ICPR(I)=-ICPR(I)
 300  IQUAD=1
      RETURN
 400  IQUAD=0
      RETURN
      END
      FUNCTION ZANG(IZ1,IZ2,A)
C     CALCULATE ANGLE BETWEEN ZONES IZ1 AND IZ2
      DIMENSION IZ1(3),IZ2(3),A(3),Z1(3),Z2(3)
      DO 100 I=1,3
      Z1(I)=IZ1(I)*A(I)
 100  Z2(I)=IZ2(I)*A(I)
      S1=Z1(1)**2+Z1(2)**2+Z1(3)**2
      S2=Z2(1)**2+Z2(2)**2+Z2(3)**2
      ARG=(Z1(1)*Z2(1)+Z1(2)*Z2(2)+Z1(3)*Z2(3))/SQRT(S1*S2)
      ABARG=ABS(ARG)
      IF(ABARG-1.) 200,200,300
 200  ZANG=ACOS(ARG)
      RETURN
 300  IF(ABARG-1.0001) 500,500,350
 350  WRITE(6,400) IZ1,IZ2,A,ARG
 400  FORMAT(/2(3X,3I4),4F12.3)
 500  ZANG=0.
      RETURN
      END
      SUBROUTINE LKH(KH,N,A,DSP,TOL,SP)
C
C     GENERATES POSSIBLE PLANES FROM SPACINGS AND TOLERANCES
C
```

```
      DIMENSION KH(3,200),A(3),SP(200),IHK(3,67),SPA(67),HK(3)
      COMMON /OVERLP/ OVLP
      DTOL=DSP*TOL/100.
      REWIND 7
      READ(7,40)
 40   FORMAT(//)
      N1=0
 50   READ(7,100,END=400) I,J,K
 100  FORMAT(BZ,1X,3I3)
      IF((I+J+K).EQ.0) GO TO 400
 200  D=1./SQRT((I/A(1))**2+(J/A(2))**2+(K/A(3))**2)
      IF(ABS(DSP-D)-DTOL) 250,250,50
 250  N1=N1+1
      IHK(1,N1)=I
      IHK(2,N1)=J
      IHK(3,N1)=K
      SPA(N1)=D
      GO TO 50
 400  CONTINUE
      WRITE(6, 500)((IHK(I,J),I=1,3),J=1,N1)
 500  FORMAT(/(10(1X,3I2,1X)))
      N=0
      DO 900 K=1,N1
      NOS=0
 600  CALL SIGN(IHK(1,K),IHK(2,K),IHK(3,K),NOS)
      IF(NOS-5) 700,900,900
 700  DO 710 I=1,3
 710  HK(I)=IHK(I,K)/A(I)
      S=SQRT(HK(1)**2+HK(2)**2+HK(3)**2)
      DO 720 I=1,3
 720  HK(I)=HK(I)/S
      IF(HK(1)+OVLP) 730,750,750
 730  IF(HK(2)-OVLP) 750,750,740
 740  IF(HK(3)-OVLP) 750,750,600
 750  IF(HK(1)-OVLP) 790,790,760
 760  IF(HK(2)+OVLP) 770,790,790
 770  IF(HK(3)+OVLP) 600,790,790
 790  N=N+1
      DO 800 I=1,3
 800  KH(I,N)=IHK(I,K)
      SP(N)=SPA(K)
      GO TO 600
 900  CONTINUE
C      WRITE(6,500) ((KH(I,J),I=1,3),J=1,N)
      WRITE(6, 1000)N
 1000 FORMAT(' NUMBER OF PLANES FORMED IS ',I6)
      RETURN
      END
      SUBROUTINE SIGN(NH,NK,NL,NSIGN)
C
C     GENERATES <HKL> FROM (HKL)
C
      IF((NH.EQ.0).AND.(NK.EQ.0))GOTO70
      IF((NK.EQ.0).AND.(NL.EQ.0))GOTO70
      IF((NH.EQ.0).AND.(NL.EQ.0))GOTO70
      IF(NH.EQ.0)GOTO71
      IF(NK.EQ.0)GOTO72
      IF(NL.EQ.0)GOTO71
```

```
      GOTO60

70    IF(NSIGN.EQ.0)GOTO50
      NSIGN=5
      RETURN
71    IF(NSIGN-1) 50,12,74
72    IF(NSIGN-1) 50,13,74
74    NSIGN=5
      RETURN

60    IF(NSIGN.EQ.0)GOTO50
      IF(NSIGN.EQ.1)GOTO13
      IF(NSIGN.EQ.2)GOTO12
      IF(NSIGN.EQ.3)GOTO13
      IF(NSIGN.EQ.4)GOTO50
      IF(NSIGN.GE.5)RETURN


12    NK=-NK
      GOTO50

13    NH=-NH

50    NSIGN=NSIGN+1
      RETURN
      END
      SUBROUTINE ICROSS (K,L,IUVW)
      DIMENSION IUVW(3),K(3),L(3)
      IUVW(1)=K(2)*L(3)-K(3)*L(2)
      IUVW(2)=K(3)*L(1)-K(1)*L(3)
      IUVW(3)=K(1)*L(2)-K(2)*L(1)
      RETURN
      END
      SUBROUTINE BEAM (A,U,C)
C
C     CALCULATES BEAM DIRECTION GIVEN THREE DIRECTIONS AND
C     COSINES OF ANGLES TO BEAM DIRECTION
C
C      USAGE   NEED TO FIRST ATTACH,IMSL,ALTLIB8,CY=30.
C                    THEN   LIBRARY,IMSL.
      DIMENSION A(3),DCM(3,3),U(3,3),C(3),WK(9)
C
C
C     CALCULATE DIRECTION COSINE MATRIX
C
      DO 300 I=1,3
      DO 300 J=1,3
 300  DCM(I,J)=U(I,J)*A(J)/SQRT((U(I,1)*A(1))**2+(U(I,2)*A(2))**2+
     +(U(I,3)*A(3))**2)
C
C      WRITE(6, 400)((U(I,J),J=1,3),ANG(I),I=1,3)
 400  FORMAT(/12H  DIRECTIONS,14X,15HANGLE FROM BEAM/
     *3(3F8.2,4X,F8.2/))
      CALL SOLVE(DCM,C)
      RETURN
      END
      SUBROUTINE SOLVE(A,C)
      DIMENSION A(3,3),C(3),CP(3)
```

```
      DETA=DET(A(1,1),C(1),0)
      DO 100 I=1,3
      CP(I)=DET(A(1,1),C(1),I)/DETA
  100 CONTINUE
      DO 200 I=1,3
  200 C(I)=CP(I)
      RETURN
      END
      FUNCTION DET(B,X,IOPT)
      DIMENSION B(3,3),X(3),W(3,3)
  100 DO 150 I=1,3
      DO 150 J=1,3
  150 W(I,J)=B(I,J)
      IF(IOPT) 500,500,200
  200 IF(IOPT-2) 210,260,280
  210 DO 250 I=1,3
  250 W(I,1)=X(I)
      GO TO 500
  260 DO 270 I=1,3
  270 W(I,2)=X(I)
      GO TO 500
  280 DO 290 I=1,3
  290 W(I,3)=X(I)
C
  500 DET=W(1,1)*(W(2,2)*W(3,3)-W(2,3)*W(3,2))
     1 -W(1,2)*(W(2,1)*W(3,3)-W(2,3)*W(3,1))
     2 +W(1,3)*(W(2,1)*W(3,2)-W(2,2)*W(3,1))
      IF(ABS(DET).GT. 1.E-10) RETURN
      WRITE(6,600) DET,IOPT
  600 FORMAT(/' DETERMINANT =',E12.4,' IOPT=',I6)
      STOP
      END
```

BIBLIOGRAPHY

ABBOTT, J.R. and MAKINSON, O.F.

J. Dent. Res., 57:790, 1978.

ABBOTT, J.R., MILLER, D.R. and NETHERWAY, D.J.

To be published, 1981.

ALLAN, F.C., ASGAR, K. and PEYTON, F.A.

J. Dent. Res., 44:1002, 1965.

APPLEMAN, D.E., EVANS Jr., H.T. and HANDWERKER, D.S.

Ann. Meet. Amer. Cryst. Ass.,
Cambridge, Mass. Program 42-43, March 1963.

ASGAR, K. and SUTFIN, L.

J. Dent. Res., 44:977, 1965.

BAIRD, H.W. and MULLER, F.A.

J. Biomed. Mater. Res. 3:375, 1969.

BERMAN, H. and HARCOURT, G.A.

Amer. Min., 23:761, 1938.

BLACK, G.V.

Dental Cosmos, 37:553, 1895a.

BLACK, G.V.

Dental Cosmos, 37:637, 1895b.

BLACK, G.V.

Dental Cosmos, 37:737, 1895c.

BLACK, G.V.

Dental Cosmos, 38:43, 1896a.

BLACK, G.V.

Dental Cosmos, 38:965, 1896b.

BLACK, G.V.

Dental Cosmos, 39:623, 1897.

BÖHME, R., BURZLAFF, H. and GOMM, M.

Acta Cryst., A31:S277, 1975.

DOYLE, P.A. and TURNER P.S.

Acta Cryst., A24:390, 1968.

DUBOIS, J.M., LECAER, G., BERNARD, B., DUMAGNY, J.G. and DUPONT, F.

Acta Met., 29:1159, 1981.

FAIRHURST, C.W.

Ph.D. Thesis, Northwestern University, 1966.

FAIRHURST, C.W. and COHEN, J.B.

Acta Cryst., B28:371, 1972.

FAIRHURST, C.W.and RYGE, G.

Advances in X-ray Analysis 5:64, Plenum Press, New York 1962.

GAYLER, M.L.V.

J. Inst. Metals, 60:379, 1937a.

GAYLER, M.L.V.

J. Inst. Metals, 60:407, 1937b.

GRAY, A.W.

J. Nat. Dent. Ass., 6:513, 1919.

GRAY, A.W.

J. Nat. Dent. Ass., 8:196, 1921.

GRAY, A.W.

J. Amer. Dent. Ass., 9:324, 1922.

GRAY, A.W.

J. Inst. Metals, 29:139, 1923.

GRUNDY, P.J. and JONES, G.A.

Electron Microscopy in the Study of Materials.
Edward Arnold (Publishers) Ltd. London, 1976.

HANSEN, M.

Constitution of Binary Allays
McGraw-Hill, New York, 1958.

HANSON, D., SANDFORD, E.J. and STEVENS, H.

J. Inst. Metals, 55:115, 1934.

HEYCOCK, C.T. and NEVILLE, F.H.

Philo. Trans., 189:25, 1897.

HILLERT, M.

"Eutectic and Peritectic Solidification" in
Solidification and Casting of Metals.
The Metals Society, 1979.

HREN, J.J., GOLDSTEIN, J.I. and JOY, D.C.

"Introduction to Analytical Electron Microscopy"
Plenum Press, New York, 1979.

JOHARI, O. and THOMAS, G.

The Stereographic Projection and its Application.
Interscience, New York, 1969.

JOHNSON, Jr. L.B.

J. Biomed. Mater. Res., 1:285, 1967a.

JOHNSON Jr., L.B.

J. Biomed. Mater. Res., 1:415, 1967b.

JOHNSON, L.B. and CARWILE, A.C.

J. Biomed. Mater. Res., 12:367, 1978.

JOHNSON, L.B., OTANI, H., NEARY, M.J., HAUCK, J.W.,
HEAVEN, T.M. and REGENITTER, R.J.

J. Biomed. Mater. Res. 8:3, 1974.

JOYNER, R.A.

J. Chem. Soc., 99:195, 1911.

KAMDAR, M.H.

Prog. Mater. Sci., 15:289, 1973.

KNIGHT, W.A. and JOYNER, R.A.

J. Chem. Soc., 103:2247, 1913.

LIND, V., WENNERHOLM, W.G. and NYSTROM, S.

Acta Odontol. Scand., 22:333, 1964.

LYNCH, S.P.

Fracture (ed. by D.M.R. Taplin)
University of Waterloo Press, Canada, 2:859, 1977.

LYNCH, S.P.

Acta Met., 29:325, 1981.

MALHOTRA, M.L. and LAWLESS, K.R.

J. Biomed. Mater. Res., 9:121, 1975.

MARCINKOWSKI, M.J., BROWN, N. and FISHER, R.M.

Acta Met., 9:129, 1961.

MCBAIN, J.W. and JOYNER, R.A.

Dental Cosmos 54:641, 1912.

MURPHY, A.J.

J. Inst. Metals, 35:107, 1926.

MURPHY, A.J. and PRESTON, G.D.

J. Inst. Metals, 46:507, 1931.

NETHERWAY, D.J.

Private Communication, 1979.

NIAL, O. ALMIN, A. and WESTGREN, A.

Z. Phys. Chem., 14:81, 1931.

NICHOLAS, M.G. and OLD, C.F.

J. Mat. Sc. 14:1, 1979.

OKABE, T., HOCHMAN, R.F. and MCLAIN, M.E.

J. Biomed. Mater. Res., 8:381, 1974.

OKABE, T., MITCHELL, R.J. and FAIRHURST, C.W.

J. Dent. Res., 58:1087, 1979.

OLD, C.F.

Met. Sc., 14:433, 1980.

OLD, C.F. and TREVENA, P.

Met. Sc., 13:591, 1979.

OGG, A.

Z. Phys. Chem., 27:285, 1895.

OTANI, H.

J. Osaka Univ. Dent. Sch., 10:57, 1970a.

OTANI, H.

J. Osaka Univ. Dent. Sch., 10:69, 1970b.

OTANI, H.

J. Osaka Univ. Dent. Sch., 10:1, 1970c.

PARTRIDGE, P.G.

Met. Rev., 12:169, 1967.

PEARCE, A.S.

Private Communication (1972).

PETRENKO, G.J.

Z. Anorg. Chem., 53:200, 1907.

PHILLIPS, R.W.

Skinner's Science of Dental Materials,

W.B. Saunders Company,

7th ed. 1973.

PIHL, C.F. and BEASLEY, W.M.

J. Dent. Res., 47:418, 1968.

REINDERS, W.

Z. Phys. Chem., 54:609, 1904.

REYNOLDS, Jr., C.L.

J. Biomed. Mater. Res., 7:335, 1973.

REYNOLDS, Jr. C.L. and BARKER, R.E.

J. Biomed. Mater. Res., 9:213, 1975.

REYNOLDS, Jr. C.L., WARNER, F.E. and WILSDORF, H.G.

J. App. Phys., 46:568, 1975.

RYGE, G., FAIRHURST, C.W. and FISCHER, C.H.

Int. Dent. J., 11:181, 1961.

RYGE, G., DICKSON, G., SMITH, D.L. and SCHOONOVER, I.C.

J.A.D.A., 45:269, 1952.

RYGE, G., MOFFETT, J.C., and BARKOW, A.G.

J. Dent. Res., 32:152, 1953.

SCHMITT, G.

Dtsch. Zahnarztl. Z., 15:736, 1960.

SCHNUCK, K.

"Strukturuntersuchungen an Zahnarztlichen Amalgamen",
Thesis (Zahnarztliche Facultat), Jena, 1958.

SIMSON, C.V.

Z. Phys. Chem., 109:183, 1924.

STENBECK, S.

"Bidrug till kannedomen om Dentala Amalgam",
lst., A-B Fahlcrantz Boktryckeri, Stockholm, 1950.

TAYLOR, D.F.

J. Biomed. Mat. Res., 6:289, 1972.

THOMAS, G.

Transmission Electron Microscopy of Metals.
John Wiley & Sons, New York, 1966.

TROIANO, A.R.

J. Inst. Metals, 63:247, 1938.

VANDERSCHAEVE, G. and SARRAZIN, T.

Phys. Stat. Sol. 43:459, 1977.

VRIJHOEF, M.M.A. and DRIESSENS, F.C.M.

J. Biomed. Mater. Res., 8:435, 1974.

WATERSTRAT, R.M. and HICHO, G.E.

J. Res. Nat. Bur. Standards, 3:317, 1964.

WING, G.

Aust. Dent, J., 10:113, 1965.

WING, G.

Aust. Dent, J., 11:105, 1966.

WING, G.

in Scientific Aspects of Dental Materials
Chapter 8, Ed. by J.A. von Fraunhofer,
Butterworths, London 1975.

WING, G. and RYGE, G.

J. Dent. Res., 44:701, 1965.

WOOD, J.V. and JACOMBS, V.

J. Mat. Sc., 11:865, 1976.

WOOD, J.V. and KING, S.C.

J. Mat. Sc., 13:1119, 1978.

YVON, K., JEITSCHKO, W. and PARTHÉ, E.

J. App. Cryst., 10:73, 1977.